Synergy of Nanoparticles and Surfactants for CO_2 Foam Enhanced Oil Recovery and CO_2 Storage in Carbonates

Master Thesis in Reservoir Physics

By

Eldri Bratland Skjelsvik

Department of Physics and Technology

University of Bergen

June 2018

Abstract

This experimental thesis is a part of an ongoing CO_2-foam project lead by the Reservoir Physics group at the Department of Physics and Technology, University of Bergen. The main thesis objective was to investigate the separate and combined use of silica nanoparticles and surfactants as foaming agents for CO_2-foam. A comprehensive study has been conducted at various experimental conditions to evaluate nanoparticle stability, foamability with different foaming agents, and the performance of CO_2-foam stabilized by nanoparticles for enhanced oil recovery (EOR).

Static stability tests of separate and combined use of hydrophilic silica nanoparticles and nonionic or cationic surfactants were conducted to qualitatively study interactions between the foaming agents at elevated temperatures. The effect of oil on nanoparticle- and/or surfactant-stabilized foam was quantitatively determined for bulk-generated foam and foam generated in porous media. Tertiary CO_2-foam for EOR injections compare the performance of nanoparticles (separate or in synergy with surfactants) as CO_2 foaming agents for foam stabilization and enhanced oil recovery. Foam was generated in-situ in Edwards limestone and Bentheimer sandstone cores with supercritical CO_2 at miscible conditions between CO_2 and oil during CO_2-foam EOR injections. Carbon storage was also quantitatively determined as an element of Carbon Capture, Utilization and Storage (CCUS). In addition, nanoparticle retention studies were performed to investigate loss of nanoparticles during core injections.

Bulk foam stability tests investigated the effect of oil on foam coalescence of N_2-generated foam stabilized by different foaming agents at ambient conditions. The experimental results indicated that oil had a detrimental effect on bulk foam stability. Presence of oil was also studied during CO_2-foam injections in porous media, where the effect of oil was detrimental on weak foams, whereas stronger foams attained a stabilizing effect from injected oil by oil-in-water emulsions. Measured nanoparticle retention was in the lower range of literature values for surfactant retention.

Optimum gas fractions for CO_2-foam EOR injections were determined during foam quality scans of co-injected CO_2 and foaming agent. A quantitative experimental analysis of oil recovery efficiency and pressure gradients during CO_2-foam EOR was used to evaluate the feasibility of using nanoparticles (separate or in synergy with surfactants) for CO_2 mobility reduction. Silica nanoparticles (NPA) were co-injected with two types of surfactants during foam scans and CO_2-foam EOR injections: a nonionic (SurfA) and a switchable cationic (SurfB) surfactant. At the experimental conditions used, NPA combined with SurfB showed better performance in terms of incremental oil recovery and increased differential pressure compared to the combination of NPA and SurfA. SurfB used separately or in combination with nanoparticles outperformed the separate use of NPA and SurfA as foaming agents in limestone.

Carbon negative oil production (more carbon stored than produced during combustion of produced oil) was achieved during SurfA-stabilized foam in sandstone and NPA-stabilized foam (with and without SurfA) in limestone, and generation of strong foam and/or emulsions were beneficial for CO_2 storage. Limestone dissolution due to the acidic effect of co-injected CO_2 and brine positively affected the carbon storage capacity due to expansion of the pore volume.

Acknowledgements

First of all, I would like to express my gratitude to my supervisor, Professor Martin Fernø, and to Professor Arne Graue at the Department of Physics and Technology at the University of Bergen, for giving me the opportunity to work on interesting research subjects. Thank you Martin for the support, guidance and valuable discussions.

I would also like to thank PhD Øyvind Eide for the experimental collaboration and for guidance along the way. Thanks to PhD candidates Arthur Uno Rognmo and Sunniva B. Fredriksen for willingly sharing valuable experience and knowledge. I would also like to thank scientist Andreas Sundblom at AkzoNobel for experimental analyzes, excellent guidance and for providing me with nanoparticles and surfactants.

A special thanks to my lab partner and friend, PhD candidate Tore L. Føyen. Thank you for your collaboration, guidance, patience and motivation. Thank you for your positivity and for always being helpful. The endless hours spent at the lab would not have been the same without you.

I would also like to thank all my friends and fellow students, especially Stine Marie Kristiansen, Anders Sundgot Saunes and Simon Inge Smenes Reite, for making these years memorable. Thank you for valuable discussions, everlasting procrastinating and for always making me laugh. I am forever grateful for our friendship.

Finally, a special thanks to my parents, Sigve and Unni, and my sister, Silje. Thank you for your endless love and support, and for always believing in me.

Bergen, June 2018

Eldri B. Skjelsvik

Table of Contents

Part I – Introduction and Theory

1. Introduction

As much as 70% of oil originally in place in a reservoir can remain unswept after implementation of conventional oil recovery methods such as pressure depletion and water injection. The increasing worldwide demand for oil and gas, together with a decreasing rate of new oilfield discoveries, have initiated the interest in enhanced oil recovery (EOR) technology on mature oil and gas fields (Romero-Zerón, 2012). Injection of CO_2 for increased oil production has been performed for over 40 years with commercial success in the U.S, due to CO_2 availability and low cost. However, density and viscosity differences between injected CO_2 and the displaced oil promote gravity override, viscous fingering, early gas breakthrough and reduced oil recovery (Enick et al., 2012; Lee & Kam, 2013).

Injection of CO_2 as foam can mitigate problems associated with unfavorable mobility ratios by reducing the CO_2 mobility, and thus increase the macroscopic sweep efficiency (Talebian et al., 2014). Foams are in general not stable, and foaming agents are required to achieve long-term foam stability (Sheng, 2013). Surfactants are widely used as foaming agents for CO_2 mobility control during EOR. However, lack of long-term foam stability often limits surfactant application at high temperatures and in high-salinity reservoirs. Using nanoparticles to stabilize CO_2 foam may overcome issues of long-term instability and adsorption loss associated with surfactant-based CO_2 EOR processes (Bennetzen & Mogensen, 2014; Grigg & Bai, 2005).

Present CO_2 EOR projects are frequently linked to global warming and climate changes due to the recent focus on reducing anthropogenic CO_2 emissions (Lee & Kam, 2013). Carbon dioxide emissions can be reduced by implementation of carbon capture, utilization and storage (CCUS), which involves capture, transport and utilization of anthropogenic CO_2, and ultimately long-term storage of CO_2 for sequestration. Utilization of CO_2 can be realized with CO_2-foam EOR, by replacing the naturally occurring CO_2 used for injection with anthropogenic sources of CO_2. CCUS is therefore a process with both environmental and economic benefits, as captured carbon is stored simultaneously as oil is recovered (Hasan et al., 2015).

This thesis presents a comprehensive experimental investigation on the feasibility of combining CO_2 and hydrophilic silica nanoparticles with surfactants as foaming agents for EOR. The synergy between nanoparticles and surfactants was studied during static stability tests and during foam generation in bulk and porous media with and without presence of oil. The effect of foaming agent was determined by quantitative comparison of differential pressure buildup and incremental oil recovery during co-injections. The degree of nanoparticle retention was evaluated, as high foaming agent retention influences foaming efficiency and the economic viability of foam-injection. Carbon storage potential was also quantitatively determined to investigate the feasibility of carbon neutral oil production during CO_2-foam EOR injections.

2. A Brief Introduction to Reservoir Engineering

Oil production from a reservoir is generally divided into three phases: primary, secondary and tertiary recovery. Primary recovery involves utilization of the natural energy available in a reservoir, such as expansion of the rock and fluid content, or gas cap drive. Secondary recovery consists of injecting water and/or gas into the reservoir for pressure support, and to increase the volumetric sweep efficiency (Sheng, 2010). Both of these recovery methods are frequently associated with low oil recovery, where less than 30% of oil originally in place (OOIP) is recovered during primary recovery, and 30-50% is recovered during secondary recovery (Alagorni et al., 2015). Low recovery during primary recovery is caused by rapid pressure depletion, developing solution gas cap drive and high gas production rates. Waterflooding, which is the most frequently used production strategy in the North Sea, often leads to poor volumetric sweep efficiency due to reservoir heterogeneity and the unfavorable mobility ratio between water and oil (Zolotuchin & Ursin, 2000). Tertiary recovery methods or enhanced oil recovery (EOR) methods are conducted when secondary recovery methods no longer are economically beneficial, where the main goal is to recover additional hydrocarbons (Alagorni et al., 2015). Bentheimer sandstone and Edwards limestone cores were used in the experimental work of this thesis, and characteristics of sandstone and carbonate reservoir will therefore be discussed below.

2.1 EOR: Enhanced Oil Recovery

Tertiary recovery or EOR is the implementation of various techniques used to increase the amount of produced oil from a reservoir after performing conventional recovery strategies like waterflooding and gas flooding (Green & Willhite, 1998). As the rate of new oil discoveries is declining, and most of the oil today is produced from mature fields, EOR technologies will play an essential role in meeting the continuously increasing energy demand. EOR methods reduce residual trapped oil by increasing the microscopic and macroscopic displacement efficiency, both contributing to the overall displacement efficiency. The microscopic displacement efficiency, which is defined as mobilization of oil at pore scale, can be increased by reducing capillary forces, oil viscosity, or the interfacial tension between oil and the displacing fluid. The macroscopic displacement efficiency describes the displacing fluids ability to sweep through the reservoir, displacing oil towards the production well. An enhancement of the macroscopic displacement efficiency is obtained by generating a more favorable mobility ratio between the oil and the displacing fluid, i.e. increasing oil mobility or decreasing the mobility of the displacing fluid (Romero-Zerón, 2012).

EOR methods are classified into five categories: mobility control, chemical, miscible, thermal and other processes. Polymer flooding or foam injections are examples of mobility control processes with increased macroscopic displacement efficiency, where the reduction in mobility of the injected phase results in a more favorable mobility ratio. Chemical processes are primarily based on enhancing the microscopic displacement efficiency by reducing the interfacial tension between oil and the displacing fluid, typically being chemicals like surfactants or alkaline agents. Miscible processes, with injection of fluids like hydrocarbon solvents or CO_2, take advantage of first-contact miscibility. Injection of thermal energy by steam or in-situ combustion from air or oxygen is defined as thermal processes. The thermal energy enhances oil recovery mainly by alteration of oil viscosity and favorable phase behavior. Processes that do not coincide with the mentioned categories are termed “other processes”, such as microbial-based techniques and immiscible CO_2 injection (Green & Willhite, 1998). The use of mobility control EOR in the form of CO_2-foam injection will be further discussed in Chapter 4.

2.2 Sandstone reservoirs

Making up as much as 60% of all petroleum reservoirs, sandstone reservoirs are the most common reservoir type in the world based on lithology (Bjørlykke & Jahren, 2010). Sandstone reservoirs mainly consist of sand grains with diameters ranging from 1/16 to 2 mm, cemented together with silica, calcium carbonate, clay and/or iron oxides. The main chemical component is silicon dioxide, SiO_2 (Zolotuchin & Ursin, 2000). Porosity and permeability are the most critical parameters in terms of oil recovery from sandstone reservoirs, but pore geometry and properties associated with wetting preferences will also affect the production (Bjørlykke & Jahren, 2010). As porosity and permeability in sandstones are closely related, and small core samples can represent an average of larger cores and areas of sandstone, these reservoirs are considered to be homogenous (Ahr, 2008).

Sandstone reservoirs are characterized as good candidates for EOR technology methods. Reservoir properties determine the oil production potential from sandstone reservoirs, and improved production technologies have achieved recovery factors up to 70 % for high-quality reservoirs in the North Sea (Bjørlykke & Jahren, 2010). High potential to implement EOR projects are shown in sandstone, but it is noteworthy that most of the methods used for EOR are mainly tested in sandstone at pilot and commercial scale. Based on a collection of 1507 EOR projects, 78 % were conducted in sandstone. Sandstone reservoirs are mainly the optimal choice for EOR applicability screening as reservoir lithology often is a limiting factor for particular EOR methods (Alvarado & Manrique, 2010).

2.3 Carbonate reservoirs

It is estimated that 60% of the world's remaining oil reserves and 40% of remaining gas reserves are placed in carbonate reservoirs, where the majority are located in The Middle East (Schlumberger, 2007). Carbonates are described as anionic complexes of the carbonate ion CO_3^{-2} and divalent metallic cations, predominantly consisting of calcite and dolomite. Carbonates consist of biological components such as skeleton remains, fecal pellets, lime mud and microbially mediated cement and lime muds. Deposition by biological, chemical and detrital processes ultimately leads to the formation of carbonate rocks. Unlike sandstones, carbonates are heavily influenced by diageneses, such as dissolution, cementation and recrystallization. As a result, carbonate porosity and permeability do not necessarily relate to each other, and these reservoirs are considered heterogeneous (Ahr, 2008). Carbonate reservoirs can be divided into limestone, dolomite and chalk (Austad, 2013), where calcite dominated limestone and dolomite make up 90% of all naturally occurring carbonates (Ahr, 2008).

Despite containing considerable amounts of oil and gas reserves, only 18% of the EOR projects were conducted on carbonate reservoirs, compared to 78% in sandstone (Alvarado & Manrique, 2010). Carbonates are often characterized by low porosity and large amounts of fractures, and exhibit oil-wet to mixed-wet wettability. These unfavorable rock properties generally lead to rapidly declining production and low hydrocarbon recovery, and EOR methods are therefore more commonly used in sandstone reservoirs, as the injected fluids in carbonates often will flow through the high-permeable fractured network rather than displace the oil situated in the rock matrix. However, there are examples of successfully pilot studies verifying the feasibility of different EOR methods in carbonates (Alvarado & Manrique, 2010). The average oil recovery from carbonate reservoirs is below 30% (Austad, 2013), and as approximately 50% of all hydrocarbon reserves are located in these reservoirs, it is necessary to continue studying EOR techniques especially targeted for carbonates. High residual oil saturation after waterflooding makes carbonate reservoirs good candidates for EOR, especially methods utilizing CO_2.

3. CO_2 for EOR

Injection of CO_2 for increased oil production by EOR technologies has been performed for over 40 years with commercial success (Lee & Kam, 2013). Due to availability and low cost, gas flooding is especially widespread in the U.S, where injection of CO_2 contributes to approximately 5% of the total domestic crude oil production (Enick et al., 2012; Lee & Kam, 2013). CO_2 is often the preferred choice for gas injection due to its phase behavior at typical reservoir conditions, where the fluid forms a dense or supercritical phase, which is more favorable for oil recovery (Lee & Kam, 2013). This section describes why CO_2 is used for EOR by introducing the physical properties of CO_2 and explaining the mechanisms behind miscible displacement of oil.

3.1 Physical Properties of CO_2

Understanding of the physical properties of CO_2 at different temperature and pressure is essential for successful application of CO_2 EOR methods. The physical state of CO_2 is a function of temperature and pressure, and CO_2 is a gas at ambient conditions. As pressure increases, the gas becomes denser and condenses from gas to liquid state (see Figure 3.1). The critical point of carbon dioxide is situated at 31.1°C and 73.9 bar (Freund, 2005), above which the CO_2 is termed "dense". For both pressure and temperature higher than the critical point, CO_2 becomes supercritical and with higher densities and viscosities compared to other gases. The supercritical state of CO_2 is more favorable for EOR injection as it, compared to pure gas injection, mitigate gravity segregation and viscous fingering (Lee & Kam, 2013).

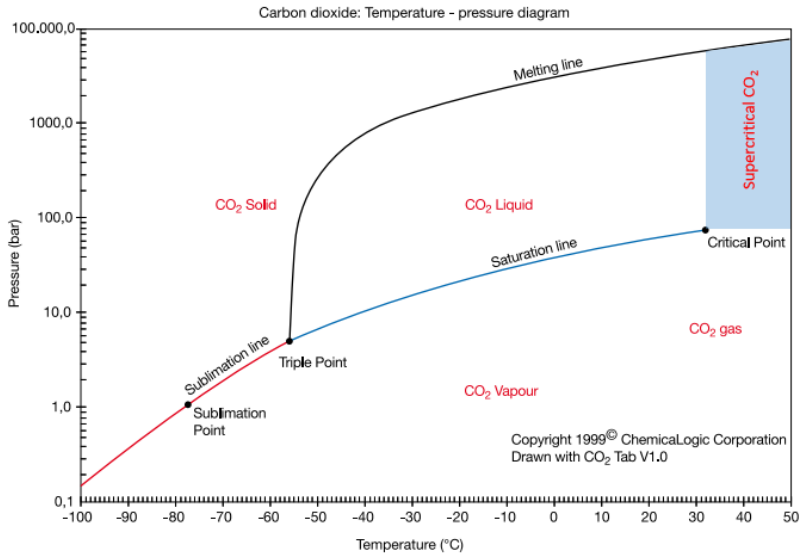

Figure 3.1 – Phase diagram for CO_2, showing phase behavior at different temperatures and pressures. The sublimation line states the transition conditions between solid and vapor CO_2, whereas the saturation line similarly shows transition conditions between vapor and liquid. CO_2 becomes supercritical for pressures and temperatures above the critical point at 31.1°C and 73.9 bar. Modified from (Freund, 2005).

3.2 Miscibility

In addition to obtaining higher viscosity and density compared to other gases, another aspect of CO_2 making it favorable for EOR application is its ability to miscibly displace oil. Two or more fluids are miscible if they form a single, homogeneous phase without the presence of an interface, in contrast to immiscible fluids where an interface between the two fluids always will be present and the interfacial tension (IFT) will be above zero. Waterflooding, performed prior to all tertiary CO_2 EOR injections conducted in this thesis, is an example of an immiscible displacement of oil. Because of a non-zero IFT between water and oil, capillary forces inhibit a complete displacement of oil. For a miscible displacement, however, it is theoretically possible to recover all of the oil in place in the swept porous (Fernø et al., 2015b; Holm, 1986). Nevertheless, this is rarely seen in practice as viscous fingering, local heterogeneities and water shielding result in low volumetric sweep efficiency (Muller & Lake, 1991).

A miscible displacement process can either be first-contact miscible or multi-contact miscible. First-contact miscibility is achieved when an arbitrary amount of the injected solvent, e.g. propane, butane or liquefied petroleum gas (LPG), exist as a single phase together with the reservoir oil. However, solvents obtaining first-contact miscibility are rarely economically beneficial due to high solvent cost. Multi-contact miscibility is obtained by the mechanism of condensing-gas drive or vaporizing-gas drive, where both types require a transfer of hydrocarbon components between the injected and the displaced fluid (Holm, 1986). Injection of CO_2 obtains miscibility through vaporizing-gas drive, where intermediate components are vaporized from the reservoir oil, resulting in miscibility between the oil and the enriched gas (Skarestad & Skauge, 2012). Compared to lean gases, dense or supercritical CO_2 injection allows for a miscible displacement at lower pressures, due to an extraction of heavier hydrocarbons from the reservoir oil (Holm, 1986).

Minimum Miscibility Pressure (MMP)

For a displacement process between two fluids to be miscible, the reservoir pressure must exceed a minimum pressure known as Minimal Miscibility Pressure (MMP), often determined from slim tube experiments. MMP is schematically established by plotting the experimental pressure against measured recovery, where the shape of the curve is used for determining MMP. If miscibility is achieved, the minimal miscibility pressure is characterized by a plateau on the plotted curve (Skarestad & Skauge, 2012), as seen in Figure 3.2. Knowledge of the MMP between CO_2 and the reservoir oil is crucial for screening reservoirs used for CO_2 injection (Yellig & Metcalfe, 1980), as it is desirable to obtain a miscible displacement front.

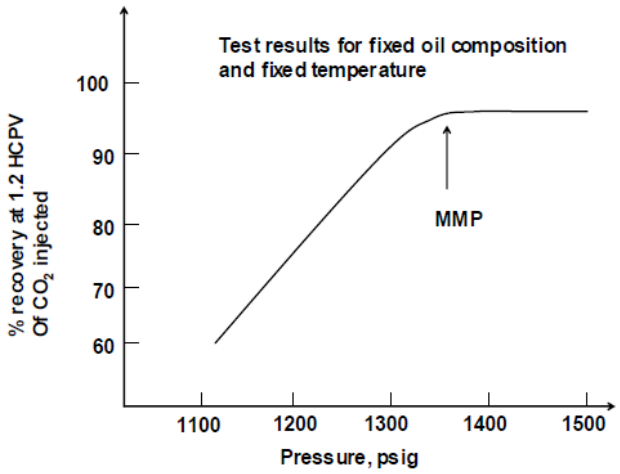

Figure 3.2 – Graphical illustration of the determination of MMP in a slim tube experiment. The MMP is characterized by a plateau (Skarestad & Skauge, 2012).

MMP for CO_2 and n-Decane

The oleic phase used in this experimental thesis is n-Decane, which is a mineral oil composed of a single hydrocarbon component, $C_{10}H_{22}$. Figure 3.3 graphically illustrates MMPs between n-Decane and CO_2 at different experimental pressures and temperatures, found by using high spatial magnetic resonance imaging (MRI) (Song et al., 2011). Pressure and temperature conditions used in this experimental thesis (see Figure 3.3) indicate that all CO_2 EOR injections are performed at miscible conditions of CO_2 and n-Decane.

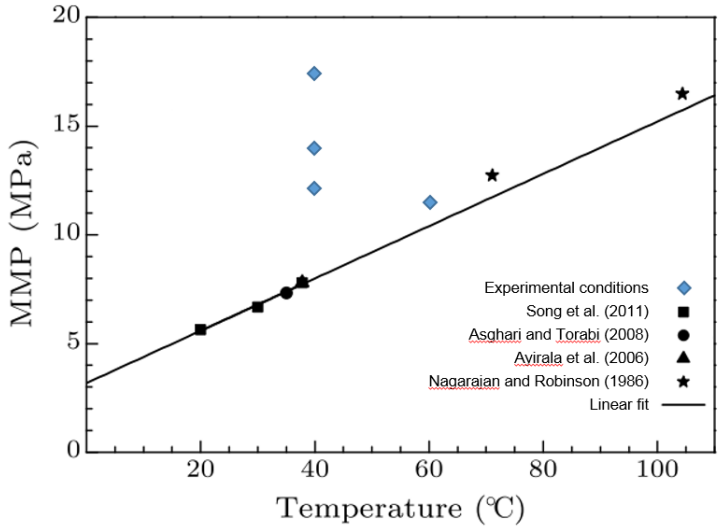

Figure 3.3 – MMPs of CO_2/n-Decane system as a function of temperature experimentally measured by Song et al. (2011), Nagarajan and Robinson (1986), Ayirala et al. (2006) and Asghari and Torabi (2008), with a correlation line fitted based the experiments of Song et al. (2011). Experimental pressures and temperatures used for CO_2 EOR injections thesis are plotted in blue. Modified from (Song et al., 2011).

3.3 Dispersion and Diffusion

In a miscible displacement of oil by CO_2, the phenomenon of dispersion has to be considered. Due to diffusion, local velocity gradients and mechanical mixing in pores, dispersion generates a mixing zone between the injected CO_2 and hydrocarbons stored in the reservoir (Skarestad & Skauge, 2012).

Dispersion

Dispersion describes the mixing of two fluids in a porous medium during a miscible displacement process, and is a measure of the degree of mixing between the miscible fluids (Lake et al., 2014). Dispersion is the combined effect of the physical phenomena of diffusion and convection induced mixing and causes reduction of concentration gradients as CO_2 is transported through a porous media (Skjæveland & Kleppe, 1992). Dispersion is affected by differences in viscosity and density between CO_2 and oil, heterogeneity of the porous media and turbulence (Perkins & Johnston, 1963). Oil recovery from a miscible displacement of oil by CO_2 is affected by the size of the transition zone, which increases with decreased core lengths. A high level of dispersion will decrease oil recovery, both for multi-contact miscibility and first-contact miscibility between gas and oil (Skjæveland & Kleppe, 1992).

The mixing mechanisms of dispersion are scale dependent. Microscopic dispersion at pore scale is described by molecular diffusion and flow in a single pore, or in a few neighboring pores. At reservoir scale, however, the denoted macroscopic or megascopic dispersion is dominated by large-scale heterogeneities such as stratification, shales and regions of variable permeability. The mixing mechanism at laboratory scale can be a variation of those observed for both microscopic and megascopic dispersion, but mechanisms seen on microscopic scale are more likely to occur if the porous system is homogeneous (Skjæveland & Kleppe, 1992). Thus, molecular diffusion and pore flow dominate the mixing mechanisms in sandstone cores, whereas the more heterogeneous carbonate cores will more likely have a mixture of mechanisms controlling the dispersion.

Diffusion

Diffusion is defined as a process between miscible fluids, where molecules are transported from areas of high concentration to areas of lower concentration, and can occur in gases, liquids and dense phases (Skjæveland & Kleppe, 1992). Diffusion is driven by concentration gradients, temperature gradients and pressure gradients, referred to as molecular diffusion, thermal diffusion and pressure diffusion, respectively (Haugen & Firoozabadi, 2006). When CO_2 and oil co-exist in a porous media, a sharp interface will arise, separating the two phases. With time, diffusion between the fluids gradually transforms the sharp interphase to a diffuse mixing zone grading the two pure fluids. The diffusion occurs due to random motion of the fluid molecules (Perkins & Johnston, 1963; Skjæveland & Kleppe, 1992).

A number of theoretical and experimental works have proven diffusion to be an essential mechanism for oil recovery for both secondary and tertiary EOR processes, especially at laboratory scale (Grogan & Pinczewski, 1987; Morel et al., 1993; Perkins & Johnston, 1963). When CO_2 is injected into a formation, it may contact the oil directly or by diffusing through a water phase blocking the oil (Grogan et al., 1988).

3.4 Oil Swelling

If CO_2 is injected into a formation as a miscible displacement of oil, CO_2 mixes with and dissolves into the reservoir oil. The mixing causes a volume increase of the oleic phase, termed oil swelling (Lee & Kam, 2013). Oil swelling has a beneficial impact on oil recovery, as it mobilizes residual oil by increasing the oil saturation and consequently increasing the relative permeability of oil. The degree of oil swelling is influenced by temperature, pressure and composition of the oil present (Mangalsingh & Jagai, 1996). Swelling occurs due to the solubility of CO_2 in the oleic phase, but CO_2 does not have the capability of displacing all methane molecules present in the oil. The oil swelling efficiency is thus controlled by methane content, where an increased amount of methane has a detrimental effect on the swelling process (Skjæveland & Kleppe, 1992).

Presence of water reduces the effect of oil swelling, as water blocks the direct contact between oil and injected CO_2. This phenomenon is known as water shielding, which prevents development of miscibility and reduces the microscopic displacement efficiency, and consequently the total oil recovery. However, experiments conducted by Campbell and Orr show that CO_2, given sufficient time, diffuses through the blocking water phase, causing swelling of trapped oil. The fluid movement is illustrated in Figure 3.4, where initially trapped oil in a dead-end pore is mobilized by swelling induced by diffusion. All of the blocking water was displaced within 26.5 hours, creating direct contact between the oil and gas, enhancing oil recovery. Water shielding occurs naturally if CO_2 is injected in tertiary mode, where the reservoir previously has been flooded with water. Even though initially trapped oil can be produced due to oil swelling and diffusion through the blocking phase, oil recovery is usually higher if the gas is injected in secondary mode due to the high water saturation in the tertiary process (Grogan & Pinczewski, 1987). All CO_2 EOR injections conducted in this thesis are performed as a tertiary process, i.e. subsequently to a waterflooding. Water shielding will affect diffusion in CO_2-foam displacements, as injected gas bubbles are divided by a thin liquid film. Foam injection of CO_2 will be further discussed in the following section.

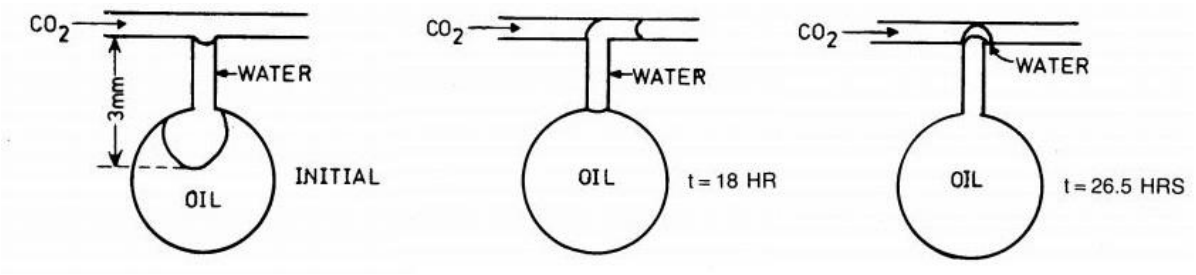

Figure 3.4 – Oil swelling over time due to diffusion through the blocking water phase in a dead-end pore. Modified from (Grogan & Pinczewski, 1987).

4. Foam for CO_2 Mobility Control

Despite achieving high microscopic sweep efficiency by miscible injection of CO_2, the volumetric sweep efficiency and gas utilization are limited due to the density and viscosity of the injected CO_2, promoting gravity override and reduced sweep efficiency in the lower reservoir regions. In addition, dense or supercritical CO_2 viscosity is low compared to typical crude oils, resulting in an unfavorable mobility ratio between the displaced (oil) and the displacing fluid (CO_2). The mobility differences cause propagation of viscous fingering, early gas breakthrough, high gas production and reduced oil production rates, all resulting in low final oil recovery. The low oil recovery may be further reduced if CO_2 is injected in reservoirs with considerable permeability variations (Enick et al., 2012; Lee & Kam, 2013).

Injection of CO_2 as foam can mitigate problems associated with unfavorable mobility ratios by reducing the CO_2 mobility, and thus increase the macroscopic sweep efficiency (Talebian et al., 2014). Foam enhances oil recovery compared to gas injection by stabilizing the displacement front due to improved gas viscosity, by blocking high-permeable layers and by reducing capillary forces as IFT is reduced by the foaming agent (discussed in Chapter 5) (Farajzadeh et al., 2012). An illustration of the different displacement fronts obtained during gas flooding and injection of foam is given in Figure 4.1. The sections below will be discussed in terms of CO_2 acting as the injected gaseous foam phase, as all injections conducted in this thesis is performed with CO_2-foam.

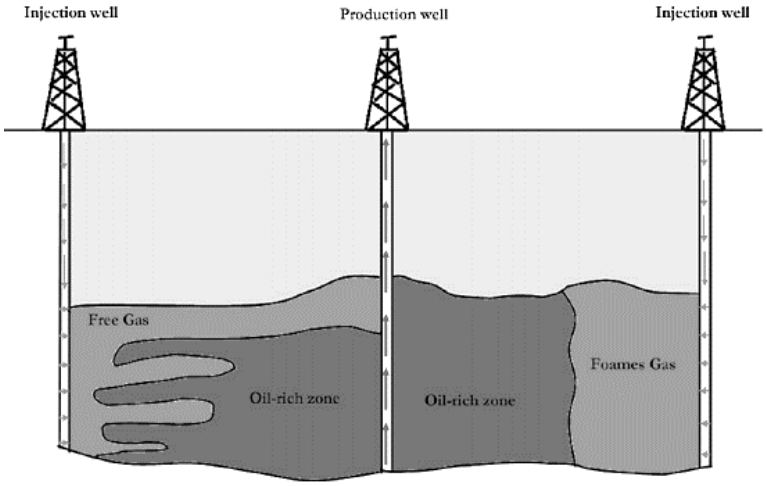

Figure 4.1 – Illustration of gas flooding (left) and foam flooding (right), showing how the gas mobility reduction in foam flooding generates a more favorable displacement (Farajzadeh et al., 2010).

4.1 Foam Characteristics

Foam is defined as a colloidal dispersion where discontinuous or continuous gas is dispersed in a continuous liquid phase (Prud'homme & Khan, 1996). The liquid phase is generally water or brine. Figure 4.2 visualizes a two-dimensional intersection of a generalized foam system, where the magnified section displays different foam structures. The gas phase is separated by a thin, continuous film termed lamellae, whereas a connection of three lamella is referred to as a Plateau border (Schramm & Wassmuth, 1994). Schramm (2014) defines foam as gas dispersed in a liquid, whereas liquid dispersed in liquid is termed an emulsion. It should be mentioned that even though CO_2 is injected as a supercritical phase for all experiments conducted in this thesis, co-injection of CO_2 and brine is characterized as foam throughout the thesis.

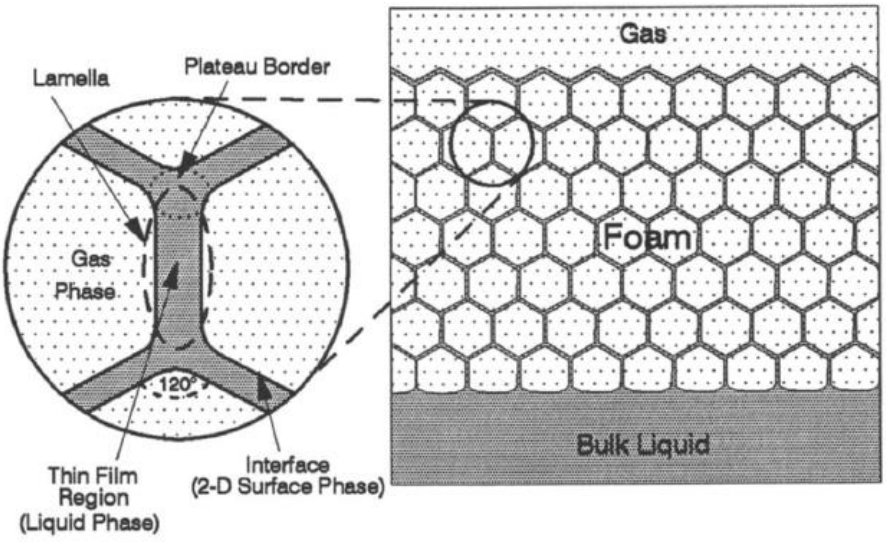

Figure 4.2 – A two-dimensional illustration of a generalized foam system, where the magnified section show the different foam structures (Schramm & Wassmuth, 1994).

A foam displacement requires increased energy beyond water and gas alone to stabilize foam structures, and a foaming agent must therefore be included to achieve foam stability (Skjæveland & Kleppe, 1992). The primary purpose of adding a foaming agent is to reduce the surface tension between the dispersed phase and the dispersion medium, resulting in an increased interfacial area and ultimately improving the generation, stability and lifetime of the foam. Surfactants are widely used as foaming agents, but macromolecules and finely divided solids like nanoparticles may also stabilize foam (Schramm & Wassmuth, 1994). The following chapters describing flow behavior is based on literature mainly focusing on surfactant-stabilized foam. This experimental thesis is investigating foam stabilized by surfactants and/or nanoparticles, and the use of surfactants and nanoparticles as foaming agents is presented in Chapter 5.1 and 5.2, respectively.

4.2 Foam Generation in Porous Media

Stable foams are generated by mixing of gas, liquid and a foaming agent, either as a co-injection of gas and liquid containing foaming agent, or as a cyclic injection with alternating injections of gas and liquid with foaming agent (referred to as surfactant alternating gas (SAG) for surfactant-stabilized foam) (Farajzadeh et al., 2012). In porous media, foam is generated in liquid-filled pores if the generation rate of bubbles exceeds the drainage rate. The generation rate depends on pore sizes and complexity and is roughly proportional to the injection rate (Heller, 1994). Foam generation mechanisms determine foam texture (bubble size and bubble size distribution), which influences both flow properties and apparent viscosity of the injected foam (Farajzadeh et al., 2012). Foam apparent viscosity is discussed in section 4.4. The generation of foam in porous media is primarily caused by the mechanism of *leave-behind*, *snap-off* or *lamella-division* (Ransohoff & Radke, 1988), which all are illustrated in Figure 4.3.

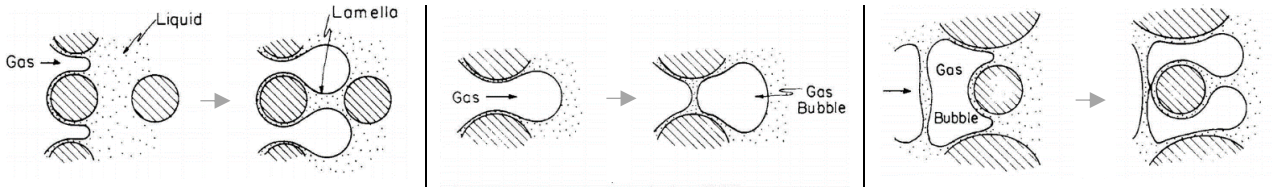

(a) Leave-behind (b) Snap-off (c) Lamalla-division

Figure 4.3 – Illustration of the different mechanisms for foam generation in porous media. Modified from (Ransohoff & Radke, 1988).

The mechanism of leave-behind (Figure 4.3 (a)) is considered a local fingering of gas in adjacent pores initially filled with liquid. Leave-behind does not generate separate gas bubbles, but establish a continuous gas flow path. Snap-off (Figure 4.3 (b)) is a mechanical process, controlled by liquid saturation, pore geometry of the porous media and rock wettability, and is the dominant foam-generation mechanism. Gas fingering through a narrow pore space causes liquid accumulation in the pore throat, resulting in separation of gas bubbles and lamella generation. Figure 4.3 (c) illustrates the mechanism of lamella-division, a dual gas fingering process of previously generated gas bubbles in adjacent pores initially filled with liquid. Lamella division primarily occurs when generated gas bubbles exceed the pore size (Ransohoff & Radke, 1988; Skarestad & Skauge, 2012). Weak foam is produced during leave-behind, as the mechanism maintains a continuous gas flow, inadequate to effectively reduce the gas mobility. Due to the creation of separate gas bubbles and reduced gas permeability, both snap-off and lamella-division leads to strong foam. However, a strong foam is usually obtained with a combination of the three mechanisms (Dicksen et al., 2002)

4.3 Foam Stability

Foams are not permanently stable and will collapse with time. Foam stability is therefore not defining the thermodynamical stability of foam, but rather mean relative stability in kinetic sense. The ability to maintain a stable foam is essentially controlled by lamella stability, and a uniform bubble distribution will generate stronger lamella, and consequently more stable foam (Sheng, 2013). The constant change in foam stability is driven by foam coarsening as diffusion causes gas transportation through the liquid lamella (Weaire, 1999). Both foam film properties and petrophysical properties determine the degree of foam stability (Farajzadeh et al., 2012), some of which are presented below.

The Effect of Temperature and Pressure

Reservoir conditions generally imply elevated temperatures and pressure, where both properties influence foam stability. Increased temperature has a detrimental effect on foam stability. Firstly, increased temperature increases the aqueous solubility of the foaming agent, making less of the foaming agent available for IFT reduction between the liquid and gas. Secondly, elevated temperatures increase the rate of liquid film drainage (Sheng, 2013). The third effect of increased temperature is reduction of the critical salt concentration (CSC), where aggregation and sedimentation of particles occurs. The result of reduced CSC will especially influence foam stability if nanoparticles are used as foaming agents, reducing their ability to stabilize the foam (Metin et al., 2011). Increased pressure will, on the other hand, stabilize foams by decreasing the bubble size, resulting in retardation of liquid drainage due to thinner and larger liquid films. However, if the pressure exceeds a specific value, the high pressure applies excessive stress on the gas bubbles, causing them to rapture (Sheng, 2013).

The Effect of Permeability

All reservoirs are to some extent heterogeneous, which often includes layers of variable permeability. Foam has lower mobility in layers of high permeability (low capillary pressure) compared to low-permeability layers (high capillary pressure) (Farajzadeh et al., 2012). Foam injection into a heterogeneous reservoir with permeability variations will therefore generate stronger foam in the high-permeability regions, forcing fluid movement into regions of lower permeability (Khatib et al., 1988). This blocking of high-permeable layers is a result of reduced gas mobility, ultimately enabling foam to smooth out reservoir heterogeneities (Skjæveland & Kleppe, 1992).

The Effect of Oil

The application of foam for EOR purpose is profoundly influenced by interactions between the foam and the reservoir oil, as presence of oil has a detrimental effect on foam films. Several core flood experiments show that foam generation does not occur if the oil saturation is higher than a specific maximum value, a critical foaming oil saturation (Friedmann & Jensen, 1986; Hudgins & Chung, 1990). Injected oil spreads on the gas/liquid interface, causing it to break (Sheng, 2013). Oil spreads on both sides of the foam film, displacing the original liquid film, and as the oil film is unstable, the gas bubble coalesces (Ross & McBain, 1944).

Several mechanisms explain the detrimental foam effect of oil. In addition to the spontaneously spreading on foam lamella, oil may also spontaneously emulsify and generate bubble rupture. Emulsification, described by absorption or adsorption of the foaming agent by the oil, causes film drainage and weaken the ability to reduce IFT between the gas and liquid. Foaming agent from the oil may re-adsorb on the foam lamella, which reduces the foam stability. Wettability alteration may also occur due to oil adsorption at the porous medium, which hinders foam generation and regeneration. Light oils (short chain hydrocarbons) show a tendency to destabilize foam to a higher degree than heavier oil (long chain hydrocarbons) (Schramm, 1994).

4.4 Foam Flow Behavior

An understanding of foam flow behavior is required to evaluate the applicability of using foam for mobility control of CO_2. The behavior of foam can be described by the study of different properties and mathematical relations (Chang & Grigg, 1999), where relevant equations for this experimental thesis are presented below.

Foam Quality

Foam flow behavior is highly influenced by foam quality, described as the ratio between gas flow rate and the sum of the gas and liquid flow rates:

$$f_g = \frac{q_g}{q_g + q_{liq}} \tag{4.1}$$

where f_g is the foam quality, and q_g and q_{liq} is the gas flow rate and liquid flow rate, respectively (Farajzadeh et al., 2012). Foam quality is essentially an expression of the gas fraction of the foam, typically ranging from f_g= 0.75-0.90 (Farajzadeh et al., 2012; Sheng, 2013). Increasing gas fractions will reduce foam mobility, but only up to a critical foam-quality stability limit. Foam mobility will not be effectively reduced if the gas fraction exceeds this stability limit. (Derikvand & Riazi, 2016). The foam quality is also linked to gas bubble size; when the bubbles increase in size, the foam stability is reduced, and the foam quality is consequently reduced (Sheng, 2013). The optimal gas fraction (highest achieved apparent viscosity) during CO_2-foam injections will be denoted f_g^* throughout this thesis.

Apparent Viscosity

The unfavorable mobility ratio during CO_2 injection for oil recovery is mainly a result of low gas viscosity. It is therefore desirable to increase the effective CO_2 viscosity to obtain an efficient displacement process. The apparent viscosity of foam is defined as the apparent viscosity of gas in the presence of foam (Svorstol et al., 1996) and a combination of gas permeability and Darcy's law, defined as:

$$\mu_{app} = \frac{KA\Delta P}{q_g L} \tag{4.2}$$

where K is the absolute permeability of the porous media, A is the cross-sectional area, ΔP is the differential pressure drop across the capillary, q_g is the volumetric foam rate and L is the capillary length (Svorstol et al., 1996). The apparent viscosity is a function of flow rate, pressure drop, bubble size and bubble distribution (Chambers, 1994; Hirasaki & Lawson, 1985).

Mobility Reduction Factor

The foam efficiency, which is its ability to reduce gas mobility compared to pure gas flooding, can be evaluated by the mobility reduction factor (MRF). MRF is defined as (Svorstol et al., 1996):

$$MRF = \frac{\mu_{app}\ (foam)}{\mu_{app}\ (gas\ before\ foam)} \tag{4.3}$$

where μ_{app} is the apparent viscosity shown in Eq. 4.2. Low values of MRF indicate weak foam, where the gas has continuous flow through the porous media. Consequently, high values of MRF are calculated for strong foams (Zhang et al., 2009). Both apparent viscosity and MRF are calculated as average values over periods with steady state pressure drop (Svorstol et al., 1996).

5. Foaming Agents: Surfactants and Nanoparticles

It is possible to generate foams purely with brine and gas, but such foams rapidly break. A foaming agent is therefore needed, not only to generate but also stabilize the foam (Sheng, 2013). Surfactants are widely used as foaming agents, but macromolecules and finely divided solids like nanoparticles may also stabilize foam (Schramm, 1994). Surfactant-stabilized foam successfully reduces CO_2 mobility, but the effectiveness of surfactants is limited at high temperatures and when dispersed in brine with high salinity. In the search for an alternative and more robust foaming agent, nanoparticles have gained interest in recent years (Bennetzen & Mogensen, 2014; Grigg & Bai, 2005). This chapter discusses the use of surfactants and nanoparticles as foaming agents, as both foaming agents were to stabilize CO_2-foam in this experimental thesis. Nanoparticles retention is also studied, with and without presence of surfactants. Finally, emulsions of foaming agents and oil are presented, as fractions of fluid production during CO_2 EOR injections were measured as emulsions.

5.1 Surfactants as Foaming Agent

Surfactants, or surface-active agents, are mainly injected in reservoirs to reduce the IFT between brine and oil or to generate and stabilize foam. (Sheng, 2013). Surfactants consist of a hydrophilic and a hydrophobic part and are classified into four groups: anionics, cationics, nonionics and amphoterics. When dissolved in water, anionics have a negative charge, cationics have a positive, nonionics are not charged, and amphoterics can have both a negative and a positive charge. For sandstone reservoirs, having a negatively charged surface, anionics are the preferred choice of surfactant. As anionics are negatively charged, the repulsive effect between the surfactant and the rock surface minimizes loss of surfactant to adsorption. Similarly, cationic surfactants are preferred for the positively charged surface area of carbonate reservoirs (see Table 5.1) (Lake et al., 2014). A nonionic and a switchable (amphoteric) cationic surfactant have been used in the experimental work of this thesis.

Table 5.1 – Surfactant type and charge with preferred reservoir type

Surfactant type	Surfactant charge	Preferred reservoir type
Anionic	Negative	Sandstone
Cationic	Positive	Carbonates
Nonionic	No charge	Sandstone / Carbonates
Amphoteric	Negative or positive	Sandstone / Carbonates

Surfactants that reduce IFT do not necessarily perform well as a foaming agent. Foaming ability, thermal stability, salinity resistance, compatibility with formation fluids, performance in the presence of oil, and adsorption must be evaluated in addition of IFT reduction before selecting surfactants for foam stabilization (Sheng, 2013). Retention of surfactants is a significant drawdown during EOR, as it reduces the amount of surfactant available to foam generation and IFT reduction. Surfactant retention is a combination of adsorption, precipitation, ion exchange and phase trapping, and the retention is intensified with increased temperature and salinity (Skarestad & Skauge, 2012; Ziegler & Handy, 1981). A profound reduction in surfactant-stabilized foam stability can therefore be observed at harsh reservoir conditions with elevated temperatures and high-salinity brines. A constant need for foam regeneration due to high retention also leads to increased material cost (Guo & Aryana, 2016).

5.2 Nanoparticles as Foaming Agent

Surfactant-stabilized CO_2-foam have successfully been tested at both lab scale and field scale through pilot tests. However, an interest in nanoparticle-stabilized foam is emerging due to problems occurring when surfactant solutions are flowing in porous media over long distances, such as adsorption loss and chemical instability. Instability problems linked to surfactants are generally intensified at harsh reservoir conditions, i.e. high temperatures and pressure (Bennetzen & Mogensen, 2014; Enick et al., 2011). As a result of high adhesion energy in solid nanoparticles, stable foam can be generated due to strong adsorption to the liquid interface. Adsorbed nanoparticles at the liquid interface do not desorb easily, and are practically irreversibly adsorbed (Binks & Horozov, 2005). On the contrary, surfactant molecules adsorb and desorb reversibly due to weak CO_2 solvation capability, profoundly reducing the ability for long time stability (Guo & Aryana, 2016).

Promising results are observed from using nanoparticles for foam mobility control of CO_2 on lab scale, but the practical use in pilot test has yet to be adequately assessed (Talebian et al., 2013). Nanoparticles can contribute to increasing oil recovery by several mechanisms, such as wettability alteration, decreased oil viscosity or increased viscosity of the displacing fluid (Ogolo et al., 2012). This experimental thesis examines the use of nanoparticles for the purpose of foam stability, and this chapter will therefore only present foam stability characteristics of nanoparticles.

Nanoparticle Properties

Nanoparticles are small particles with diameters ranging from 1-100 nm, composed of a particle core and a chemically modified surface consisting of grafted of covalently linked surface molecules (Bennetzen & Mogensen, 2014). Oxides of Aluminum, Zinc, Magnesium, Iron, Zirconium, Nickel, Tin and Silicon are examples of selected types of nanoparticles tested for EOR screening, where oxides of Aluminum and Silicone have shown potential to increase oil recovery (Ogolo et al., 2012). The most common used nanoparticles are spherical fumed silica particles, with diameters in the range of tens of nanometers (Zhang et al., 2010). All experiments involving nanoparticles conducted in this thesis are performed with silica nanoparticles (Silica oxides) dispersed in brine containing both monovalent and divalent ions.

Nanoparticle Retention

Retention of nanoparticles in a porous media is considered a complex process due to reservoir heterogeneity. Particle flow paths are driven by several factors which ultimately affects retention, such as particle shape and surface properties, morphology of the medium, chemistry of the carrying fluids and a variation of forces between the particles and the porous media (Gao, 2007). Retention of nanoparticles is both determined by the interactions between nanoparticles and liquids (at the interface between brine and oil) and between nanoparticles and the mineral surface (Metin, 2012). As for surfactants, nanoparticle retention may result in reduced foamability due to loss of particles at the pore wall. Retention can impact rock properties such as porosity, permeability and wettability, and can negatively affect fluid injectivity by reducing the flow capacity near the injection well due to particle accumulation (Rognmo et al., 2017).

Retention of nanoparticles in a porous media is induced by three different mechanisms, illustrated in Figure 5.1. The first mechanism is adsorption of nanoparticles caused by Brownian motion, and by electrostatic interactions between the migrating particles and the pore surface. The second is size exclusion, which occurs when the migrating particle size exceeds the size of the pores. Sedimentation or gravity settling due to density differences between moving particles and the liquid they are dispersed in is the final mechanism causing retention (Gao, 2007). Skauge et al. (2010) have shown that silica nanoparticles are too small for pore blocking and that particles propagate easily through sandstone cores, resulting in low retention. Presence of CO_2 during co-injections which are performed in the experimental work of this thesis will result in lower retention as nanoparticles adhere to the CO_2-liquid interface (Prigiobbe et al., 2016).

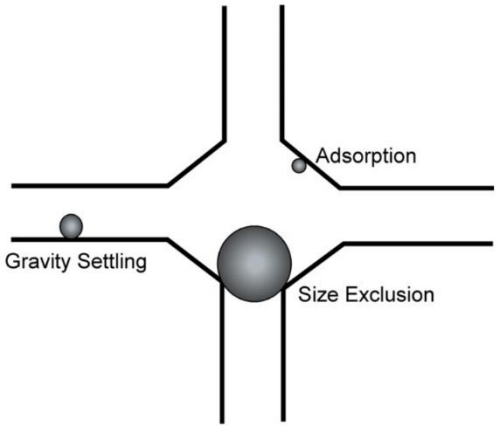

Figure 5.1 – Schematic illustration of mechanisms of particle retention: gravity settling, size exclusion and adsorption (Gao, 2007).

Aggregation of Nanoparticles

When nanoparticles are dispersed in brine, the repulsive forces between the particles are greater than the attractive forces. If the attractive forces exceed the repulsive, the nanoparticles will aggregate (Kovalchuk & Starov, 2012). Aggregation occurs when dispersed colloidal particles are clumping or sticking together, and the aggregated particles may be loosely tied together and re-dispersed when shaken (agglomerates), or be cemented together (aggregates) (Pratsinis, 1998).

The stability of nanoparticle dispersion in porous media is dependent on factors such as temperature, pH and ion concentration in the liquid phase. Aggregation is a function of a diffuse electrical layer surrounding the nanoparticles, where the layer thickness is determined by electrolytes present in the brine solution. High salinity levels will therefore advocate aggregation by increasing the electric layer thickness. Increased temperature has a detrimental effect on the nanoparticle stability by reducing the CSC, and by increasing the average kinetic energy. This provokes particle collision, and ultimately cause aggregation. (Azadgoleh et al., 2014). Increased pH values will also induce nanoparticle aggregation. For silica nanoparticles, an increase in pH results in dissociation of negatively charged functional groups (SiO^-), which attract more counter-ions near the particle surface (Mei et al., 2016).

Silica Nanoparticles for EOR

The most common used nanoparticles, which also have shown potential to increase oil recovery, are silica nanoparticles (Ogolo et al., 2012). Investigation of silica nanoparticles for stabilizing CO_2 in water was first described by Dickson et al. in 2004. This work was not explicitly described for EOR purpose, but several experimental studies have investigated the feasibility of using silica nanoparticles as foam stabilizers in previous years (Espinoza et al., 2010; Rognmo et al., 2018b; Sofla et al., 2018; Worthen et al., 2013). Low fabrication cost, ready availability and the ability for surface modification make silica nanoparticles good candidates for foam EOR purpose. Surface modification allows for hydrophilicity control, which increases the nanoparticle tolerance for elevated salt concentrations by increasing the critical salt concentration (CSC, see chapter 4.3). The CSC is especially improved for the divalent ions Ca^{2+} and Mg^{2+} (Metin, 2012). Another reason for the arising interest in using silica nanoparticles as foaming agents is their natural occurrence in reservoirs, posing no harm to the environment (Skauge et al., 2010).

5.3 Emulsions of Foaming Agent and Oil

Understanding emulsion generation between oil and foaming agents is of importance for this thesis, as emulsions was produced during the majority of CO_2 EOR injections. Listed below are emulsion characteristics which will be of importance for further discussion.

Emulsion Definition

Emulsions are colloidal dispersions where a liquid is dispersed in a continuous liquid phase of a different composition, where the two fluids are immiscible. As for foams, emulsions are not thermodynamically stable, but possess to some extent kinetic stability. Water (brine) and oil are liquid phases for petroleum emulsions, where the type of emulsion formed is distinguished by which liquid that forms the continuous phase. Oil-in-water (O/W) emulsions are formed when oil droplets are dispersed in water, and water-in-oil (W/O) emulsions are consequently formed if water droplets are dispersed in oil. As formation of emulsions does not occur spontaneously, an emulsifying agent is required for IFT reduction between the two liquids (Schramm, 1992). Both nanoparticles and surfactants can act as an emulsifying agent (Bennetzen & Mogensen, 2014), and emulsions are generally easy to distinguish from pure oil and water as they often appear with “milky” opaqueness. Texture evaluation, mixing, dyeing and fluorescence methods are some techniques which are used for determining the physical nature of emulsions (Schramm, 1992).

Emulsion Flow in Porous Media

Rheology properties of emulsions are of great importance, as emulsions often are associated with high viscosity values. The flow of a high-viscous fluid in porous media can be desirable or undesirable, depending on whether flow resistance is the aim of the injection process. (Schramm, 1992). For heterogeneous reservoirs, it is often desirable to restrict fluid flow through high-permeable layers, directing the fluid to low-permeable layers. Emulsion generation can therefore positively influence oil production by blocking high permeable layers, as seen in Figure 5.2. The figure illustrates the blockage mechanism of oil droplets in O/W emulsions with sizes exceeding the pore throat size (McAuliffe, 1973). The blockage effect reduces the fluid permeability and consequently increases the differential pressure (Schramm, 1992).

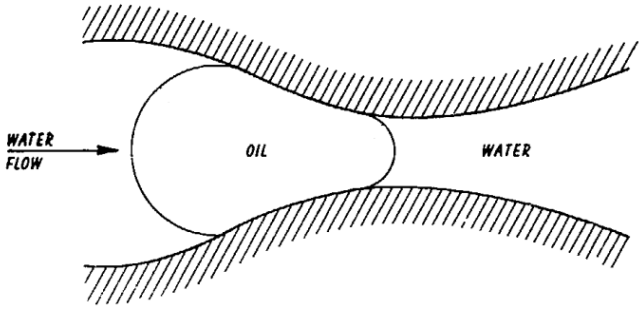

Figure 5.2 – An oil droplet entering a pore constriction, illustrating the mechanism of emulsion blocking (McAuliffe, 1973).

Similar to foams, emulsion flow in a porous media is dependent of a vast number of variables, such as emulsion stability and quality, droplet size distribution, oil viscosity and interfacial properties between water and oil. However, a high degree of complexity is associated with emulsion flow in porous media, as both the fluid composition and porous media is complex, in addition to the flowing fluid lacking thermodynamically stability (Kokal et al., 1992).

6. Carbon Utilization and Storage

Global warming and recent climate changes have intensified the focus on reducing greenhouse gas (GHG) emissions. Anthropogenic CO_2, being the main contributor, accounted for 83% of the total GHG emissions in the US in 2009 (Lee & Kam, 2013). Carbon dioxide emissions can be reduced by implementation of carbon capture and storage (CCS), which involves capture and transport of anthropogenic CO_2, and ultimately long-term storage of CO_2 for sequestration (Hasan et al., 2015). Injection of CO_2 into subsurface formations began already back in the early 1970s. The aim was to increase oil recovery, and there was no focus on the environmental benefit of CO_2 storage. The first pure CO_2 storage project started up in 1996, with the Sleipner project on the Norwegian Continental Shelf (NCS), which was a pioneer for future CCS projects (Nordbotten & Celia, 2012). Further development of CCS is CCUS, where the "U" implements utilization of anthropogenic captured CO_2. Utilization of CO_2 can be realized with CO_2 EOR, by replacing the naturally occurring CO_2 used for injection with anthropogenic sources of CO_2. CCUS is therefore a process with both environmental and economic benefits, as captured carbon is stored simultaneously as oil is recovered (Hasan et al., 2015).

Utilization of CO_2 has been performed as foam injection in the experimental work of this thesis. The use of CO_2-foam for EOR has already been discussed in chapter 4. A quantitative investigation of carbon storage potential has been conducted in both sandstone and limestone, with the aim of examining the possibility of carbon neutral or carbon negative oil production. These terms will be presented in chapter 6.2. The carbon capture aspect of CCUS is beyond the scope of this thesis, and will therefore not be further discussed.

6.1 CO_2 Storage Mechanisms

A combination of both physical and geochemical mechanisms of CO_2 trapping determine the effectiveness of geological storage. Four main mechanisms of CO_2 trapping exists: stratigraphic and structural trapping, residual CO_2 trapping, solubility trapping and mineral trapping. Stratigraphic and structural trapping is controlled by the nature of the geological storage site. Due to buoyancy, injected CO_2 rises to the top of the formation. Structural or stratigraphic arrangements, such as faults or anticlines may act as a seal for fluid flow, resulting in stored CO_2. Residual trapping is a rapid process compared with the other storage mechanisms. Injected CO_2 displaces the resident fluid, and as the carbon dioxide moves through the formation, brine traps CO_2 in the pore space as residual droplets. Solubility trapping is a considerably slower process and is the primary mechanism for long-term sequestration of CO_2. CO_2 dissolves in the formation brine, and the increased solution density cause settlement of brine and dissolved CO_2 for sequestration. As carbon dioxide dissolves in brine, the solution pH is lowered. The acidified solution may react with the porous media and induce mineral trapping as it encounters chemical complexes. The mineral trapping mechanism is a slow process, but it is a permanent sequestration process, as it ultimately results in chemical precipitation of solid carbonate minerals (Abidoye et al., 2015; Benson et al., 2005)

6.2 Carbon Neutral and Carbon Negative Oil Production

Saline aquifers and depleted reservoir fields are generally candidates for CO_2 storage sites in a CCS process, but such storage of CO_2 has no other function than to reduce CO_2 emission. For CCUS processes, reservoirs can act as storage sites simultaneously as oil is recovered. As previously mentioned, this can be an environmental benefit as anthropogenic CO_2 is sequestered (Hasan et al., 2015). It is however of great importance to account for the hydrocarbons that are produced from the reservoir during injection of CO_2, as combustion of produced hydrocarbons produces CO_2. For CO_2-foam EOR experiments conducted in this thesis, n-Decane is used as the oleic phase, consisting of 10 carbon atoms and 22 hydrogen atoms ($C_{12}H_{22}$) (Smallwood, 1996). In the presence of sufficient oxygen, combustion of n-Decane generates CO_2, water and heat. The combustion reaction for n-Decane is expressed as (Hucknall, 1985):

$$2C_{10}H_{22} + 31O_2 \rightarrow 20CO_2 + 22H_2O + \text{Heat} \tag{6.1}$$

The reaction in Eq. 6.1 evidently reveals that CO_2 containing 10 carbon atoms are generated by the combustion of 1 molecule of n-Decane.

For this thesis, carbon neutral and carbon negative oil production will be defined as a net total of carbon stored equal or greater than the net total of carbon produced, respectively. As mentioned in chapter 3.1, the physical properties of CO_2 are highly dependent of pressure and temperature. Consequently, the amount of carbon stored in a reservoir is a function of the reservoir conditions.

Part II – Experimental Procedures

7. Experimental Procedures

This chapter presents fluids, rock materials, experimental preparations and procedures used in the experimental work. As the main objective of this thesis was to investigate the separate and combined use of nanoparticles and surfactants as foaming agents, a comprehensive study was conducted under various experimental conditions. In addition to fluid injections in porous media to evaluate the performance of nanoparticles and surfactants as foam agents, temperature stability tests were executed on samples of nanoparticles and surfactants dispersed in brine for qualitative investigation of the interaction between the foaming agents. Bulk foam stability tests were conducted at ambient conditions to evaluate foam generation and coalescence with and without presence of oil.

For experiments conducted in porous media, nanoparticle retention studies were conducted for both limestone and sandstone cores. Foam experiments in core samples was generated by co-injecting supercritical CO_2 and foaming agent dispersed in brine. This includes foam scans, tertiary CO_2-foam EOR injections and foam screenings. The ability of foaming agents to generate and stabilize CO_2-foam was quantitatively analyzed by studying oil recovery efficiency, pressure gradients and foam stability in the presence of oil. A list of all experiments is shown in Table 7.1 All experiments were performed at the Department of Physics and Technology, University of Bergen, while concentration of nanoparticles and surfactant in effluent samples for retention studies were measured by AkzoNobel in Bohus, Sweden.

Table 7.1 - Experimental overview

Experiment	Saturation fluids	Injection fluids	Experimental conditions (*)	Number of experiments
Long term foam stability test	-	NPA + Surf	LT-MT/LP	15
Bulk foam stability test	-	NPA + Surf + n-Decane	LT/LP	10
Retention study	Brine	NPA	HT/LP	2
	Brine	NPA	HT/LP	3
	Brine	Surf	MT/HP	1
	Brine	NPA + Surf	MT/HP	2
Foam scan	Brine	CO_2 + Brine	MT/HP	1
	Brine	CO_2 + NPA	HT/MP	1
	Brine	CO_2 + NPA + Surf	MT/HP	3
EOR	Brine, n-Decane	CO_2 + Brine	MT/HP	1
	Brine, n-Decane	CO_2 + NPA	MT/HP	1
	Brine, n-Decane	CO_2 + Surf	MT/HP	2
	Brine, n-Decane	CO_2 + NPA + Surf	MT/HP	5
Foam screening	Brine, n-Decane	CO_2 + NPA + Surf + n-Decane	MT/HP	3

* LT: Low temperature (20°C) MT: Medium temperature (40-60°C) HT: High temperature (120°C)
LP: Low pressure (1-3bar) MP: Medium pressure (80 bar) HP: High pressure (110-175 bar)

7.1 Fluids

Table 7.2 gives an overview of properties and characteristics of fluids used at experimental conditions. Limestone cores were saturated with Brine A or B, whereas sandstone cores were saturated with Brine C. Primary drainage with oil flooding prior to CO_2 EOR injections was conducted using filtered n-Decane mineral oil.

Both nanoparticles and surfactants were used as foaming agents in this experimental thesis. The nanofluid used during all experiments, referred to as Nanoparticle A (NPA), is a silane-modified colloidal silica dispersed in Ethanol (Levasil CC301) from AkzoNobel. Two different surfactants were used; a nonionic, alpha olefin sulfonate surfactant from Huntsman (SURFONIC L24-22), and a bis(2-hydroxyethyl)cocoalkylamine surfactant from AkzoNobel (Ethomeen C/12). The surfactants are referred to as SurfA and SurfB, respectively. Both NPA and the surfactants were dispersed in Brine A, B or C, depending on core type used in the experiment. Foaming agent was dispersed in Brine C for experiments conducted in sandstone cores to compare results with previously conducted nanoparticle injections in sandstone by the research department at the University of Bergen. Foaming agent was dispersed in Brine B for preliminary experiments conducted in limestone, while the majority of experiments conducted in limestone were performed with foaming agent dispersed in Brine A for comparison with previous experiments of surfactant-stabilized foam in limestone, and to study the effect of divalent ions. The NPA concentration for all experiments was 1500 mPPM (concentration in part per million by mass of foaming agent), all will be referred to as NPA without explicitly including its concentration. The surfactant concentration varied between 0.5 wt.% or 1 wt.%, and the surfactant concentration will therefore be explicitly expressed for each experiment.

The tertiary amine surfactant (SurfB) has the ability to switch from a nonionic to a cationic surfactant, depending on solution pH. The amphoteric surfactant is a nonionic surfactant in its original form, with pH values ranging from 9-10 with 1 wt.% surfactant dissolved in water. As the pH is reduced, protonation of the tertiary amine causes the surfactant to switch to a cationic surfactant. As the surfactant does not dissolve in brine in its nonionic form, the pH was reduced to 3-4 by adding hydrochloric acid to the surfactant-brine solution.

Table 7.2 – Fluid properties

Fluid	Composition	Viscosity [cP]	Density [g/cm^3]	Experimental Conditions
Brine A	22.797 g/L NaCl 0.458 g/L KCl 2.760 g/L $MgCl_2$ $6H_2O$ 5.825 g/L $CaCl_2$ $2H_2O$	1.077(1)	1.025(1)	20°C
		0.710(1)	1.019(1)	40°C
		0.509(1)	1.009(1)	60°C
Brine B	Distilled water w/ 5 wt.% NaCl	1.010	1.030	20°C
Brine C	Distilled water w/ 2 wt.% NaCl	1.010	1.030	20°C
NPA	Brine A/B/C w/ 1500 ppm NPA	NM	NM	40°C /120 bar /140 bar /175 bar 60°C /110 bar 120°C /3 bar /80 bar
NPA	Brine C w/ 500-5000 ppm NPA	NM	NM	20°C /1 bar 40°C /1 bar 60°C /1 bar 80°C /1 bar
SurfA	Brine A/B/C w/ 0,5/1 wt.% L24-22	NM	NM	40°C /120 bar /140 bar /175 bar 60°C /110 bar
SurfA	Brine C w/ 1 wt.% L24-22	NM	NM	20°C /1 bar 40°C /1 bar 60°C /1 bar 80°C /1 bar
SurfB	Brine C w/ 0,5/1 wt.% Ethomeen C/12	NM	NM	40°C /175 bar
n-Decane	$C_{10}H_{22}$	0.792(2) 0.809(2) 0.840(2) 0.616(2)	0.725(2) 0.726(2) 0.729(2) 0.709(2)	40°C /120 bar 40°C /140 bar 40°C /175 bar 60°C /110 bar
CO_2	> 9.999% CO_2	0.059(2) 0.065(2) 0.073(2) 0.027(2) 0.022(2)	0.718(2) 0.763(2) 0.813(2) 0.658(2) 0.128(2)	40°C /120 bar (Supercritical) 40°C /140 bar (Supercritical) 40°C /175 bar (Supercritical) 60°C /110 bar (Supercritical) 120°C /80 bar (Supercritical)

NM: Not Measured
1) Values retrieved from (El-Dessouky, 2002)
2) Values obtained from (Lemmon et al., 2018)

7.2 Rock Material

7.2.1 Bentheimer Sandstone

Three experiments were performed on 2” diameter cylindrical outcrop core plugs of Bentheimer sandstone from Germany. The core plugs are composed of 95% quartz, 3% clays and less than 2% feldspar (Dautriat et al., 2007). The two core plug samples used in this experimental thesis have a measured permeability of 1650 mD and 1863 mD, and a porosity of 23%. The cores are considered homogeneous and assumed strongly water-wet.

Figure 7.1 – 2’’ homogeneous Bentheimer sandstone core plugs

7.2.2 Edwards Limestone

The majority of core experiments were performed on 2’’ diameter cylindrical Edwards limestone core plugs from near Garden City, Texas. Edwards limestone consists of calcite minerals and is considered to be a highly heterogeneous rock, where the pore space is made up of mainly moldic pores and interparticle porosity (Fernø et al., 2015a). Measured porosities for core plugs used in this experimental thesis ranges from 22-28% and the absolute permeability ranges from 14-68 mD. The outcrop core plugs are assumed to be strongly water-wet based on previous experiments (Fernø et al., 2010).

Figure 7.2 – 2’’ diameter Edwards limestone core plugs displaying heterogeneity

7.3 Core Preparations and Core Analysis

A total of 2 sandstone cores and 17 limestone cores were used in this experimental work, all prepared equally prior to retention studies and CO_2-foam injections tests. After cut to lengths, the cores were gently rinsed with water and dried for at least 48 hours at 65°C. Core parameters such as length, diameter and matrix weight were measured before the cores were saturated with brine for porosity and permeability determination. The experimental procedure for porosity and permeability measurements is described in detail in Appendix A. Core parameters for each core are listed in Table 8.1 in Chapter 8. Six limestone cores were scanned with computerized tomography (CT) at Haukeland University Hospital before and after CO_2-foam injections to qualitatively and quantitatively study core plug dissolution as an effect of CO_2-injection.

7.4 Experimental Setup and Procedures

This section presents experimental preparations and procedures used in the experimental work. Static foaming agent stability tests were conducted to study interactions between nanoparticles and surfactants at elevated temperatures. Bulk foam tests were performed to investigate the feasibility of foam generation with the combined use of nanoparticles and surfactants at ambient conditions, and to study the effect of oil on foam stability. For experiments conducted in porous media, nanoparticle retention was studied to calculate the loss of foaming agent during injection, as loss of foaming reduces the economic feasibility of foam injection. Foam scans investigated foam behavior and optimal gas fraction for tertiary CO_2-foam EOR injections. Foam screenings were used to evaluate foam behavior using different foaming agents, with and without presence of oil.

7.4.1 Long-Term Foaming Agent Stability

Long-term stability of foaming agent dispersed in Brine C was studied at elevated temperatures (40°C, 60°C and 80°C) using 15 sealed glass bottles with NPA and/or SurfA for a range of pH and nanoparticle concentrations placed in a heating cabinet. The solutions were visually monitored for a total of 44 days.

Table 7.3 – Overview of glass bottle content

Glass bottle	Foaming agent	NPA concentration [mPPM]	Surfactant concentration [wt.%]	pH (± 0.3)
1	NPA	1500	-	6
2	NPA	1500	-	4
3	NPA	1500	-	7
4	SurfA	-	1	6
5	SurfA	-	1	4
6	SurfA	-	1	7
7	NPA + SurfA	1500	1	6
8	NPA + SurfA	1500	1	4
9	NPA + SurfA	1500	1	7
10	NPA + SurfA	500	1	6
11	NPA + SurfA	500	1	4
12	NPA + SurfA	500	1	7
13	NPA + SurfA	5000	1	6
14	NPA + SurfA	5000	1	4
15	NPA + SurfA	5000	1	7

7.4.2 Bulk Foam Coalescence Study

Bulk foam coalescence studies were conducted to determine the stability and half-decay time of foam stabilized by nanoparticles and/or surfactants with and without presence of oil at ambient conditions, using N_2 as the gaseous phase. The objective was to determine the feasibility of using a combination of nanoparticles and surfactants for foam generation and to study the effect of presence of oil. 1500 mPPM NPA and/or 0.5 wt.% SurfA or SurfB dispersed in Brine A were used as foaming agents. Brine A was used to implement the effect of divalent ions.

Experimental Setup and Equipment

The experimental setup used for determining bulk foam stability by quantifying bulk foam height as a function of time at ambient conditions is shown in Figure 7.3. The setup was originally built and tested by PhD candidate Zachary Paul Alcorn. The experimental setup consists of:

- EL-FLOW Mass Flow Controller to control N_2 flow
- Check valve to avoid back flow of fluids through the mass flow controller
- Graded glass cylinder with a porous frit
- POM end piece
- Vacuum grease and thread tape to avoid leakage
- N_2 tank to inject gas through mass flow controller
- Swagelok valves, fittings and plastic tubing
- Web camera for monitoring foam height
- Computer to control web camera

The graded glass cylinder had a length of 50 cm and an inner diameter of 2.04 cm. The porous frit located towards the bottom is a porous glass filter with pore sizes ranging from 40-100 µm used for gas sparging. An inlet end piece at the lower end enabled controlled injection of N_2 gas.

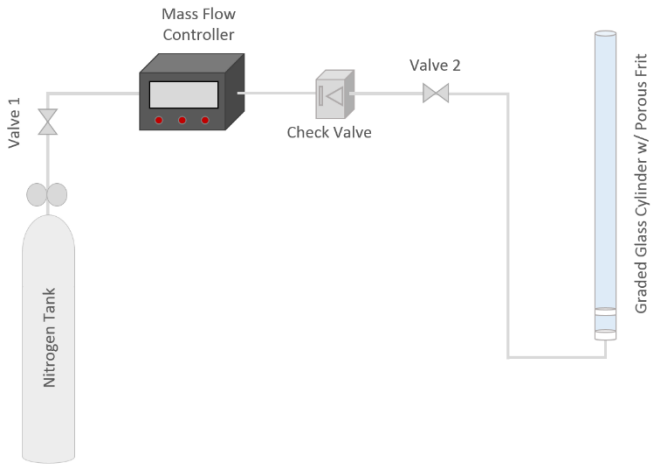

Figure 7.3 – Experimental setup for bulk foam coalescence test. A mass flow controller was used to inject 10 ml/min of N_2 through the porous for foam generation. The check valve avoided back flow of fluids through the mass flow controller.

Experimental Procedure

4 cm of foaming agent was gently poured into the glass cylinder. Valve 2 (see Figure 7.3) was closed, blocking the liquid from flowing downstream of the porous frit. The valve was then opened, and foam was generated by adjusting the mass flow controller to inject 10 ml/min of N_2 through the porous frit. When 30 cm of foam was reached, time was noted and valve 2 was closed. Foam decay height and increase in liquid height was recorded as a function of time to study the stability and half-decay time of the generated foam. For experiments investigating the influence of n-Decane, a 5% volume factor of oil relative to the foaming agent solution was added to the system. Oil was gently poured into the glass cylinder on top of the foaming agent prior to foaming.

7.4.3 CO_2-Foam Injection: Foam Scans in Porous Media

After determining the foam generation using nanoparticles, surfactants and combinations in bulk tests, foam stability in porous media was investigated using core plugs. Foam scans with co-injection of CO_2 and foaming agent were conducted to quantitatively measure foam strength by apparent foam viscosity as a function of gas fractions (foam quality scan), or as a function of injection rates (foam rate scan). 1500 mPPM NPA was injected separately or combined with 1wt. % SurfA or SurfB dispersed in Brine A to implement the effect of divalent ions. Foam scans were performed using Edwards limestone cores.

Experimental Setup and Equipment

The experimental foam scan setup is illustrated in Figure 7.4. The setup was built to perform foam scans and CO_2-foam EOR injections (section 7.4.4) at elevated temperatures and high pressures. Several changes and improvements were continuously implemented as a vital part of this thesis.

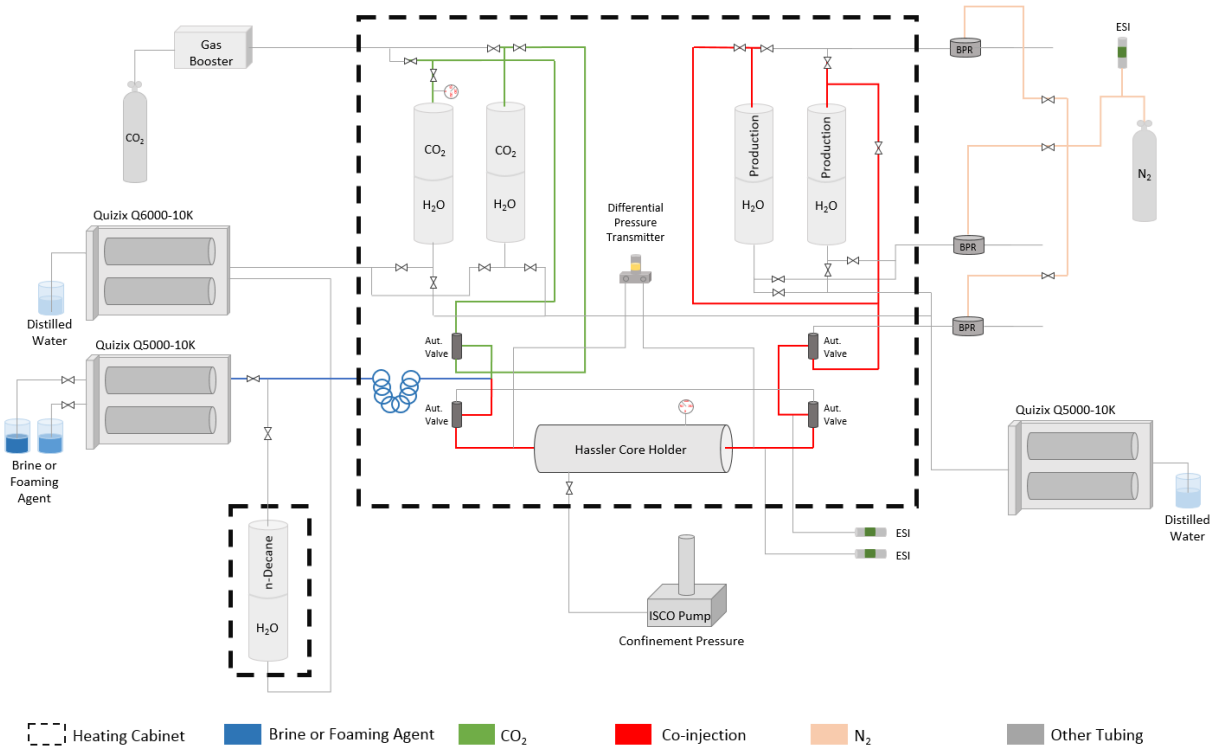

Figure 7.4 – Illustration of the experimental setup used for foam scan experiments with co-injection of CO_2 and foaming agent. Fluid flow is characterized by different colors, where a color description is given at the bottom of the figure. Tubing marked in grey as "other tubing" was used for refilling or discharging fluids to/from accumulators or for CO_2-foam EOR.

The experimental setup consists of:

- Heating Cabinet
- 2" diameter Hassler Core Holder
- ISCO Syringe Pump for confinement pressure
- Quizix Q5000-10Kpump for injection of brine, nanoparticles and/or surfactants
- Quizix Q6000-10K pump for injection of CO_2
- Quizix Q5000-10K pump for refilling CO_2 accumulators and empty production accumulators
- Stainless Steel Accumulator for pressurized CO_2 (x2)
- Stainless Steel Accumulator for production collection (x2)
- Equilibar Back Pressure Regulator (BPR) regulated by a N_2 tank
- APLISENS Smart Differential Pressure Transmitter (range 0-16 bar)
- ESI Pressure Transducers to measure inlet at outlet pressure (range 0-250 bar) and pressure at the BPR (range 0-400 bar)
- CO_2 tank (maximum 50 bar) and Haskel gas booster to supply pressurized CO_2 to the CO_2 accumulators
- Swagelock tubing, fittings and valves
- Autoclave fittings and valves
- Automatic valves (x4)
- Manometers to measure pressure for accumulators and confinement pressure
- Computer to operate Quizix pumps, automatic valves, ESI pressure transducers and differential pressure transducer

APLISENS Smart Differential Pressure Transmitter

The PRE-28 SMART differential pressure from APLISENS has a nominal measuring range of 0-16 bar differential pressure, with a static pressure limit up to 250 bar. The instrument uncertainty is below 0.032 bar (Aplisens, 2018), and pressure uncertainties for differential pressures measured with the differential pressure transmitter will not be displayed in future graphs.

ESI Pressure Transducer

Three ESI pressure transducers were used in the experimental setup. One transducer ranging from 0-400 bar recorded the gas pressure applied to the back pressure regulator (BPR), whereas two transducers ranging from 0-250 bar measured the inlet and outlet pressure of the core plug. The uncertainty of the pressure transducers is 0.1% of full scale, respectively 0.4 and 0.25 bar.

Production Accumulator

A BPR is required when production measurements are performed at ambient conditions and the pore pressure is at elevated pressures. As CO_2 and brine have a corrosive effect on o-rings in BPRs, CO_2 through the BPR may with time negatively affect the system pressure in terms of fluctuations. The fluctuations cause production of sudden slugs of fluid, and a risk of permanent plugging of the BPR. For CO_2 EOR injections (see chapter 7.4.4), where fluid saturation of each phase must be recorded at different time steps, it is essential to produce fluids through a BPR. Foam scans are run for a substantially longer period than CO_2 EOR injections, and rely on stable differential pressures for each gas fraction. To eliminate pressure fluctuations associated with the BPR, produced CO_2 and brine was collected in

the top of a stainless steel piston accumulator simultaneously as distilled water from the bottom of the piston accumulator was produced through a N_2-leaded BPR maintaining the system pressure.

Foam scans rely on stable differential pressures for each gas fraction. Refilling of discharging of fluids (necessary for an empty CO_2 accumulator or full production accumulator) delayed stabilization of differential pressures due to discontinuous co-injections. An additional set of accumulators was therefore used to streamline the experimental process and maintain stable differential pressures.

Experimental Procedure

All foam scans were performed as co-injection of CO_2 and nanoparticles and/or surfactants at elevated temperatures and pressures. CO_2 becomes supercritical at elevated pressures and temperatures, and the change in compressibility in addition to the corrosive effect the gas obtains in contact with water can have a destructive effect on the equipment. CO_2 and brine especially cause damage to rubber equipment, such as the core holder sleeve and o-rings placed in the core holder and the BPR. To reduce harmful effects, aluminum foil was wrapped around the core plugs, acting as a diffusion barrier between the rubber equipment and the CO_2 and brine. A diffusion barrier was also applied for cores used in CO_2-foam EOR injections and foam screenings (discussed in following sections).

After mounting the core plug in the core holder, absolute permeability (see Appendix A) was measured using brine, before the system was pressurized by injecting brine (both core and bypass) against the BPR set to the desired pore-pressure. A confinement pressure was constantly kept 20 bar above the pore-pressure for limestone. Permeability was again measured at experimental pore-pressure.

Foam quality scans were conducted as a "drainage-like" process with increased gas fractions (by 10% points) from 0.1 to 0.95, and a constant superficial velocity of 1 or 2 feet/day. CO_2 and foaming agent dispersed in brine were injected with a constant gas fraction until steady state flow and pressure were obtained, and apparent foam viscosity (Eq. 4.2) was calculated for each gas fraction. An "imbibition-like" process (decreasing gas fractions) was also conducted on one of the limestone cores prior to a drainage-like injection to evaluate hysteresis.

Foam rate scans show the effect of injection rate on foam strength. The gas fraction was held constant at f_g = 0.7, and the injection rate was increased from 1 feet/day to 3 feet/day. Each rate was held constant until steady state flow and pressure were obtained, and apparent viscosities were calculated for each rate.

7.4.4 CO_2-Foam Injection for EOR

This section describes the experimental setup and procedures for CO_2-foam injections where foaming agents (nanoparticles and/or surfactants) were co-injected with supercritical CO_2 for EOR. Enhancement of oil production subsequent to waterflooding was quantitatively determined by measuring volumetric oil production as a function of pore volumes injected. CO_2 EOR injections in limestone cores were performed using 1500 mPPM NPA solution in Brine A, separately, or combined with 0.5 wt.% SurfA or 1 wt.% SurfB. The foaming agent used in sandstone CO_2-foam EOR injections was 0.5 wt.% SurfA dispersed in Brine C.

Experimental Setup and Equipment

The experimental setup for CO_2-foam EOR injections is illustrated in Figure 7.5. The setup was constructed to perform foam scans (see section 7.4.3) and CO_2-foam EOR injections at elevated temperatures and high pressures. Several changes and improvements were continuously implemented as a vital part of this thesis.

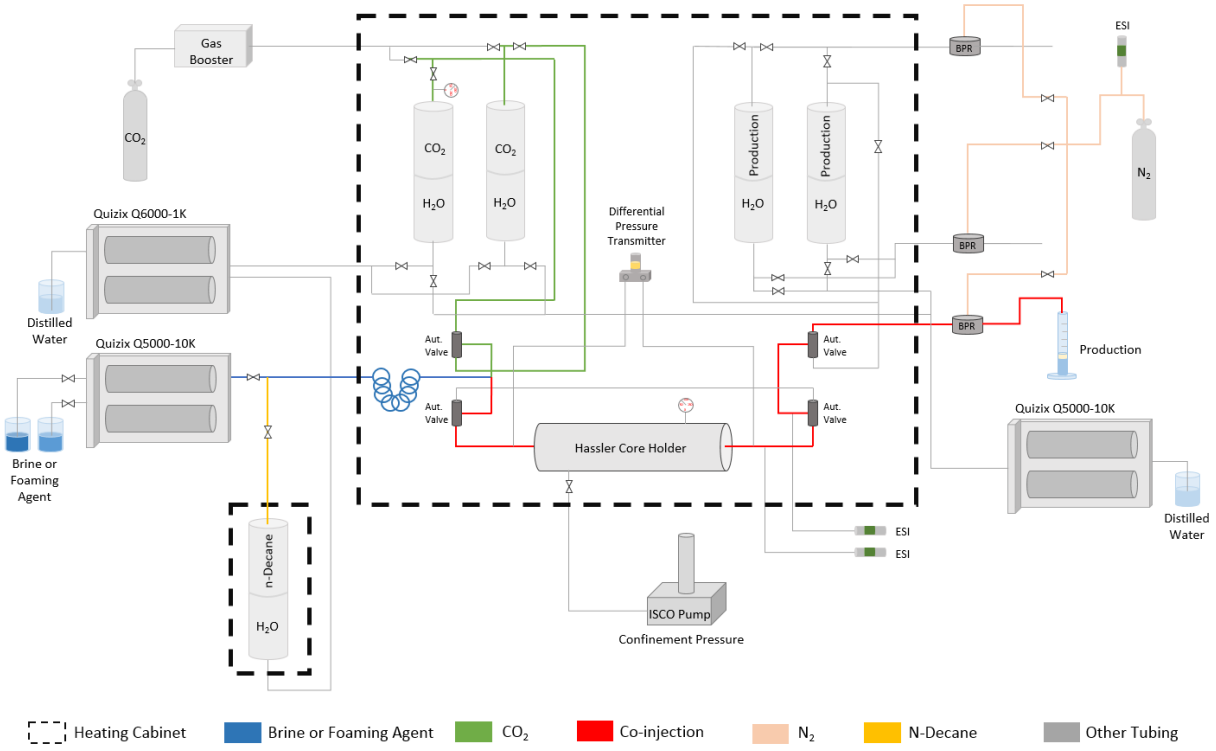

Figure 7.5 – Illustration of the experimental setup used for CO_2-foam EOR with co-injection of CO_2 and foaming agent dispersed in brine. Fluid flow is characterized by different colors with a color description given at the bottom of the figure. Tubing marked in grey as "other tubing" was used for refilling or discharging fluids to/from accumulators or for CO_2-foam scan purpose. The accumulator containing n-Decane was placed in a separate heating cabinet due to limited storage capacity. Produced fluids through the BPR was measured in graded cylinders.

Minor adjustments were made to the experimental setup used for foam scans prior to CO_2 EOR injections. A drainage process was conducted to saturate the cores with oil. The pump used for CO_2 injection was additionally used for injecting n-Decane, which was stored in an accumulator in a separate heating cabinet. Measurements of fluid saturation in the core were crucial for determining oil recovery. The production was therefore not collected in the production accumulator, but sent through a BPR and measured in an inverted imbibition cell and graded glass cylinders of 5 ml and 10 ml for precise fluid measurements.

Experimental Procedure for EOR Experiments

Pressurization

After mounting the core plug in the core holder, absolute permeability was measured using brine before the system was pressurized by injecting brine (both core and bypass) against the BPR set to the desired pore-pressure. A confinement pressure was constantly kept 20 or bar above the pore-pressure for limestone and sandstone, respectively. Permeability was again measured at experimental pore-pressure.

Primary Oil Drainage

All cores were initially 100% saturated with brine, and primary drainage with oil flooding was therefore required ahead of CO_2 EOR injections. Oil was first injected through the bypass, displacing brine in the tubing. At a rate corresponding to a pressure gradient of 1.5 bar/cm, the core plugs were drained at experimental conditions with n-Decane until irreducible water saturation (S_{wi}) was reached. S_{wi} and S_{oi} (initial oil saturation) was calculated by measuring the total brine production from the drainage process.

At S_{wi}, oil originally in place (OOIP) was calculated:

$$OOIP = S_{oi} \cdot PV \tag{7.2}$$

where S_{oi} is the initial oil saturation after primary drainage and PV is the total pore volume [ml]. By using Equation 7.2, it is assumed that all of the produced water during drainage is replaced by oil in the core, as calculation of S_{oi} involves produced water volume V_w [ml]:

$$S_{oi} = 1 - S_{wi} = \frac{PV - V_w}{PV} \tag{7.3}$$

It is essential to specify that not all of the measured water production origins from the core plug. Brine or oil left in the tubing upstream and downstream of the core after injecting fluids through the bypass is defined as dead volumes. These volumes are necessary to accurately measure and take account for, as they overestimate calculations of OOIP. Dead volumes also affect pressure data, as the inlet dead volume delays contact between the injected fluid and the core. The outlet dead volume delays measured volume from the core. Dead volumes were also taken account for during waterflood and co-injection calculations in the following sections.

Waterflood

A waterflood was performed prior to tertiary co-injection of CO_2-foam. Brine was first injected through the bypass, displacing remaining oil in the tubing. Brine was then directed through the core plug to displace oil from the core. The produced oil was collected downstream of the BPR in an inverted imbibition cell and accurately measured as a function of time. The Quizix pump was programmed to inject water for 1 PV at a superficial velocity of 2 feet/day. Pressure gradients from the ESI pressure transducers and the differential pressure transmitter were recorded during the waterflood.

The volumetric oil recovery factor was calculated for evaluation of displacement efficiency. The volumetric oil recovery factor, R_f, is the ratio of oil produced to the oil volume originally in place:

$$R_f = \frac{V_{o,prod}}{OOIP} \tag{7.4}$$

where $V_{o,prod}$ [ml] is volume of oil produced during waterflooding, and $OOIP$ [ml] is the oil originally in placed, as calculated in Eq. 7.2 during oil drainage. The volumetric oil recovery is given as percentage of OOIP (% OOIP).

Co-injection of CO_2 and foaming agent

Subsequent to waterflooding, CO_2 and foaming agent (nanoparticle and/or surfactant) were co-injected to evaluate the performance of CO_2-foam for EOR. The fluids were co-injected with f_g = 0.7, as this gas fraction gave the highest foam apparent viscosity during foam quality scans. Similar to the waterflood, produced fluids were collected in an inverted imbibition cell, and the cumulative oil production was accurately measured at different time steps. If the produced fluids formed emulsions, oil content was determined gravimetrically using the density differences between oil and brine containing foaming agent. CO_2 and foaming agent were injected at a superficial velocity of 2 feet/day, and pressure gradients and oil production was recorded during oil production in the imbibition cell. Equation 7.4 was used to calculate R_f for the co-injection. The incremental oil recovery during co-injection compared to waterflooding, $\Delta R_{f,co-inj}$, is given as percentage points of calculated OOIP (%* OOIP).

7.4.5 CO_2-Foam Injection: Foam Screenings

Foam screenings were conducted on two limestone cores and one sandstone core directly after (and as an extension of) CO_2-foam EOR injections. The main goal of running foam screenings was to investigate foam flow behavior using different foaming agents with and without the presence of oil. CO_2 and foaming agent were co-injected with a superficial velocity of 2 ft/day and f_g = 0.7. During foam screenings, different types of foaming agents were used, switching between injecting only nanoparticles (NPA), only surfactants (SurfA) or a combination of NPA and SurfA. At the onset of foam screenings, oil saturation was equal to final oil saturation after CO_2-EOR injections. Because stable pressure measurements were needed during foam screening, the produced fluids were collected in an accumulator at the outlet. Hence, subsequent fluid saturation changes could not be quantified, although it was suspected that the oil saturation would decrease with time due to large amounts of CO_2 injected at miscible conditions with the oleic phase. Oil was therefore injected into the system simultaneously as CO_2 and foaming agent to evaluate the presence of oil during foam screening.

7.4.6 Retention Study

A retention study was performed in order to quantitatively measure the loss of foaming agent (nanoparticle and/or surfactant) dispersed in the aqueous phase during injection through the porous media. Retention was investigated both in sandstone and in limestone in this thesis.

Experimental Setup and Equipment

Using the experimental setup in Figure 7.5, a fractional collector was placed downstream of the BPR to accurately distribute effluent samples in plastic vials placed on a tray to quantify retention as a function of time (see Figure 7.6). A pH-meter (Model Q45P from Analytical Technology Inc.) was used to measure pH of the injected foaming agent dissolved in brine both prior and subsequent to retention studies. The plastic vials were covered with plastic foil to prevent evaporation of the collected fluids.

Figure 7.6 – Fractional collector controlling the production and tray with plastic vials to collect production.

Experimental Procedure

Core mounting, pressurization and permeability measurements for retention studies followed the same procedure as for CO_2 EOR injections. Foaming agent (NPA and/or surfactant) dispersed in brine was injected with a rate of 50 ml/h for a total of 5 or 10 PV. Effluent samples were distributed in plastic vials by a fractional collector set to produce in each vial for 12 minutes (10 ml in each vial). The vials were covered with plastic foil to reduce the effect of evaporation. A brine injection was performed subsequently to foaming agent injection, with the same injection rate for the same amount of PVs injected. The pH was reduced for some of the brine solutions injected in limestone. Effluent pH and pressure gradients were logged during both injections. The effluent samples were packed and shipped to AkzoNobel in Sweden for analyzation of foaming agent concentrations.

7.5 Equipment Maintenance

Maintenance of the experimental setup was a continuous process during the experimental work of this thesis. As co-injections were performed for the majority of core experiments, presence of CO_2 and brine heavily affected the rubber equipment due to etching and abrasion, as seen in Figure 7.7. The core holder rubber sleeve and o-rings in the BPR were therefore replaced after each experiment conducted with CO_2. The BPR and inlet and outlet end pieces were disassembled, cleaned and dried using compressed air between every experiment.

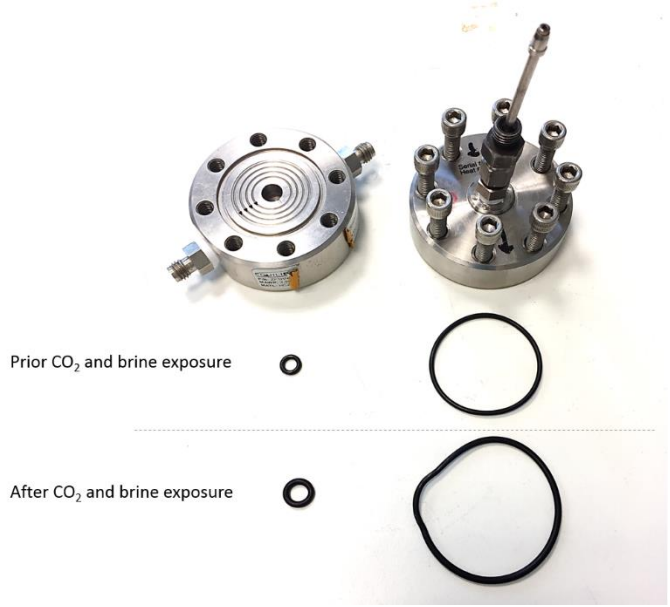

Figure 7.7 – BPR with associated o-rings damaged by etching and abrasion from CO_2 and brine after foam injection

Part III – Results and Discussion

8. Experimental Overview and General Observations

This section presents results and discussions of the experimental work conducted in this thesis. A series of experiments have been performed in order to investigate the separate and combined use of nanoparticles and surfactants as CO_2 foaming agents. Stability of nanoparticles and surfactants dispersed in brine was tested to qualitatively study the interaction between the two foaming agents at elevated temperatures. Bulk foam stability tests were conducted at ambient conditions to evaluate foam generation and coalescence with and without presence of oil. Foaming agent retention, foam stability and EOR potential of CO_2-foam in porous media were also investigated.

A total of 19 cores were used in the experimental work of this thesis (17 Edwards limestone cores and 2 Bentheimer sandstone cores), see Table 8.1, where EDW stands for Edwards limestone and SS for Bentheimer sandstone. Core properties are listed in Table 8.2. Retention studies were conducted to examine retention of nanoparticles and/or surfactants in limestone and sandstone. Foam experiments in core samples were generated by co-injecting supercritical CO_2 and foaming agent dispersed in brine. This includes foam scans, tertiary CO_2-foam EOR injections and foam screenings. The ability of foaming agents to generate and stabilize CO_2-foam was quantitatively analyzed by studying oil recovery efficiency, pressure gradients and foam stability. General observations made during the experimental work of this thesis is presented below.

General Observations

- Mixtures of nanoparticles (NPA) and surfactants (SurfA) were assumed stable during co-injections with CO_2 based on results from static stability tests.

- Measured nanoparticle retention was in the lower range of reported literature values for surfactants.

- Bulk foam experiments showed that oil had a detrimental effect on N_2-foam at ambient conditions. The effect of injected oil in porous media containing foam was influenced by the foam strength.

- Shear-thinning behavior (decreasing apparent viscosity with increasing injection rate) was observed for nanoparticle- and surfactant-stabilized CO_2-foam.

- Foam quality scans showed that the optimal gas fraction (highest apparent viscosity) was achieved with $f_g = 0.6$ for NPA-stabilized CO_2-foam and $f_g = 0.7$ for NPA- and SurfA-stabilized CO_2-foam in limestone.

- SurfB separately or combined with NPA as foaming agents generated stronger CO_2 foam and achieved higher oil recovery compared with the separate and combined use of NPA and SurfA.

- Oil-in-water emulsions were produced during co-injection of CO_2 and surfactants, both separately and combined with NPA.

- Carbon negative oil production was achieved with SurfA as foaming agent in sandstone, and with NPA as foaming agent separately or combined with SurfA in limestone.

- Co-injection of CO_2 and foaming agents dispersed in brine caused dissolution of the limestone surface and interior.

Table 8.1 – Overview over cores, injected fluids and conditions used for each type of experiment

Experiment	Cores used	Injection fluids	Conditions (*)
Retention study	SS05 EDW01 EDW03 EDW04 EDW05 EDW10 EDW12 EDW14	NPA NPA + SurfA NPA + SurfB SurfB	HT/LP MT/HP
Foam scan	EDW06 EDW10 EDW11 EDW12	CO_2 + NPA CO_2 + NPA + Brine CO_2 + NPA + SurfA CO_2 + NPA + SurfB	HT/MP MT/HP
EOR	SS06 EDW07 EDW08 EDW09 EDW13 EDW15 EDW16 EDW17 EDW18	CO_2 + SurfA CO_2 + SurfB CO_2 + NPA CO_2 + NPA + Brine CO_2 + NPA + SurfA CO_2 + NPA + SurfB	MT/HP
Foam screening	SS06 EDW08 EDW09	Brine SurfA NPA Brine + n-Decane SurfA + n-Decane CO_2 + SurfA CO_2 + NPA CO_2 + NPA + Brine CO_2 + NPA + SurfA CO_2 + SurfA + n-Decane CO_2 + NPA + n-Decane CO_2 + NPA + SurfA + n-Decane	MT/HP

* LT: Low temperature (20°C) MT: Medium temperature (40-60°C) HT: High temperature (120°C)
LP: Low pressure (1-3bar) MP: Medium pressure (80 bar) HP: High pressure (110-175 bar)

Table 8.1 – Core properties

Core	Length ± 0.01 [cm]	Diameter ± 0.01 [cm]	Pore Volume ± 0.8 [ml]	Porosity ± 0.3 [%]	Permeability ± 1 [mD]
EDW01	15.16	4.86	75.8	27.0	32
EDW03	15.18	4.84	70.5	25.2	17
EDW04	15.48	4.97	75.2	25.5	50
EDW05	15.44	4.97	69.9	23.4	29
EDW06	15.50	4.97	74.5	24.8	35
EDW07	15.13	4.84	71.2	25.6	68
EDW08	15.15	4.83	76.8	27.7	41
EDW09	15.32	4.82	70.2	25.1	48
EDW10	15.30	4.84	69.7	25.0	21
EDW11	15.13	4.84	76.2	27.4	21
EDW12	15.35	4.83	64.9	23.1	42
EDW13	15.18	4.84	72.0	25.8	20
EDW14	15.15	4.84	61.5	22.0	14
EDW15	15.16	4.84	77.7	27.8	31
EDW16	15.15	4.85	77.6	27.8	25
EDW17	15.15	4.84	68.1	24.4	22
EDW18	15.28	4.84	63.9	22.7	29
SS05	25.10	5.04	116.2	23.2	1650*
SS06	25.50	4.89	108.3	22.7	1863*

*Uncertainty: ± 24

9. Static Temperature Stability of Nanoparticles and Surfactants

A study of interactions between nanoparticles and surfactants was conducted to evaluate the feasibility of their combined effect for CO_2-foam EOR. The stability of nanoparticles (500-5000 mPPM NPA) and surfactants (1 wt.% SurfA) dispersed in Brine C (2 wt.% NaCl) was therefore evaluated for a range of temperatures and pH values. Foaming agents were evaluated both separately and in combination. The temperature was initially set to 40°C and held constant for 40 days. Stability was observed visually once a day, and solutions were considered unstable when they became cloudy/non-transparent. The temperature was increased to 60°C and held constant for 22 days. Finally, the temperature was set to 80°C and held for 12 days. A graphical presentation of results obtained from the static temperature stability test is shown in Figure 9.1, showing stability duration (days) for solutions at elevated temperatures. Table 9.1 lists 15 bottle samples differentiated by foaming agent content, concentration and pH. Samples with a pH of 6 and 7 are defined as "Neutral pH", whereas samples of pH = 4 are defined as "Low pH".

Table 9.1 – Overview of glass bottle content

Glass bottle	**Foaming agent**	**NPA concentration [mPPM]**	**Surfactant concentration [wt.%]**	**pH (± 0.3)**
1	NPA	1500	-	6
2	NPA	1500	-	4
3	NPA	1500	-	7
4	SurfA	-	1	6
5	SurfA	-	1	4
6	SurfA	-	1	7
7	NPA + SurfA	1500	1	6
8	NPA + SurfA	1500	1	4
9	NPA + SurfA	1500	1	7
10	NPA + SurfA	500	1	6
11	NPA + SurfA	500	1	4
12	NPA + SurfA	500	1	7
13	NPA + SurfA	5000	1	6
14	NPA + SurfA	5000	1	4
15	NPA + SurfA	5000	1	7

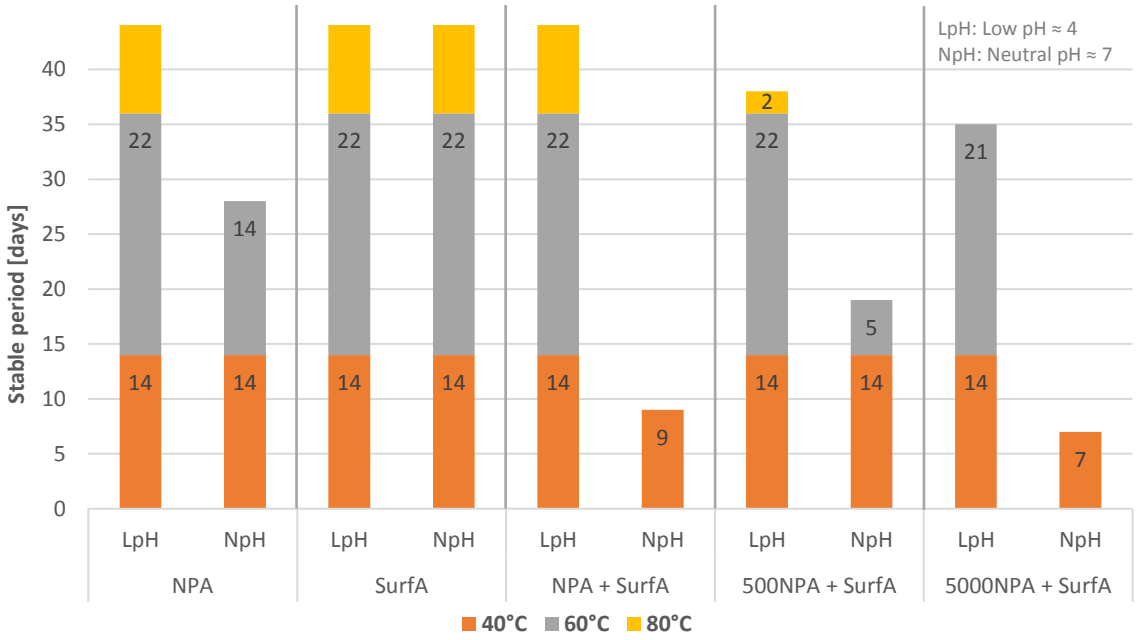

Figure 9.1 – Duration (days) of stability for solutions of NPA and/or SurfA dispersed in Brine C at different temperatures (40, 60 or 80°C) with variating pH (4 or 7) and nanoparticles concentration (500, 1500 or 5000 mPPM). LpH implies low pH of 4, while NpH is a neutral pH of 7. NPA with no further denotation has a concentration of 1500 mPPM, while 500NPA and 5000NPA represents 500 mPPM and 5000 mPPM, respectively. The surfactant concentration is 1 wt.% for all surfactant solutions. The number on top of each colored column represent total stable days at given temperature. The temperature was increased from 40°C to 60°C after 14 days and from 60°C to 80°C after 36 days. The test was stopped after a total of 44 days, resulting in no labeled number for solutions maintaining stability at 44 days.

Results shown in Figure 9.1 indicate that solution stability is a function of temperature, pH and nanoparticle concentration. As discussed in Chapter 5.2, a rise in temperature provokes particle collision and aggregation by increasing the kinetic energy and reducing the CSC. The effect of temperature is observed for several foaming agent solutions: NPA (neutral pH), NPA+SurfA (neutral pH), 500 mPPM NPA+SurfA (low and neutral pH) and 5000 mPPM NPA+SurfA became unstable as the temperature increased.

At neutral pH values, mixtures of nanoparticle and surfactant exhibited lower stability when the nanoparticle concentration was increased. This is expected, as higher nanoparticle concentration increase the probability of nanoparticle aggregation. At reduced pH, however, 1500 mPPM nanoparticle with surfactant is stable for a longer period than the mix with lower nanoparticle concentration.

All solutions containing nanoparticles (separately or combined with surfactant) maintain higher stability with reduced pH than with neutral pH. An increase in pH induces nanoparticle aggregation due to dissociations of negatively charged SiO^- attracting more counter-ions near the particle surface (see Chapter 5.2). All co-injections in this thesis was performed with CO_2 and brine. In presence of brine, CO_2 acts as an acid and reduces the pH of the injected liquid. It can therefore be assumed that the results from "low pH-solutions" reflect conditions obtained during co-injections conducted in this thesis. Further investigation is needed to comment on the pH effect on pure surfactant solutions as both solutions were stable after 44 days.

Interactions between nanoparticles and surfactants seem to adversely affect the static stability at neutral pH: separate solutions of nanoparticles and surfactants were stable longer compared to the combined solutions. At pH-reduced conditions, however, both separate and combined solutions remained stable at all temperatures throughout the entire test (44 days). Hence, it is assumed that all co-injections of nanoparticles and surfactants (1500 mPPM NPA and 1 wt.% SurfA) conducted in this thesis are stable as CO_2 reduced the solution pH and no co-injections are run for a period exceeding 44 days.

10. Bulk Foam Stability

Foam stability is crucial for obtaining an effective oil displacement, and foam stability for different foaming agents were therefore studied with absence and presence of oil prior to CO_2-foam EOR injections. In addition to foam generation, the gradual decay of foam was measured as a function of time to investigate stability and half-decay time of foam stabilized by nanoparticles (1500 mPPM NPA) and/or surfactants (0.5 wt.% SurfA and SurfB) with and without presence of oil. Brine A was used to include a potential effect of presence of divalent ions. All bulk foam stability experiments were performed at ambient conditions, with N_2 as the gaseous phase. Figure 10.1 illustrates the foam decay process, where foam height and liquid height were measured at different time steps. This section shows that oil has a detrimental effect on foam stability. SurfA, SurfB and combinations of these surfactants with NPA are able to stabilize foam generated with N_2 at ambient conditions.

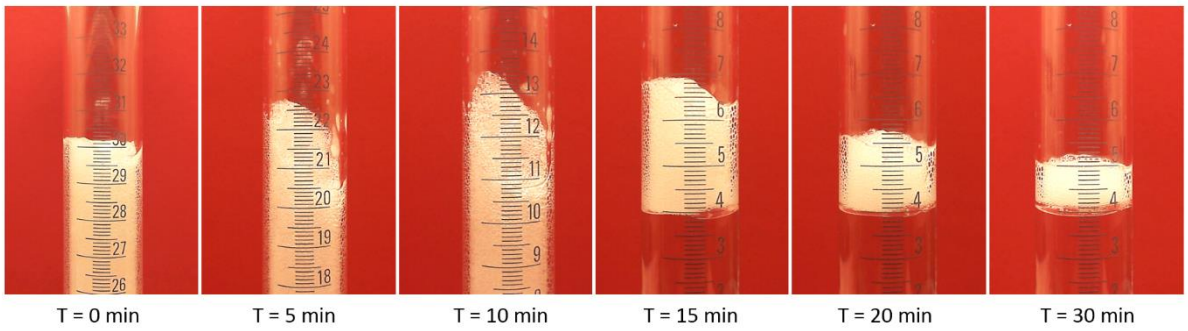

Figure 10.1 – Observed foam decay (SurfB dispersed in Brine A) with presence of oil as a function of time. Initial foam height was 30 cm at T=0 min.

Figure 10.2 displays foam decay time for foam stabilized by surfactants (SurfA and SurfB) and surfactants combined with NPA (SurfA and SurfB). The influence of oil on foam coalescence was also studied. Normalized foam height (to initial height of 30 cm) is plotted as a function of time. Foam decay time for SurfA is an average based on seven experiments with corresponding standard deviations. Remaining experiments were only performed once for each foam agent combination without uncertainties: uncertainty associated with repeatability is substantially larger than the uncertainty associated with foam height measurements.

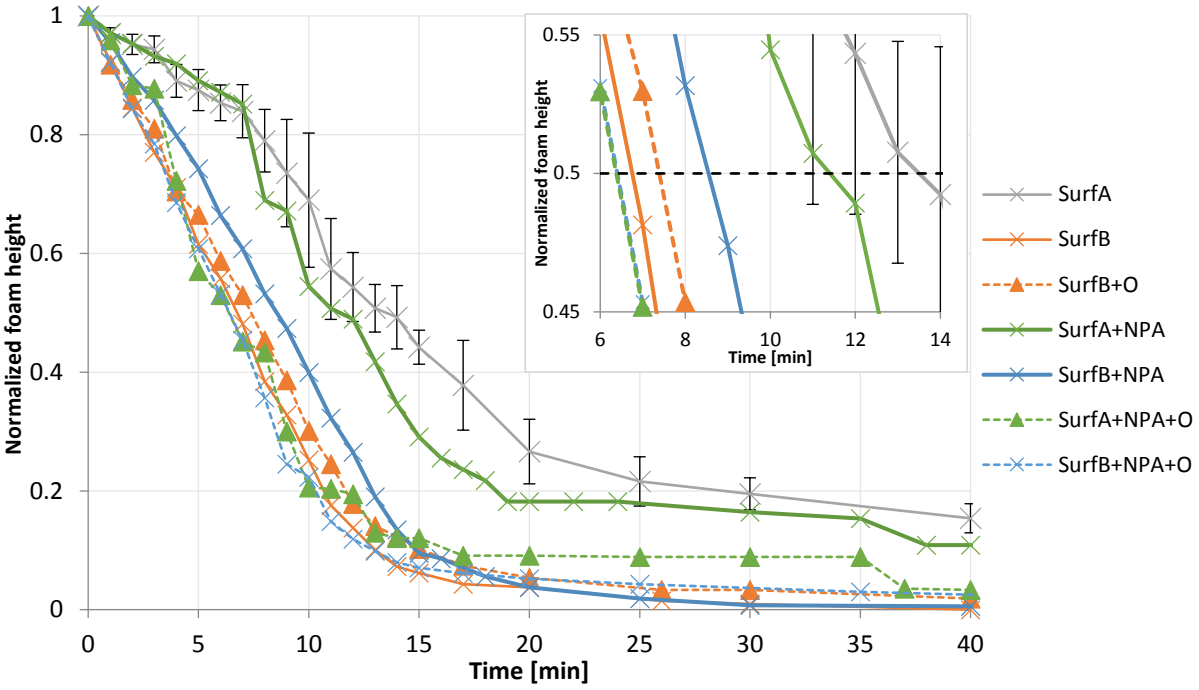

Figure 10.2 – Foam decay illustrated for different combinations of foaming agent with and without presence of oil as normalized foam height as a function of time. The normalized foam height correspond to the measured foam height relative to the initial foam height. Foaming agent combinations are differentiated by colors, where dashed lines corresponds to the foaming agent of the solid line of similar color, but with presence of oil. The grey line is an average of seven foam experiments performed with SurfA, with corresponding standard deviation. The concentration was 0.5 wt.% for SurfA and SurfB, whereas the nanoparticle concentration was 1500 mPPM. Top right corner: half-decay time illustrated for different combinations of foaming agent with and without presence of oil as a function of time. The dashed horizontal black line illustrates half-decay time (normalized height = 0.5).

Half-decay time (normalized height = 0.5) was used to quantify and compare foam strengths. Results are highlighted in Figure 10.2 and listed in Table 10.1. SurfA generates the most stable foam (13.5 min), followed by SurfA combined with NPA (11.4 min) and SurfB combined with NPA (8.5 min), whereas SurfB (6.8 min) generated the least stable foam. However, no conclusion of foam agent stability should be made based solely on these results, as each experiment (except SurfA) was performed only once. The average of seven experiments conducted with SurfA with corresponding standard deviation reveals great uncertainty associated with these bulk foam experiments. Uncertainties are thus not included in Table 10.1.

Table 10.1 – Half-decay time for foam generated with different foaming agents

	SurfA	**SurfB**	**SurfB + Oil**	**SurfA + NPA**	**SurfA + NPA + Oil**	**SurfB + NPA**	**SurfB + NPA + Oil**
Half-decay time [minutes]	13.5	6.8	7.7	11.4	6.4	8.5	6.4

Figure 10.2 also displays how presence of oil affect foam stability (dashed lines). Oil has a detrimental effect on foam stability for combinations of nanoparticles and surfactants, whereas presence of oil suggests to establish a more stable foam when stabilized with SurfB. However, as generated foam reached 30 cm, a fraction of the oil remained on top of the foaming agent solution, at the foam-liquid interface at the bottom part of the glass tube used in the experimental setup. As a result, a varying amount of oil may have been available for foam destabilization. The presence of oil has less effect on foam stabilized by Surf B compared with the other foaming agents, and the observed foam stabilizing effect of oil may not be repeatable. As discussed in chapter 4.3, oil spreads on the interface between liquid and gas bubbles, resulting in foam coalescence. It is therefore more likely that results obtained from foam stabilized by nanoparticles and surfactants are more representative of oil-foam interactions, with a half-decay reduction of 44% and 25% for SurfA combined with NPA and SurfB combined with NPA, respectively. Short chain hydrocarbons have a more destabilizing effect on foam than hydrocarbons of longer chains (see chapter 4.3), and the detrimental oil effect will therefore be less severe for crude oils than for n-Decane used in this experimental thesis.

Experiments performed at ambient conditions cannot explain foam behavior at elevated temperatures and pressures, and bulk foam experiments cannot determine generation, stability or behavior of foam in porous media, as different physics govern foam behavior and stability at bulk and pore scale (Osei-Bonsu et al., 2017). Results obtained from conducted bulk foam stability tests therefore not transferable foam stabilized by nanoparticles and/or surfactants during foam scans (without presence of oil) or during CO_2-foam EOR injections (with presence of oil), discussed in the following chapters. Nevertheless, bulk stability tests have proven the feasibility of combining nanoparticles and surfactants for foam generation and stability.

11. Loss of Foaming Agent: Retention of Nanoparticles in Porous Media

Foaming agent applicability for foam EOR injections in porous media is profoundly affected by the degree of retention, as loss of foaming agent debilitates the effectiveness of foam generation and IFT-reduction between reservoir fluids, reducing the economic feasibility of foam injection. A retention study of silica nanoparticles in Bentheimer sandstone and of silica nanoparticle and/or surfactant (1500 mPPM NPA and 1 wt.% SurfA or SurfB) in Edwards limestone was therefore performed at different experimental conditions to quantitatively measure the loss of foaming agent as the dispersed phase was injected through the porous media. Table 11.1 lists cores used for retention tests and studies. This section shows that retention of NPA with and without presence of SurfA was in the lower range of reported literature values for surfactants, and that pH reduction of injected nanoparticles dispersed in brine was needed to avoid nanoparticle aggregation at 120°C and 3 bar pore pressure in limestone.

Table 11.1 – Overview of core used for retention tests with corresponding experimental parameters

Core	Injection fluid	Experimental conditions	Injection rate [ml/h]	Brine	Reduced pH [YES/NO]
SS05	NPA	120°C / 3 bar	50	Brine C	NO
EDW02**	NPA	120°C / 3 bar	50	Brine B	NO
EDW03	NPA	120°C / 3 bar	50	Brine B	NO
EDW04	NPA	120°C / 3 bar	15	Brine B	YES
EDW05	NPA	120°C / 3 bar	30	Brine B	YES
EDW12	NPA + SurfA	40°C / 175 bar	50	Brine A	YES
EDW10	NPA + SurfB	40°C / 175 bar	50	Brine A	YES*
EDW14	SurfB	40°C / 175 bar	50	Brine A	YES*

* pH was reduced to solubilize SurfB
** This experiment was conducted by PhD Øyvind Eide

11.1 Retention of Nanoparticles in Sandstone

Results from the retention study of nanoparticles in sandstone (SS05) are shown in Figure 11.1, where normalized effluent concentrations are represented as a function of PV injected. Normalized concentration is the ratio of measured effluent NPA concentration to the initial concentration of injected NPA, where a value of 1 means that the retention is satisfied. NPA dispersed in Brine C was injected with a rate of 50 ml/h, at 120°C and a pore pressure of 3 bar to prevent evaporation. The NPA concentration increased after breakthrough (observed before 1 PV injected) and reached its maximum value after 4 PV injected. The maximum concentration was equal to the injected concentration (hence, a normalized value of 1 was achieved), suggesting that retention was satisfied after approximately four pore volumes injected. Brine was subsequently injected to measure recovery of re-mobilized NPA (NPA elution), with a higher rate of elution than retention.

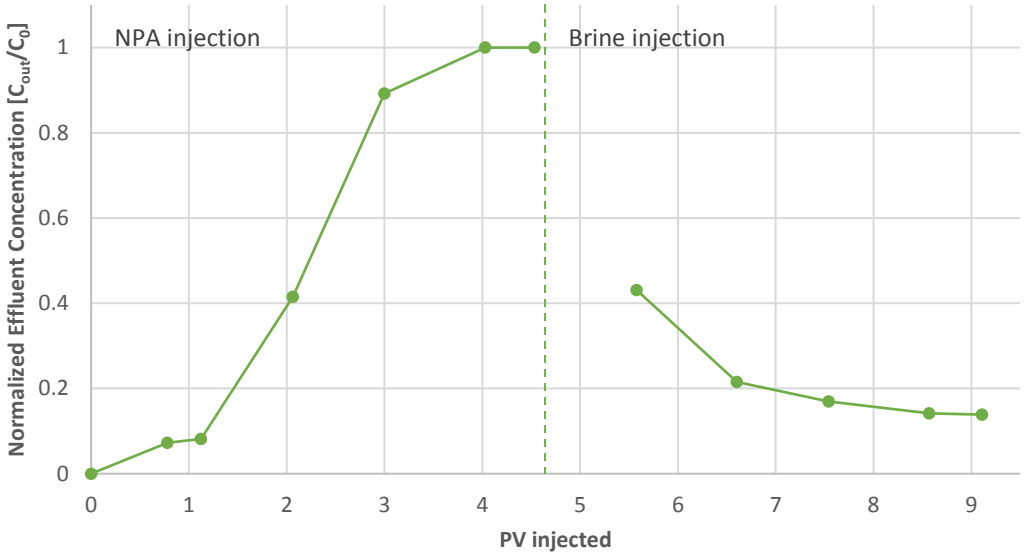

Figure 11.1 – Retention of nanoparticles in sandstone displayed as normalized effluent concentration (the ratio between the measured concentration of effluent sample (C_{out}) and initial concentration (C_o)) as a function of PVs injected. 1500 mPPM NPA dispersed in Brine C was injected with a rate of 50 ml/h in sandstone core SS05 at pore pressure of 3 bar and temperature of 120°C. The dashed vertical line represents the end of NPA injection and the start of brine injection.

The nanoparticle retention was calculated by dividing the total mass of nanoparticles injected (at volume injected when normalized concentration reached 1) by the total mass of the core. The calculated nanoparticle retention in sandstone was (0.48 ± 0.06) mg/g, which is in the lower range of reported literature values for surfactant retention (Enick et al., 2011). Retention of silica nanoparticles in Bentheimer sandstone is lower when the temperature decrease (Rognmo et al., 2018a), showing that an increase in temperature adversely affects nanoparticle retention.

11.2 Retention of Nanoparticles in Limestone

Aggregation of Nanoparticles

Retention of nanoparticles was investigated in limestone cores at the same conditions as for sandstone in section 11.1 (50 ml/h, 120°C, 3 bar). The experimental conditions and change in rock type led to injectivity complications, and effluent samples were not measurable as nanoparticles aggregated in the core inlet (see Figure 11.2), blocking the injection. Dissolution of $CaCO_3$, naturally occurring in limestone, increases the pH of the injected fluid. As discussed in chapter 5.2, a rise in pH results in dissociation of negatively charged function groups of silica nanoparticles (SiO^-), which attract more counter-ions near the particle surface and consequently induce nanoparticle aggregation. The high experimental temperature (120°C) may have exacerbated the aggregation process due to increased kinetic energy and reduction of the CSC (critical salt concentration).

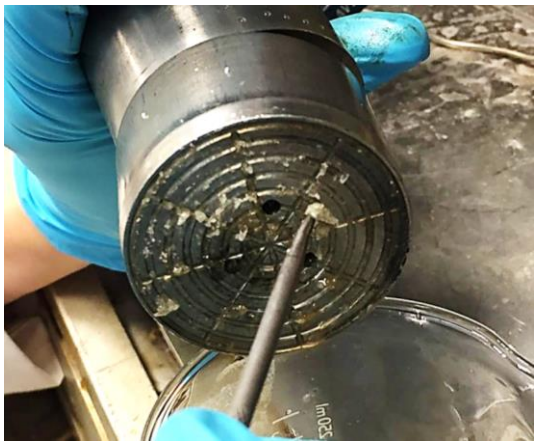

Figure 11.2 – NPA aggregates at inlet end-piece during adsorption test on EDW03. Aggregation generated a "gel" of nanoparticles at the inlet end-piece.

Retention of pH-reduced Nanoparticles

A pH-reduction (3.7 ± 0.2) of the injected nanoparticle solution eliminated aggregation issues in limestone at 120°C and 3 bar (see Figure 11.3). NPA dispersed in Brine B was injected with a rate of 15 ml/h (EDW04) and 30 ml/h (EDW05) to evaluate the effect of injection rate.

Nanoparticle retention was not calculated for retention tests in EDW04 and EDW05 because the measured effluent concentrations did not coincide with the injected NPA concentration. The injected NPA concentration was 1500 mPPM, whereas the highest concentration measured at the outlet was 570 mPPM, and there is reason to believe that the measured concentrations are unreliable for retention calculations. Effluent samples were sent to Sweden for analyzes, and the contents may have transformed over time due to contamination or decomposition. However, the shape of curves obtained from these experiments resembles curves from the sandstone experiment (previous section) and previous UoB (University of Bergen) experiments (Rognmo et al., 2017). The measured concentration stabilizes at 4 PVs injected for EDW04, implying satisfied retention based on previous assumptions.

Nanoparticle retention for EDW04 and EDW05 is therefore qualitative described based on the trends observed in Figure 11.3. An increase in NPA concentration was observed after breakthrough, with a similar increasing trend in both core samples. Stable normalized effluent concentration was not achieved, and retention satisfaction is therefore not justified for the limestone cores. A longer injection period of NPA should have been conducted in order to study the effect of injection rate on nanoparticle retention in limestone.

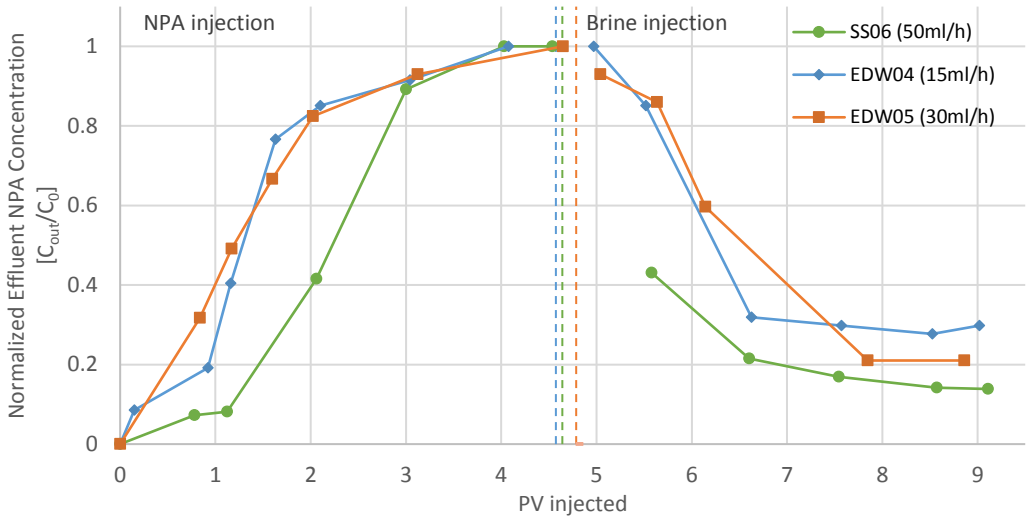

Figure 11.3 – Retention of nanoparticles in limestone (EDW04 and EDW05) and sandstone (SS06) displayed as normalized effluent concentration (measured concentration of effluent sample (C_{out}) over initial concentration (C_o)) as a function of PVs injected. 1500 mPPM NPA dispersed in Brine C was injected with a rate of 50 ml/h (SS06), 30 ml/h (EDW05) or 15 ml/h (EDW04) at pore pressure of 3 bar and temperature of 120°C. The dashed vertical lines represent the end of NPA injection and start of brine injection.

The shape of the curves obtained from retention in EDW04 and EDW05 deviates from the sandstone retention curve: nanoparticle concentrations that are measured for limestone cores after 1 PV injected are higher than for sandstone, indicating a more dispersed front. A breakthrough of nanoparticles prior to 1 PV injected suggest a volumetric sweep efficiency below 1, which can be caused by fractures. Bentheimer sandstone and Edwards limestone do not contain fractures, but the latter is a highly heterogeneous rock (see Figure 7.2, Chapter 7.2.2), where high-permeable layers can explain the detection of nanoparticles prior to 1 PV of injected fluid. This could, however, also be caused by uncertainties associated with concentration measurements.

Retention experiments were performed by injecting dispersed foaming agent into brine-saturated cores with absence of CO_2 and oil. It is unknown how the presence of supercritical CO_2 (foam scans) and of supercritical CO_2 and oil (CO_2-foam EOR injections) impacts retention. As discussed in Chapter 5.2, it is assumed that nanoparticle retention will decrease with presence of CO_2, as nanoparticles adsorb on the CO_2-liquid interface. Retention tests on EDW02 and EDW03 caused nanoparticle aggregation, whereas no aggregation was observed for pH-reduced nanoparticle injection at similar experimental conditions. Presence of CO_2 during co-injections conducted in this thesis reduces the solution pH, and pH alteration of the foaming agent solution is therefore not necessary (as proven in Chapter 12).

11.3 Retention of Nanoparticles with Presence of Surfactants

Nanoparticle retention in limestone (EDW12) was also investigated when co-injected with SurfA (1 wt.%) (see Figure 11.4). This retention study was conducted at 40°C and 175 bar pore pressure, and cannot directly be compared with results in chapter 11.2 where the injection was performed at 120°C and 3 bar, as temperature and pressure can affect the retention process. Nevertheless, nanoparticle retention in EDW12 is satisfied after 6 PVs injected compared to 4 PVs for SS06. The nanoparticle retention is higher for EDW12 (see Table 11.2) without concluding the cause of increase; the separate or combined effect of reduced temperature, increased pressure or presence of surfactant may cause higher retention.

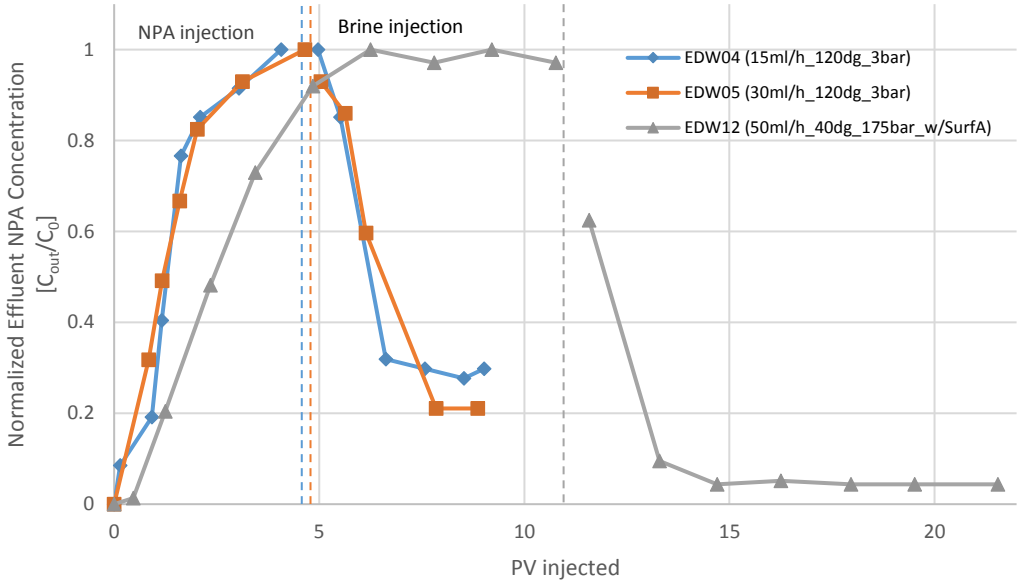

Figure 11.4 – Retention of nanoparticles in limestone (EDW04, EDW05 and EDW12) displayed as normalized effluent concentration as a function of PVs injected. 1500 mPPM NPA dispersed in Brine B or Brine C was injected with a rate of 50 ml/h (EDW12), 30 ml/h (EDW05) or 15 ml/h (EDW04) at 40°C and 175 bar (EDW12) or 120°C and 3 bar (EDW04, EDW05). NPA was co-injected with SurfA in EDW12, but only nanoparticle retention was studied. The dashed vertical lines represent the end of NPA injection and start of brine injection.

Measured nanoparticle retention in sandstone (SS06) and limestone (EDW12) is listed in Table 11.2. The calculated nanoparticle retention was (0.48 ± 0.06) mg/g and (0.8 ± 0.1) mg/g for sandstone and limestone, respectively. The calculated retention values are in the lower range of reported literature values for surfactant retention (Enick et al., 2011). Eluted values indicate recovery of nanoparticles by re-mobilization during brine injection, resulting in a nanoparticle recovery of 38% in SS06 and 25% in EDW12. Re-mobilized nanoparticles are beneficial during field application, as the stabilizing effect of nanoparticles can reach further into the reservoir (Rognmo et al., 2017).

Table 11.2 – Retention and recovery of NPA in core plugs

Core	Foaming Agent	Retention [mg/g]	Eluted [mg/g]	Total particle recovery [%]
SS06	NPA	0.48 ± 0.06	0.18 ± 0.02	38 ± 2
EDW12	NPA + SurfA	0.8 ± 0.1	0.20 ± 0.02	25 ± 3

Retention tests were also conducted with SurfB separately and combined with NPA in limestone. Nanoparticle concentrations were however not measurable as increased pH due to dissolution of $CaCO_3$ caused clouding of SurfB. Effluent pH-measurements as a function of PV injected is shown in Figure 11.5 for all retention tests. The initial reduction in pH (shown in the data legend) prior to injection of SurfB with and without NPA was not sufficient to prevent clouding of SurfB. Lower retention of SurfB than SurfA is expected in limestone when the pH is sufficiently low to maintain the cationic state of SurfB. However, for increased pH, SurfB may switch to an anionic surfactant, resulting in high retention due to electrostatic attraction (see Table 5.1, Chapter 5.1).

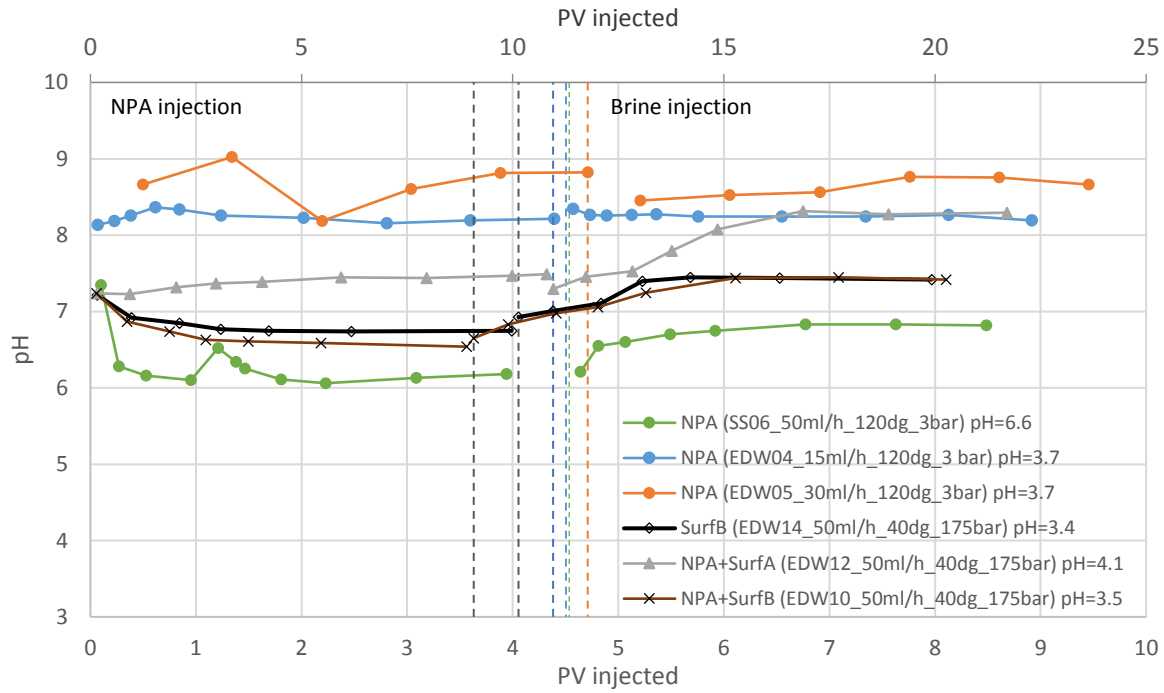

Figure 11.5 – Effluent pH measurements as a function of PV injected for each retention study. Each foaming agent is labelled with respective core plug, injection rate, experimental conditions and initial pH. PV injected for SS06, EDW04 and EDW05 coincide with the primary horizontal axis, whereas the secondary horizontal axis display PV injected for EDW12, EDW14 and EDW10. The pH is highly increased for effluent samples regardless of initial pH reduction.

12. Foam Generation in Limestone – Investigation of Foam Quality and Foam Rate

The applicability of using foam for mobility control of CO_2 is profoundly affected by foam strength and foam behavior in porous media. A total of 6 foam scans with in-situ foam generation during co-injection of CO_2 and foaming agent (1500 mPPM NPA with and without 1 wt.% SurfA or SurfB dispersed in Brine A) were conducted in limestone to quantitatively measure foam strength by apparent foam viscosity as a function of gas fractions (foam quality scan), or as a function of injection rate (foam rate scan). Table 12.1 lists cores used for foam scan studies. This section shows that the combined effect of NPA and SurfA generate a significantly stronger foam compared with the separate use of NPA or SurfA. Further investigation is needed to quantitatively determine foam strength for SurfB-stabilized foam, as the dispersed surfactant is pH dependent. However, high apparent viscosities were observed during foam scans with NPA and SurfB, indicating generation of strong foam.

Table 12.1 – Overview of core used for foam scan studies with corresponding experimental parameters

Core	Experiment	Injection fluid	Experimental conditions	Superficial velocity [feet/day]	Reduced pH [YES/NO]
EDW11	Foam quality scan (baseline)	CO_2 + Brine	40°C / 175 bar	1	NO
EDW06	Foam quality scan	CO_2 + NPA	120°C / 80 bar	2	NO
EDW12	Foam quality scan Foam rate scan	CO_2 + NPA + SurfA	40°C / 175 bar	1	YES
EDW11	Foam quality scan	CO_2 + NPA + SurfB	40°C / 175 bar	1	YES*
EDW10	Foam quality scan	CO_2 + NPA + SurfB	40°C / 175 bar	1	YES*

* pH was reduced to solubilize SurfB

12.1 Baseline – Co-injection of CO_2 and Brine

A foam quality baseline with co-injection of CO_2 and brine was performed to establish foam strength in limestone without presence of foaming agents. The observed behavior without foaming agent served as a benchmark for subsequent injections with foaming agent to evaluate their performance of CO_2 mobility control.

CO_2 and Brine A were co-injected with a total superficial velocity of 1 ft/day at 40°C and 175 bar pore pressure in a "drainage-like" process with increasing gas fraction. Apparent viscosity as a function of gas fraction is illustrated in Figure 12.1. Fluids were produced through a BPR, resulting in substantial fluctuations and high uncertainty related to calculated apparent viscosities. Although a decreasing trend in apparent viscosity for increased gas fraction was observed, the trend cannot be justified when accounting for the uncertainty values. Nevertheless, no stable foam was generated during co-injection of CO_2 and brine due to the absence of foaming agent (see Chapter 5), and a distinct optimal gas fraction (highest apparent viscosity) should not be observed.

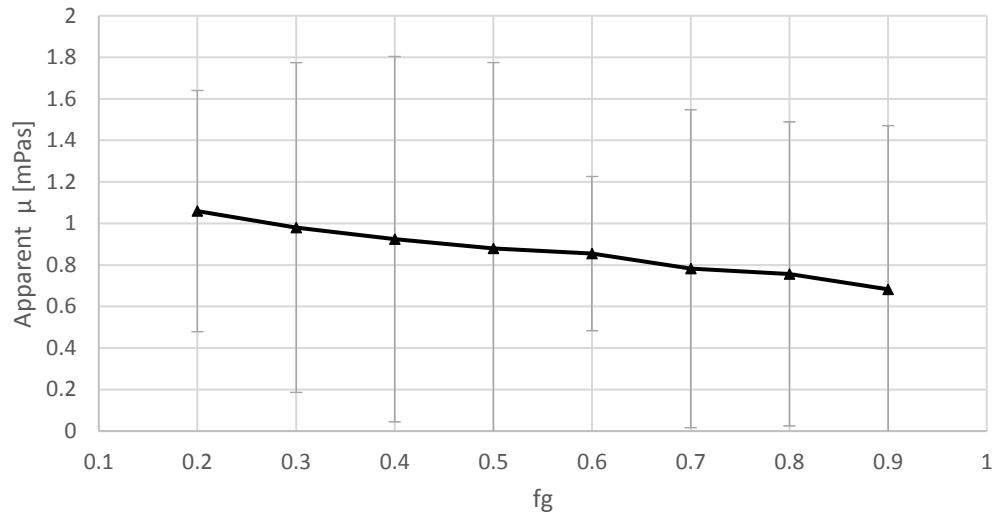

Figure 12.1 – Apparent viscosity as a function of gas fraction (f_g) during co-injection of CO_2 and Brine A in limestone (EDW11) with a total superficial velocity of 1 feet/day at 40°C and 175 bar. The gas fraction was monotonically increased from 0.2 in a "drainage-like" injection mode (increasing gas fractions). Fluids were produced through a BPR, increasing apparent viscosity uncertainties due to pressure fluctuations.

12.2 Nanoparticle-Stabilized Foam

A foam quality scan of NPA-stabilized CO_2-foam was conducted at 120°C and 80 bar pore pressure in limestone (EDW06). In addition to studying foam stability and strength at elevated temperature, the experiment was performed at 120°C to investigate co-injection of CO_2 and NPA without pH alteration. Nanoparticles aggregated at the inlet during retention studies (see Chapter 11.2) at 120°C and 3 bar, whereas pH-alteration prior to injection mitigated injectivity issues. No pressure buildup caused by aggregation was observed during co-injection of NPA and CO_2, suggesting that presence of CO_2 is sufficient to prevent nanoparticle aggregation at 120°C and 80 bar in limestone. The effect of gas fraction and hysteresis on NPA-stabilized foam is introduced in the following sections.

The Effect of Gas Fraction

Figure 12.2 shows apparent viscosity as a function of gas fraction (f_g) measured during co-injection of NPA and CO_2 in EDW06. The gas fraction was monotonically increased from 0.1 to 0.9 in a "drainage-like" process (subsequent to an "imbibition-like" injection). An increase in apparent viscosity was observed for increasing f_g, with a sharp increase from f_g = 0.5 to 0.6. The optimal gas fraction (f_g^* = 0.6) represents the strongest foam obtained for NPA at the experimental conditions used, and values of f_g exceeding 0.6 are detrimental on foam mobility reduction.

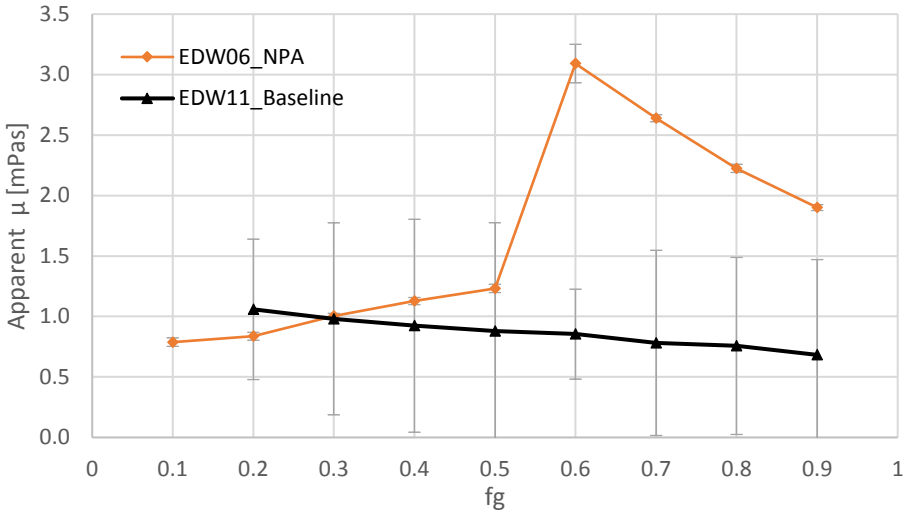

Figure 12.2 - Apparent viscosity as a function of gas fraction (f_g) during co-injection of NPA and CO_2 in limestone (EDW06, 2 ft/day, 120°C and 80 bar) in orange and former results from the baseline co-injection of CO_2 and brine in limestone (EDW11, 1 ft/day, 40°C and 175 bar) in black. Highest apparent viscosity for NPA-stabilized foam is achieved at f_g = 0.6.

The maximum apparent viscosity for co-injection of NPA and CO_2 (3.1 ± 0.2 mPas at $f_g^* = 0.6$) was 3 times higher than the baseline (average apparent viscosity for all gas fractions). However, the two co-injections cannot directly be compared because different experimental conditions were used (see Table 12.1). The difference in superficial velocity (2 ft/day for NPA-stabilized foam and 1 ft/day for the baseline) does not influence the results as constant apparent viscosities are observed for different co-injection rates of NPA and CO_2 (Rognmo et al., 2017). The NPA-stabilized foam is generated at a significantly higher temperature (120°C) than the baseline temperature (40°C), suggesting that higher apparent viscosity could be achieved for NPA-stabilized CO_2-foam generated at the baseline temperature as increased temperature adversely affect the physical properties of the fluids. Regardless of the deviating experimental conditions, increased apparent viscosities demonstrated a successful application of NPA as a foaming agent for CO_2 mobility control in limestone at 120°C and 80 bar.

The Effect of Hysteresis

An imbibition-like co-injection (decreasing f_g) of NPA and CO_2 was performed prior to the drainage-like co-injection (increasing f_g), see Figure 12.3. Apparent viscosities obtained from the drainage-like co-injection do not follow the trend observed during the imbibition-like co-injection, and the maximum apparent viscosity is obtained at different foam qualities: $f_g^* = 0.3$ (1.1 ± 0.1 mPas) for the imbibition-like and $f_g^* = 0.6$ (3.1 ± 0.2) for drainage-like process. The difference in foam behavior is a result of hysteresis, indicating that foam generation is dependent on saturation change and trapped gas caused by previous injections executed on the core (Keelan & Pugh, 1975). Hysteresis effects are also observed for NPA-stabilized foam in sandstone (Rognmo et al., 2017) and SurfA-stabilized foam in limestone and sandstone (Wergeland, 2017).

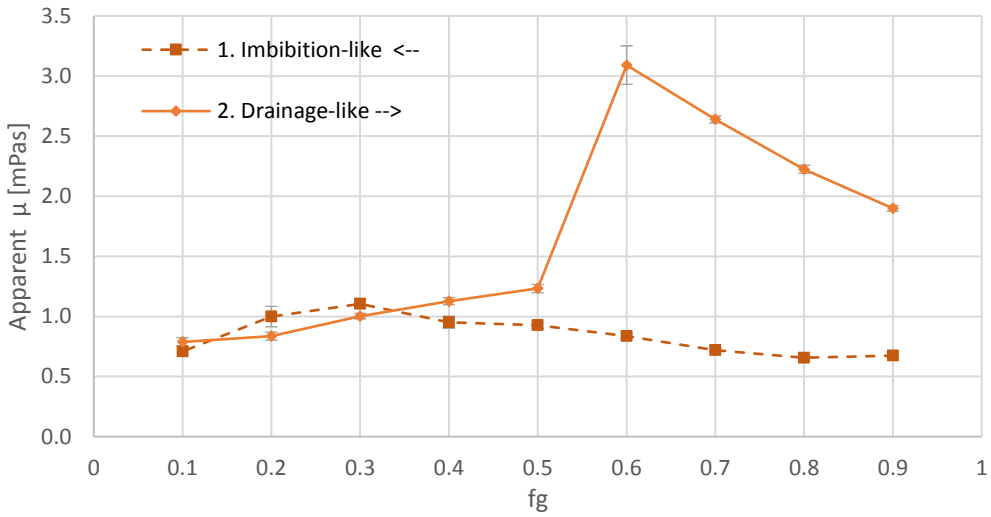

Figure 12.3 – Hysteresis effect in apparent foam viscosities during co-injection of NPA and CO_2 in limestone (EDW06). An imbibition-like co-injection with decreasing gas fractions (dashed line) was conducted prior to a drainage-like co-injection (solid line). Both injection cycles were performed at 40°C and 175 bar, with a superficial velocity of 1 ft/day.

12.3 Nanoparticle- and Surfactant-Stabilized Foam

Foam quality scans and a foam rate scan were performed with CO_2-foam stabilized by nanoparticles and surfactants to investigate the combined effect of the foaming agents. CO_2 was co-injected with 1500 mPPM NPA and 1 wt.% SurfA or SurfB dispersed in Brine A at a superficial velocity of 1 ft/day. The experimental conditions were held constant at 40°C and 175 bar pore pressure. The following sections present results achieved by a foam quality and foam rate scan of NPA and SurfA (EDW12), and from two foam quality tests of NPA and SurfB (EDW10 and EDW11). All foam quality scans are performed as drainage-like injections.

The Combined Effect of NPA and SurfA

Apparent viscosity measured as a function of gas fraction for co-injection of CO_2 and a combination of NPA and SurfA is shown in Figure 12.4 (blue line). Maximum foam strength (273 ± 2 mPas at $f_g^* = 0.7$) was 300 times higher than the baseline (average apparent viscosity for all gas fractions). The foam scan baseline (black line), co-injection of CO_2 and NPA (orange line) and results from co-injection of CO_2 and SurfA conducted in limestone by PhD candidate Sunniva Brudvik Fredriksen (grey line) are also displayed in Figure 12.4.

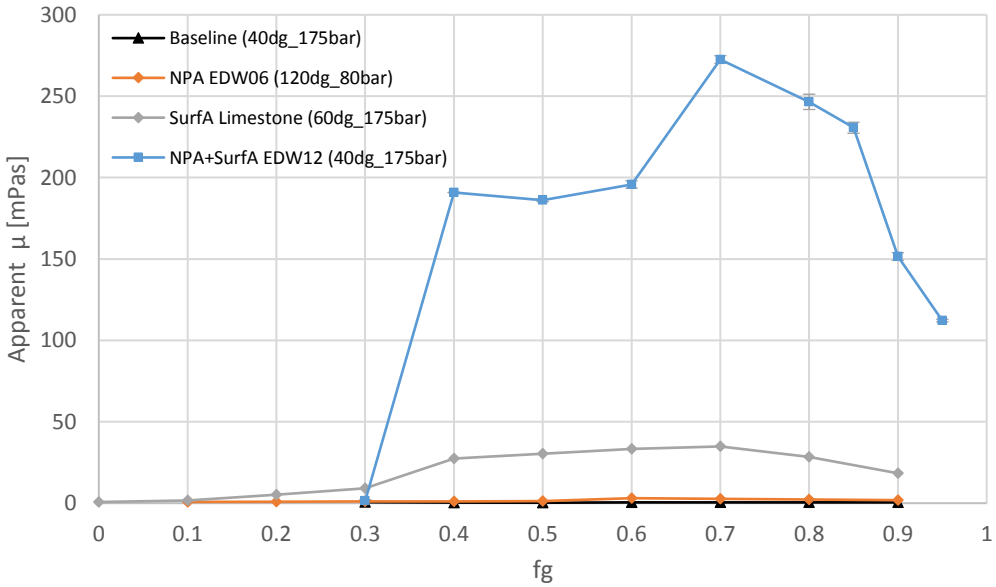

Figure 12.4 – A comparison of foam strength of foam stabilized by CO_2 and brine (baseline, black line), CO_2 and SurfA (grey line), CO_2 and NPA (orange line) and CO_2 with a combination of NPA and SurfA (blue). Foam strength is measured as apparent viscosity as a function of gas fractions, f_g. NPA and Surf A generate a significantly stronger foam compared with the separate used of NPA and SurfA.

The two foam scans with CO_2-foam stabilized separately by NPA or SurfA foam were performed at different experimental conditions compared with the baseline and foam stabilized by combining NPA and SurfA (see Figure 12.4). As previously discussed, stronger foam can be expected for NPA-stabilized foam at lower temperatures, but further experiments should be performed to reach a firm conclusion. The experiment performed with SurfA-stabilized foam is conducted at more comparable experimental conditions, with a temperature difference of 20°C (60°C compared to 40°C). Increased temperature will presumably have an unfavorable effect on the foam strength, and stronger foam (higher apparent viscosity) could therefore be expected for SurfA-stabilized foam at 40°C and 175 bar. Apparent viscosity for all co-injections is visualized in Figure 12.5. Uncertainties are not taken account for as the experimental conditions deviate. Nevertheless, a significant increase in foam strength (300 times higher) is observed for foam stabilized by NPA and SurfA compared to the baseline at identical conditions. Despite a need for further investigation at comparable experimental conditions, a considerably stronger foam is generated for the combining use of NPA and SurfA compared to the separate use of the foaming agents.

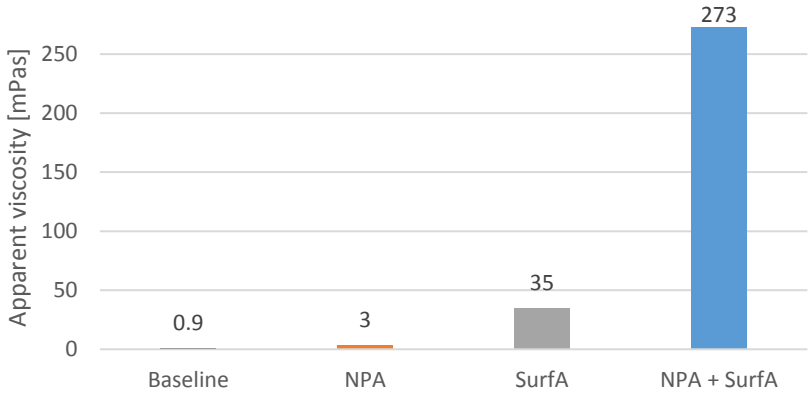

Figure 12.5 – Highest measured apparent viscosity for different foaming agents. Results obtained for NPA-stabilized foam (orange) and SurfA-stabilized foam (grey) are not directly comparable to the baseline (black) and combined use of NPA and SurfA (blue) due to deviating experimental conditions.

The Effect of Injection Rate

A foam rate scan was conducted as co-injection of CO_2, NPA and SurfA in limestone (EDW12) with constant gas fraction (f_g= 0.7) and increasing superficial velocity from 1 ft/day to 3 ft/day (solid line in Figure 12.6). The objective of the foam rate scan was to study the rheology of foam at different injection rates. Foam can be described as a Newtonian fluid if the apparent viscosity (μ_{app}) is constant with changing injection velocity, or as a non-Newtonian fluid if the μ_{app} is decreasing with increasing injection rate (shear-thinning) or increasing μ_{app} with increasing injection rate (shear-thickening). As seen in Figure 12.6, foam shear thinning was observed for injection rates higher than 1.5 ft/day, but the initially measured μ_{app} at 1 ft/day did not coincide with the shear-thinning behavior. The injection was therefore reduced back to 1 ft/day (dark green dashed line) and then increased to 3 ft/day (light green dashed line). A clear shear-thinning behavior was then observed

Shear-thinning behavior is expected for surfactant-stabilized foam, whereas NPA-stabilized CO_2 foam has shown near-Newtonian behavior (Rognmo et al., 2017). The combined effect of NPA and SurfA demonstrated shear-thinning behavior, suggesting that surfactants dominate the foam flow behavior with increasing injection rates. This could possibly be explained by the concentration relationship between dispersed NPA and SurfA, as 1500 mPPM (0.15 wt.%) of NPA was dispersed in brine compared to 1 wt.% of SurfA. The first measured apparent viscosity (1 ft/day, solid line) showed a hysteresis effect as a result of increasing injection rate.

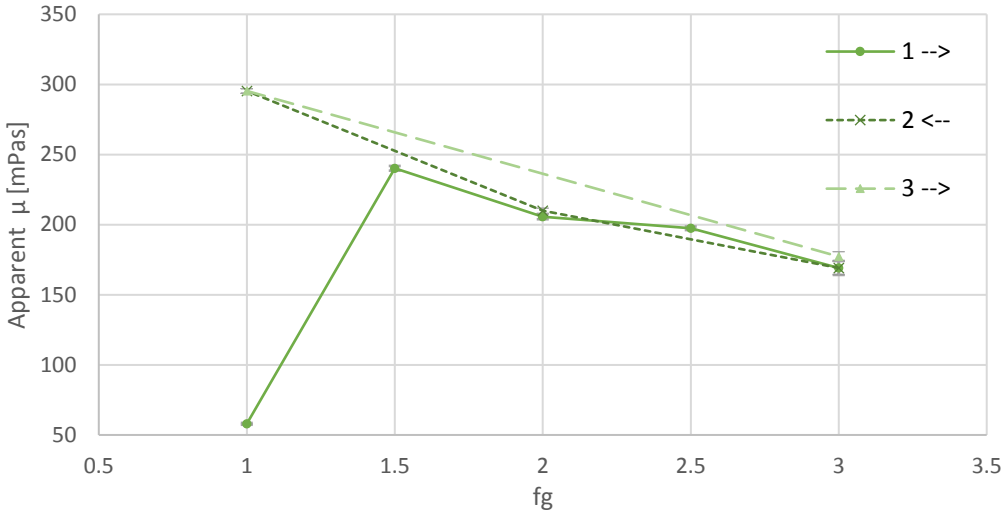

Figure 12.6 – Foam rate scan with apparent viscosity as a function of superficial velocity. Decreasing apparent viscosity for increased superficial velocity show a shear-thinning behavior for co-injection of CO_2 and NPA with SurfA at a constant gas fraction of 0.7 at 40°C and 175 bar. Superficial velocity was firstly increased from 1 ft/day to 3 ft/day (solid line). Due to abnormal behavior at 1 ft/day, the superficial was then reduced back to 1 ft/day (dark green dashed line) before increased to 3 ft/day (light green dashed line).

The Combined Effect of NPA and SurfB

Two foam quality scans were performed as co-injections of NPA and SurfB to study the combined effect of NPA with a cationic surfactant (SurfB) compared to the nonionic surfactant (SurfA) used in previous sections. SurfB is an amphoteric surfactant and acts as a cationic surfactant at low pH values (below 5). Cationic surfactants are the preferred surfactant choice for limestone reservoirs due to repulsive effects resulting in low retention (see Table 5.1, Chapter 5.1). Retention studies showed that pH reduction prior to injection in limestone was not sufficient to maintain stable SurfB-brine interactions, resulting in clouding of (cationic) SurfB (see Chapter 11.3). Retention studies were, however, not performed as co-injections with CO_2, and it was assumed that presence of CO_2 would sufficiently reduce the pH and maintain a stable surfactant injection.

Steady-state flow and stable pressures were achieved during co-injection of CO_2, NPA and SurfA in the previous sections, and apparent viscosity was therefore calculated as a measure of foam strength at variating foam qualities and injection rates. Stable pressures were not obtained for every gas fraction during co-injection of CO_2, NPA and SurfB, as seen for EDW11 (blue) and EDW10 (green) in Figure 12.7. Severe pressure fluctuations were observed for co-injection in EDW11 within each gas fraction and for increasing gas fractions. This behavior was suspected to be related to sleeve complications, as a damaged sleeve due to presence of CO_2 and water could cause leakage of confinement oil into the core, or leakage of CO_2 out of the core, and adversely affect foam stability. The co-injection in EDW11 was therefore stopped at f_g = 0.5.

A second co-injection of CO_2, NPA and SurfB was performed on EDW10 (green line in Figure 12.7). Similar results from co-injection in EDW11 was observed for EDW10: the differential pressure increased during f_g = 0.2, until a sudden pressure drop occurred. No measurable foam (differential pressure) was observed for f_g = 0.3. The gas fraction was therefore increased to 0.7, resulting in stable pressure measurements for increased f_g. Lower differential pressures for f_g above 0.7 imply that the optimal gas fraction was reached at f_g^* = 0.7 (or a lower gas fraction). Apparent viscosity was not calculated for all gas fractions during co-injections with CO_2, NPA and SurfB as stable pressures are required (see Equation 4.2). However, stable pressure at f_g = 0.9 and 0.95 in EDW10 demonstrate apparent viscosities of (19.6 ± 0.1) mPas and (12.7 ± 0.1) mPas, respectively. A significant increase in pressure gradient (above 120 bar/m) as the gas fraction was reduced from 0.95 to 0.5 (and increased from 0.5 to 0.7) indicates a strong hysteresis effect for foam stabilized by NPA and SurfB, with apparent viscosities above 80 mPas for f_g = 0.5 and f_g = 0.7.

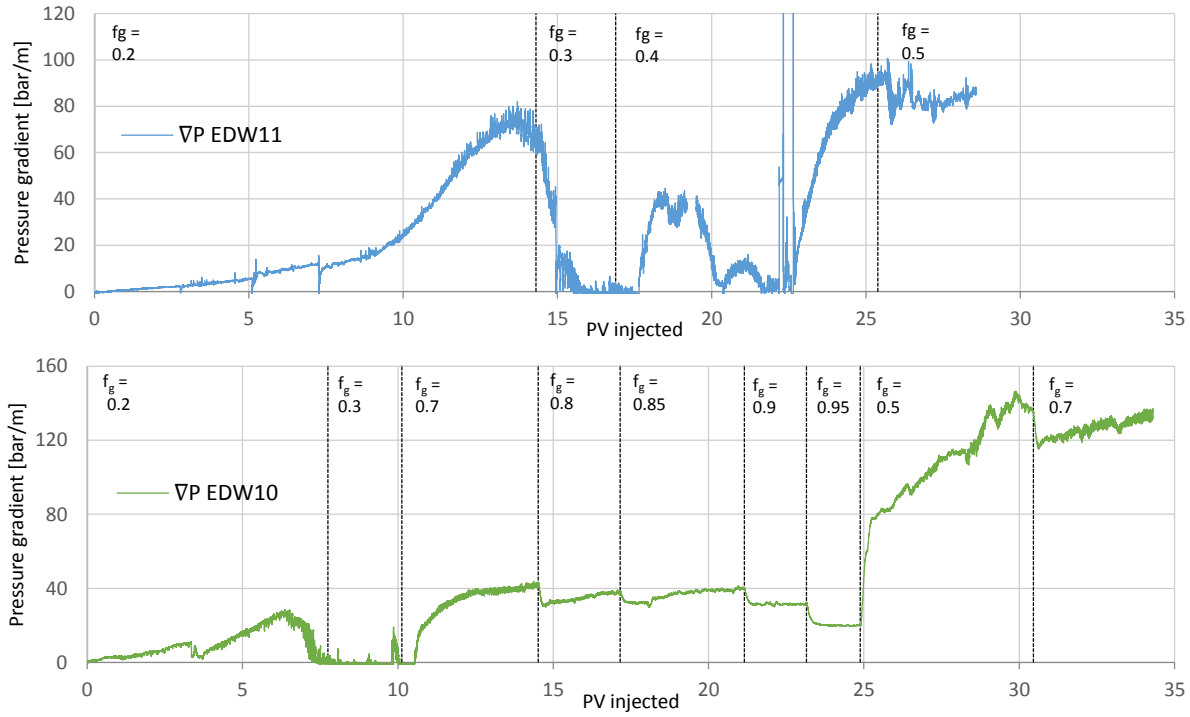

Figure 12.7 – Differential pressures during foam quality scan of EDW11 (blue) and EDW10 (green). Co-injection of CO_2, NPA and SurfB was conducted at 40°C and 175 bar pore pressure, with a superficial velocity of 1ft/day. Unstable foam is observed for fg =0.2 and 0.3, implying that the low CO_2 content (non-effective pH reduction) is not sufficient to maintain stable interactions between SurfB and brine.

Unstable differential pressures at low gas fractions were likely a result of clouding of SurfB caused by increasing pH due to dissolution of $CaCO_3$. Low pH values are required for SurfB to dissolve in brine and to act as a cationic surfactant. The acidic characteristic of CO_2 and brine were sufficient to maintain stable SurfB-brine interactions at high gas fractions, but the foam became unstable and collapsed at low gas fractions due to insufficient pH-reduction. However, all CO_2-foam EOR injections stabilized by NPA and SurfB were performed with f_g = 0.7, which were sufficient to maintain a stable surfactant dispersion and generation of stable foam. The optimal gas fraction was not determined for foam stabilized by NPA and SurfB, but f_g = 0.7 for foam EOR injections in the following sections were based on experiments conducted with NPA and SurfA. A comparison of foam strength during foam scans between NPA and SurfA or NPA and SurfB as foaming agents is not quantified, as differential pressures did not stabilize for all gas fractions during co-injection of NPA and SurfB.

13. Investigation of Foam Behavior with Presence of Oil

Foam screening with different types of foaming agents (switching between injecting only nanoparticles (NPA), only surfactants (SurfA) or a combination of NPA and SurfA) was performed in limestone cores and a sandstone core partially saturated with CO_2 and oil. A detailed description of injection fluids is listed in Table 13.1 for each core plug. The initial oil saturation was equal to the final oil saturation from the preceding CO_2-EOR injections (see Chapter 14), and fluid saturation was not quantified during foam screening because produced fluids were collected in the accumulator at the outlet (to achieve stable pressure gradients, see Chapter 7.4 for details). Oil was injected into the system simultaneously as CO_2 and foaming agent to maintain presence of oil in the core during foam screening.

This chapter focuses on the effect of oil on foam behavior, and only parts of the foam screening results will be discussed as many results were influenced by experimental difficulties when injecting CO_2 over extended periods. A comprehensive overview of the entire foam screening results are provided in Appendix B.

Table 13.1 – Overview of core used for foam screening with corresponding experimental parameters

Core	Injection fluid	Surf concentration [wt.%]	Experimental conditions	Brine
SS06	NPA CO_2 + NPA CO_2 + SurfA CO_2 + NPA +SurfA CO_2 + NPA + n-Decane CO_2 + SurfA + n-Decane CO_2 + NPA +SurfA + n-Decane	0.5	40°C / 140 bar	Brine C
EDW08	SurfA CO_2 + NPA +SurfA SurfA + n-Decane CO_2 + SurfA + n-Decane CO_2 + NPA +SurfA + n-Decane	0.5	40°C / 120 bar	Brine A
EDW09	Brine SurfA CO_2 + SurfA CO_2 + NPA +SurfA Brine + n-Decane CO_2 + NPA +SurfA + n-Decane	0.5	60°C / 115 bar	Brine A

Pressure gradients during foam screening in EDW08 (blue) and EDW09 (green) are shown in Figure 14.1 as a function of time and not PV injected due to frequent stops in the injection that influenced foam behavior. The pressure gradients were measured during co-injection of CO_2, NPA, SurfA and n-Decane subsequent to co-injection of CO_2, NPA, SurfA without presence of oil (time = 0 equals start of n-Decane injection). A decreasing pressure gradient, i.e. foam coalescence, was observed when oil was injected in EDW08. This detrimental effect of oil coincides with theory discussed in Chapter 4.3 and with results obtained during bulk foam tests in Chapter 10. The pressure gradient attained during foam screening in EDW09 (green line) did, however, not coincide with a detrimental foam effect: a distinct increase in pressure gradient was observed as oil was injected.

Foam stabilized by NPA and SurfA was generated prior to oil injection in both cores. However, the initial condition of the foam before oil injection (time = 0) varied for the two core plugs. CO_2, NPA and SurfA were continuously injected for 42 hours in EDW09 prior to oil injection. In EDW08, an extended shut-in period and subsequent foam coalescence prior to a 1 hour continuously foam generation before oil injection may have caused a weaker initial foam. It is therefore assumed that the initial foam in EDW08 was weaker and more unstable compared to the foam in EDW09. The difference in foam state can explain why the injection of oil had a detrimental effect on foam in EDW08, whereas the pressure gradient increased during oil injection for EDW09. The stable, pre-generated foam appeared to be further strengthened by the injected oil.

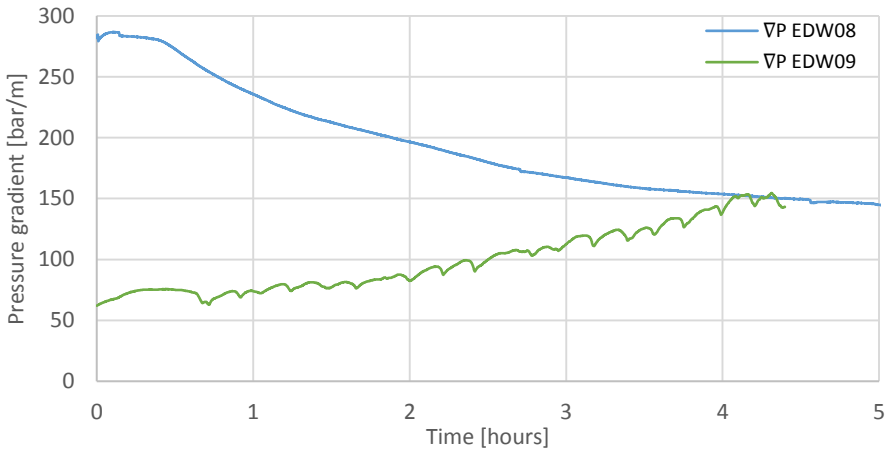

Figure 14.1 – Pressure gradient as a function of time during foam screening in EDW08 (blue line) and EDW09 (green line) during co-injection of CO_2, NPA, SurfA and n-Decane. Time = 0 indicates the start of oil injection, which was injected after 1 hour of CO_2-foam injection (after an extended shut-in period) in EDW08 and after 42 hours of CO_2-foam injection in EDW09.

The increased pressure gradient in EDW09 due to oil injection indicates that other mechanisms than foam generation contributed to the incremental pressure gradient. Foaming agents may also act as emulsifying agents, which are required for emulsion generation. Emulsions may positively influence oil production by blocking high-permeable layers and consequently increase the differential pressure (see Chapter 5.3). Emulsion generation may explain the pressure increase observed during foam screening in EDW09, and further investigation of presence of emulsion is therefore executed in the following chapter.

14. CO_2 Foam EOR in Oil Saturated Limestone Cores

CO_2-foam EOR injections were conducted to investigate the feasibility of using nanoparticles (NPA) and surfactants (SurfA or SurfB) separately or combined as CO_2 foaming agents in limestone. The feasibility of combining the two foaming agents was quantitatively analyzed by measuring oil recovery efficiency and pressure gradients during tertiary (post waterflood) co-injection of CO_2, NPA and/or surfactants for in-situ foam generation. A total of 8 CO_2-foam EOR injections were conducted at different experimental conditions (see Table 14.1) indicating a miscible displacement of CO_2 and n-Decane (c.f. Figure 3.3). 1 PV of brine was injected during all waterfloods, whereas co-injection was conducted as long as oil production was observed. The gas fraction during co-injections was 0.7 based on foam scan results from Chapter 12.

Foaming agent ability to stabilize CO_2-foam was evaluated based on the total oil recovery ($R_{F,co-inj}$) achieved during co-injection compared to waterflooding ($R_{F,wf}$), as oil recovery during waterflooding varied for each core. Foaming agent-stabilized foam was benchmarked against a baseline with co-injection of CO_2 and brine. This chapter demonstrates that a combination of nanoparticles and surfactants can be utilized as a foaming agent for enhanced oil recovery in limestone. At the experimental conditions used in this experimental work, foam stabilized by NPA and SurfB provided higher oil recovery efficiency and pressure gradients compared to the combination of NPA and SurfA. All co-injections combining nanoparticles and surfactants demonstrated high pressure gradients, but it was uncertain whether the high pressures were a result of strong foam and/or emulsions. This chapter also highlights the importance of measuring oil content of produced emulsions, as oil recovery efficiencies were significantly increased when emulsified oil production was taken into account.

Table 14.1 – Cores used for CO_2-foam EOR injections with respective experimental properties

Core	Injection fluid	Surf concentration [wt.%]	Superficial velocity [ft/day]	Experimental condition	Brine
EDW18	CO_2 + Brine	-	2	40°C / 175 bar	Brine A
EDW16	CO_2 + NPA	-			
EDW17	CO_2 + SurfB	1			
EDW13	CO_2 + NPA +SurfB	1			
EDW15	CO_2 + NPA +SurfB	1			
EDW07*	CO_2 + NPA +SurfA	1		40°C / 120 bar	
EDW08	CO_2 + NPA +SurfA	0.5		40°C / 120 bar	
EDW09	CO_2 + NPA +SurfA	0.5		60°C / 115 bar	

* Pre-flush of surfactant prior to drainage: water production from drainage and oil production from waterflooding could not be quantified due to production of emulsions

14.1 Baseline – Co-injection of CO_2 and Brine

Co-injection of CO_2 and brine was conducted in limestone (EDW18) to establish volumetric oil recovery without presence of a foaming agent, serving as a benchmark for future foam injections stabilized by foaming agents. The baseline was compared with CO_2-foam EOR injections conducted at similar experimental conditions (Chapter 14.3).

Oil recovery and corresponding pressure gradients during waterflooding and CO_2-foam injection are plotted as a function of pore volumes (PV) injected in Figure 14.1. Rapid, constant oil production was observed during the waterflood before a clean water cut after water breakthrough. This behavior during waterflood is expected, as Edwards limestone is strongly water-wet. An immediate increase in oil production was observed during co-injection of CO_2 and brine, with a final recovery of 64.7 % of original oil in place (OOIP), see Table 14.2. Pressure gradients obtained during waterflooding and co-injection show that no foam was generated during co-injection (no increasing pressure gradient). Severe pressure fluctuations during co-injection was caused by production of sudden slugs of fluids through the BPR.

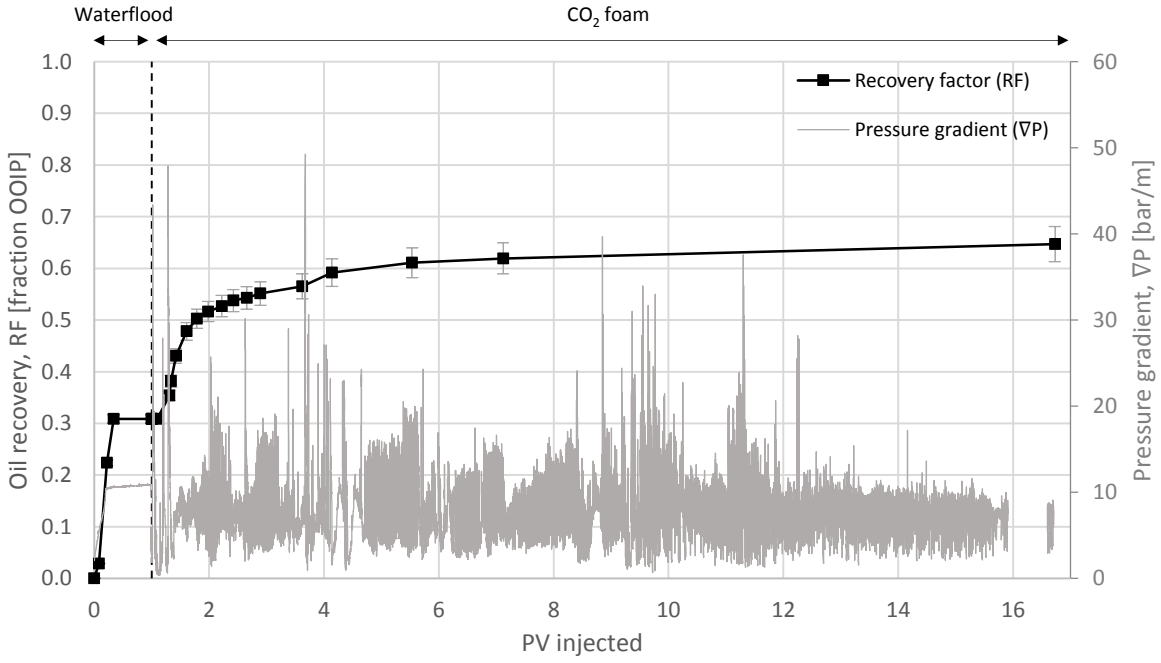

Figure 14.1 – Oil recovery and pressure gradient as a function of PV injected during waterflood (1 PV) and tertiary co-injection of CO_2 and brine (baseline). The baseline was conducted on EDW18 with a superficial velocity of 2 ft/day at 40°C and 175 bar. Sudden slugs of produced fluid through the BPR caused pressure fluctuations during the CO_2-foam injection. Connection issues with the differential pressure transmitter resulted in lack of pressure data at 16 PV injected.

Theoretically, 100% of oil from a core plug can be produced during a miscible displacement of CO_2 and n-Decane if the displacement is given sufficient time for diffusion (discussed in Chapter. 3.3). The co-injection was therefore injected for almost 17 PVs to observe the effect of diffusion. However, co-injected brine reduces CO_2-oil mixing by water shielding, as CO_2 must diffuse through the water layer for oil swelling and mobilization of trapped oil (see Chapter 3.4). Increased water saturation as a consequence of waterflooding will also have a shielding effect and reduce oil production rate. However, diffusion and water shielding are more pronounced in fractured core plugs. Edwards limestone is an unfractured carbonate rock, where forced extrusion of CO_2 through the core matrix supplies a viscous recovery component in addition to diffusion.

Foaming agent performance was evaluated during CO_2-foam EOR injections by comparing increased pressure gradients and oil recovery obtained during co-injection compared to pressure gradients and oil recovery during waterflooding. Although no stable foam was generated during co-injection of CO_2 and brine (negative ∇P increase), $\Delta R_{F,final}$ was evaluated to serve as a benchmark for foam stabilized by foaming agents in the following sections. Static parameters used for further comparison is listed in Table 14.2, with corresponding uncertainties for key values.

Table 14.2 – Static parameters for baseline with co-injection of CO_2 and brine

Core	**∇P increase [% of waterflood]**	**$R_{F,\,wf}$ [% OOIP]**	**$R_{F,\,co\text{-}inj}$ [% OOIP]**	**$\Delta R_{F,\,final}$ [%* OOIP]**
EDW18 (baseline)	-36 ± 13	30.9	64.7	34 ± 2

14.2 Co-injection of CO_2, NPA and SurfA

Oil recovery and corresponding pressure gradients during waterflooding and CO_2-foam injection stabilized by NPA and SurfA in EDW08 and EDW09 are plotted as a function of pore volumes (PV) injected in Figure 14.2. The pressure gradient for EDW07 is also shown despite not being able to measure oil production as a pre-flush of surfactants prior to drainage caused production of emulsion (discussed in detail in Section 14.3). Rapid, constant oil production was observed during the waterflood before a clean water cut after water breakthrough. An increase in oil production was observed during co-injection, with a final incremental oil recovery, $\Delta R_{F,final}$, of 9.2 and 7.2 %* (percentage points) OOIP for EDW08 and EDW09, respectively. Recovery values are also listed in Table 14.3.

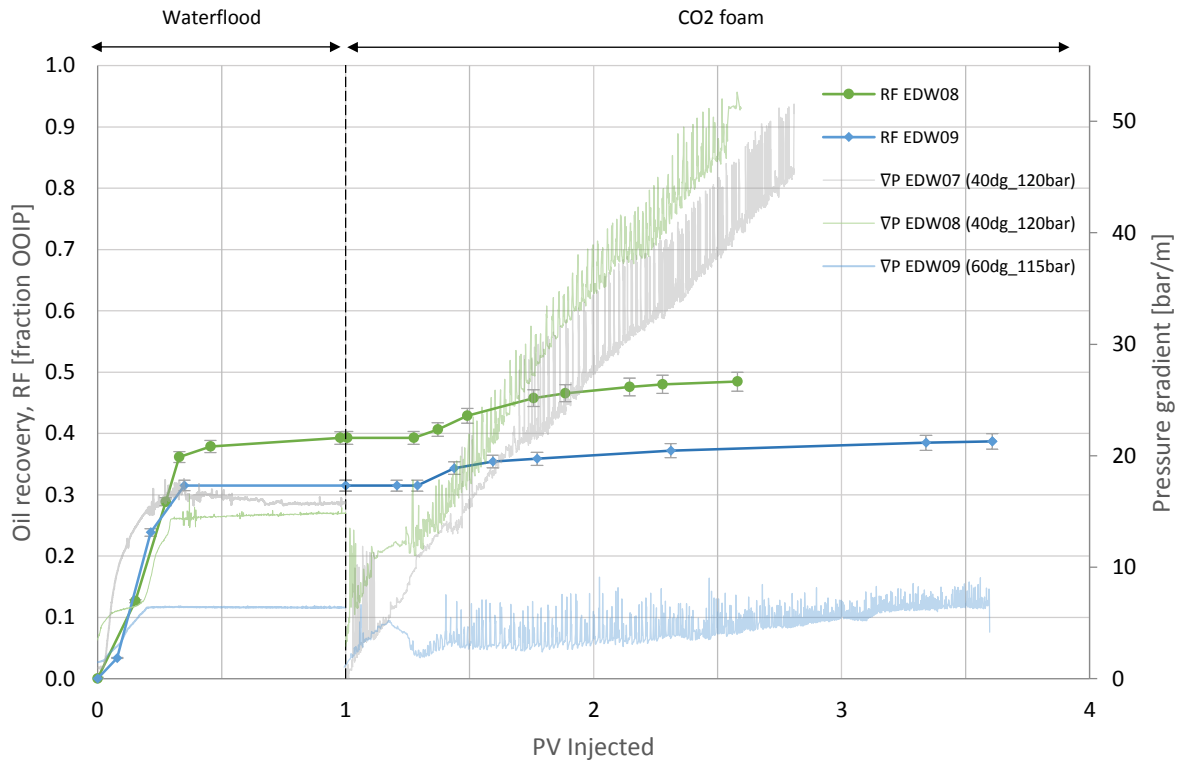

Figure 14.2 – Oil recovery and pressure gradient during waterflood (1PV) and co-injection of CO_2, NPA and SurfA as a function of PV injected for EDW08 (green) and EDW09 (blue). Pressure gradient for EDW07 is shown in grey. A significantly higher pressure gradient is observed during co-injection in EDW08 and EDW07 compared to EDW09. A low increase in pressure gradient obtained during co-injection relative to waterflooding (7.6%) indicate that a weak (or no) foam is generated in EDW09.

Foam strength is evaluated based on the average pressure gradient (∇P) obtained during co-injection compared to waterflooding (measured during the last 0.1 PV injected). A significantly higher pressure gradient was achieved for EDW08 than for EDW09 (see Table 14.3), and it appeared as a weak foam was generated in EDW09. Based on Figure 3.3 (Chapter 3.2), it is assumed that the experimental pressure used in these co-injections are above the minimum miscibility pressure (MMP) for CO_2 and n-Decane. However, experimental conditions for EDW09 (60°C and 115 bar) are closer to the line indicating MMP than for EDW08 (40°C and 120 bar), and it is possible that miscibility was not obtained for EDW09. All further CO_2-foam EOR injections in limestone were therefore conducted at higher pressures to ensure miscibility between CO_2 and n-Decane. Nevertheless, co-injection of CO_2, NPA and SurfA in EDW08 demonstrate that the combined effect of nanoparticles and surfactants can be utilized as a foaming agent for enhanced oil recovery. A more comprehensive study of the effect of surfactant type is presented in Chapter 14.4.

Table 14.3 – Static parameters for co-injection of CO_2, NPA and SurfA in EDW08 and EDW09

Core	Experimental conditions	PV injected	∇P increase [% of waterflood]	$R_{F, wf}$ [% OOIP]	$R_{F, co\text{-}inj}$ [% OOIP]	$\Delta R_{F, final}$ [%* OOIP]
EDW08	40°C / 120 bar	2.6	222 ± 16	39.9	48.5	9.2 ± 0.4
EDW09	60°C / 115 bar	3.6	8 ± 11	31.5	38.7	7.2 ± 0.3

14.3 Co-injection of CO_2, NPA and SurfB

Co-injection of CO_2 and separate and/or combined use of NPA and SurfB as foaming agents were conducted in limestone at 40°C and 175 bar pore pressure. The cationic surfactant (SurfB) was chosen because it is the preferred surfactant type in limestone cores (see Table 5.1). All experimental parameters were held constant to focus on the effect of foaming agents. Foaming agent-stabilized CO_2-foam was benchmarked against the baseline with co-injection of CO_2 and brine (Chapter 14.1). The optimal gas fraction was not determined for the combination of NPA and SurfB, but 0.7 was chosen based on experiments conducted with NPA and SurfA in Chapter 12.

Oil recovery and corresponding pressure gradients during waterflooding and CO_2-foam injection are plotted as a function of PV injected in Figure 14.3, where different colors represent different foaming agents: green for NPA (EDW16), orange for SurfB (EDW17) and blue for NPA and SurfB (light blue for EDW13, dark blue for EDW15). The black line represents the baseline discussed in the previous section. Each co-injection with foaming agent has a corresponding dashed line of similar color illustrating a significant increase in oil recovery. These dashed lines represent additional oil recovery obtained from measuring oil content of produced emulsions. Observed pressure gradient drop for EDW13, EDW15 and EDW17 is a result of reduced injection rate. Volumetric uncertainties are listed in Appendix C.

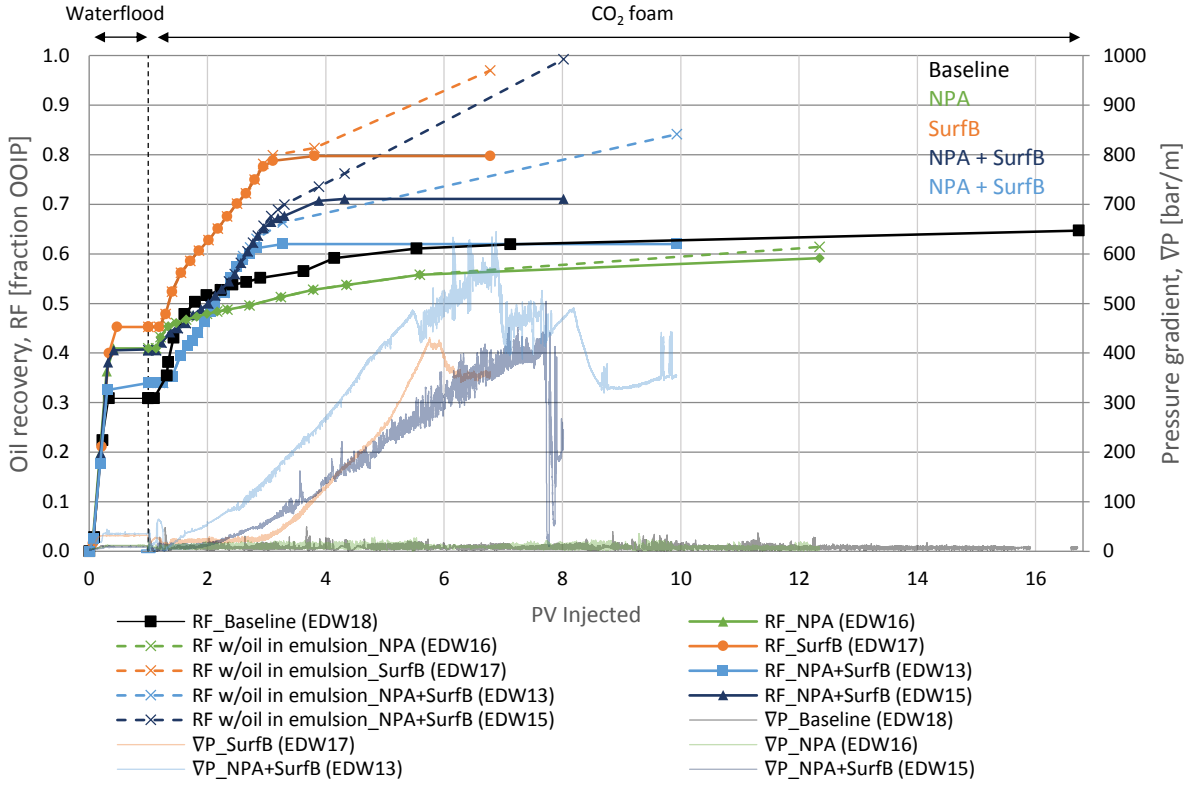

Figure 14.3 – Oil recovery and pressure gradient during waterflood and co-injection of CO_2 and foaming agent, where foaming agents are differentiated by colors: green for NPA (EDW16), orange for SurfB (EDW17), blue for NPA + SurfB (light for EDW13 and dark for EDW15) and black for the baseline. Solid lines are oil recovery without considering oil in emulsions, whereas additional oil content in emulsions is represented by dashed lines. The observed pressure gradient drop for EDW13, EDW15 and EDW17 is a result of reduced injection rate.

The Effect of Foaming Agent

The effect of different foaming agents was quantitatively analyzed by comparing oil recovery efficiency and increase in apparent viscosity during co-injection (see Figure 14.3 and Table 14.4). Oil recovery during co-injection ($R_{F,co-inj}$), and consequently final incremental oil recovery ($\Delta R_{F,final}$), was based on the total oil production achieved with oil in emulsions (discussed in detail in Chapter 14.4). The injection rate was reduced during several of the co-injections due to pressure limitations of the experimental setup. Foam strength is therefore not evaluated by increasing pressure gradients, but as an increase in apparent viscosity during co-injection compared to apparent viscosity measured during the waterflood. Apparent viscosity is a function of differential pressure and injection rate (see Eq. 4.2). Uncertainties associated with key values are listed in Table 14.4.

Table 14.4 – Static parameters for baseline co-injection and co-injection of CO_2 and foaming agent

Core	Foaming agent	PV injected	μ_{app} increase [% of waterflood]	$R_{F,wf}$ [% OOIP]	$R_{F,co-inj}$ [% OOIP]	$\Delta R_{F,final}$ [%* OOIP]
EDW18 (baseline)	-	16.7	-36 ± 13	30.9	64.7	34 ± 2
EDW16	NPA	12.4	-52 ± 17	41.0	61.4	20 ± 4
EDW17	SurfB	6.8	4379 ± 50	45.3	97.0	52 ± 9
EDW13	NPA + SurfB	9.9	8106 ± 469	34.0	84.1	50 ± 4
EDW15	NPA + SurfB	8.0	9720 ± 1031	40.6	99.2	59 ± 7

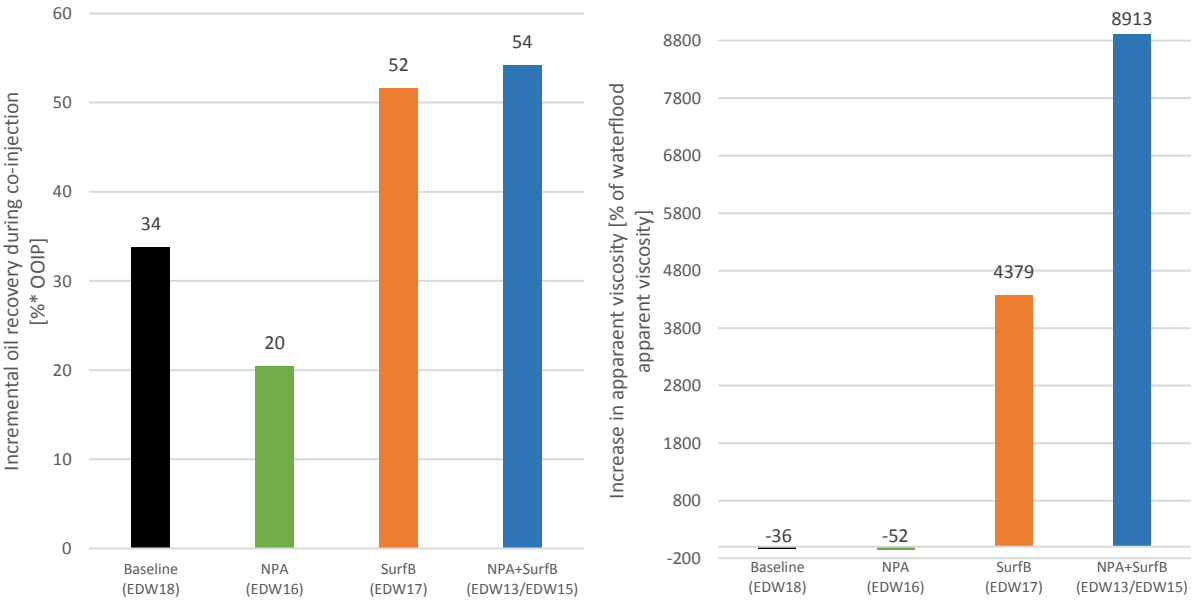

Figure 14.4 – Incremental oil recovery (left) and increase in apparent viscosity during co-injection compared to waterflood (right). Each color represents different foaming agents. The blue column for NPA and SurfB as foaming agents is an average based on results from experiments conducted on EDW13 and EDW15. The negative values for apparent viscosity increase obtained for the baseline and for NPA-stabilized foam is a result of lower pressure during co-injection than during waterflooding.

Incremental oil recovery is compared with the increase in apparent viscosity during CO_2-foam EOR injections in Figure 14.4. The measured apparent viscosity obtained during co-injection of CO_2 and NPA was lower than apparent viscosity measured during the waterflood (similar to the baseline), suggesting that no foam was generated with NPA as foaming agent. The incremental oil recovery achieved during co-injection of CO_2 and NPA is also less compared with the baseline. However, NPA has proven to stabilize foam during production of crude oil (in sandstone) at a higher temperature and lower pressure (Rognmo et al., 2018a; Rognmo et al., 2018b). The lack of foam generation with NPA can be a result of higher experimental pressure and increased pH caused by dissolution of $CaCO_3$ in limestone. Silica nanoparticles are highly hydrophilic at high pH, reducing the ability to stabilize foam with and without the presence of oil (Binks et al., 2008; Binks et al., 2007). However, when mixed with a cationic surfactant (SurfB), surfactants monomers adsorb onto the nanoparticle surface making it less hydrophilic (Binks et al., 2007). The effect of pH can explain why significantly higher oil recovery and apparent viscosity is observed when NPA is mixed with SurfB.

The average incremental oil recovery during co-injection of CO_2, NPA and SurfB (54 %) is slightly higher than achieved during the separate use of SurfB as foaming agent (52%). The incremental apparent viscosity, however, is two times higher with the combined use of NPA and SurfB, indicating generation of stronger foam. Surfactants generate strong foams, whereas nanoparticles act for as foam stabilizers, and an even stronger foam is achieved by combining SurfB and NPA compared with the separate use of SurfB. In addition, apparent viscosity values during co-injection of CO_2 and SurfB with and without NPA are underestimated, as pressure gradients during these co-injections did not stabilize before the injections were stopped. Nevertheless, higher oil recovery and substantially greater apparent viscosity is observed for both SurfB and the combination of NPA and SurfB compared with the separate use of NPA.

Emulsion Production

A collection of produced fluids during the baseline co-injection is shown in Figure 14.7 (left). A meniscus separated oil (on top) and brine (bottom), and both phases were transparent. Produced fluids during co-injection of CO_2, NPA and SurfB is displayed to the right, where the first cylinders resemble cylinders from the baseline. At increased PV injected, however, the transparent, aqueous foaming agent phase was replaced by a white, "milky" phase of oil-in-water emulsions. These o/w emulsions were also observed during co-injection of NPA and SurfA in EDW08 and EDW09 (Chapter 14.2), but it was assumed that the emulsions contained an insignificant amount of oil. Produced emulsions have previously been observed by the Reservoir Physics group at the Department of Physics and Technology but without further investigation of oil content.

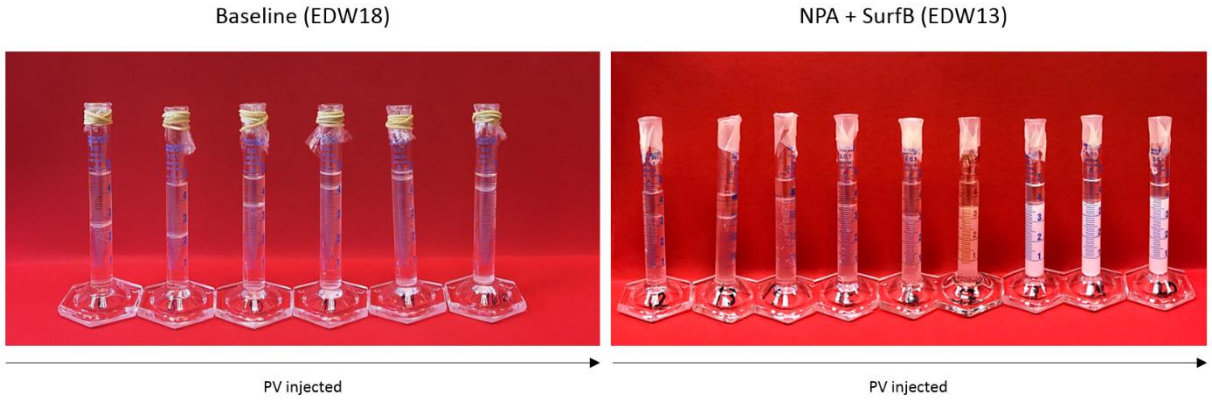

Figure 14.7 – Produced fluids of co-injection during baseline (left) and with NPA and SurfB as foaming agents (right). The three last cylinders to the right show distinct, "milky" emulsions produced during co-injection of CO_2, NPA and SurfB.

Emulsions were observed at the end of each co-injection with CO_2 and foaming agent. Produced fluids were collected in graded cylinders for as long as a measurable amount of oil was produced. As oil recovery decreased to the point where visible oil production was limited and only emulsions were observed, produced fluids were redirected into a glass beaker. Oil content was determined by measuring the density of the produced emulsion, based on density differences between n-Decane and the injected foaming agent dispersed in brine. Density measurements revealed significant amounts of oil in the emulsified phase (as seen in Figure 14.3 and 14.5). The substantial oil quantity was also proven by observing produced fluids over a period of days: the oil phase continuously increased as the "milky" emulsion phase decreased over time. Results shown in Figure 14.3 emphasize the importance of measuring oil content in produced emulsions, as the amount significantly increased the total oil recovery.

14.4 The Effect of Surfactant Type

Figure 14.5 compares oil recovery during waterflood (blue) and co-injection (green) for all co-injections of CO_2 and foaming agent/brine conducted in limestone. The dashed line separates CO_2-foam EOR injections performed under deviating experimental conditions (left) and at 40°C and 175 bar pore pressure (right). The figure emphasizes the importance of calculating oil content of produced emulsions (light green color). Small amounts of emulsions were produced during co-injection of NPA and Surf A (EDW08 and EDW09), but the oil content was not investigated as it was assumed to be negligible. However, the low oil recovery during co-injection of NPA and SurfA implies that the added emulsion oil volume would only contribute to a small increase in total oil recovery. It should be noted that the CO_2-foam stabilized by NPA and SurfA (to the left) was injected for a substantially shorter period than results to the right (see Table 14.3 and 14.4).

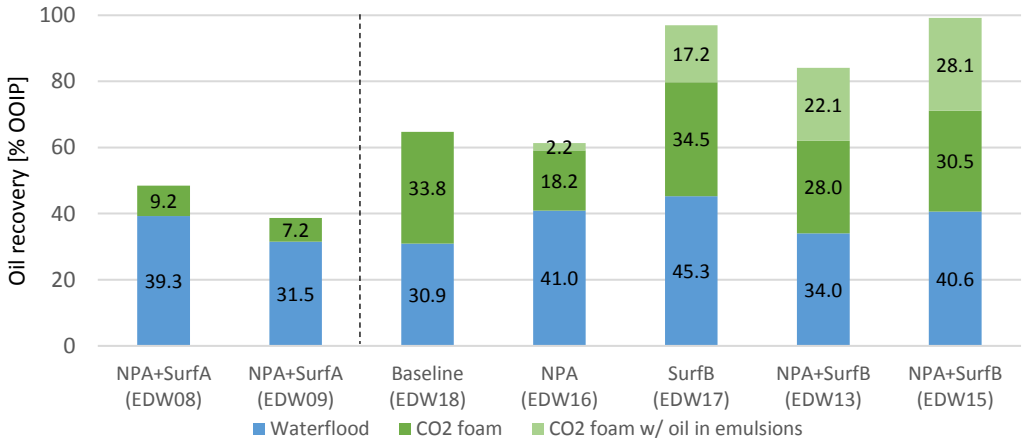

Figure 14.5 – Oil recovery (% of OOIP) during all co-injections of CO_2 and foaming agent/brine. The dashed line separates co-injections performed under deviating conditions and surfactant concentration (left) and at 40°C and 175 bar (right). The different colors represent different measurements: oil recovery during waterflood (blue), oil recovery during co-injection without considering oil content of emulsions (dark green) and oil recovery during co-injection with added oil volume from emulsions (light green). The uncertainty associated with emulsion content is more significant compared to waterflood and co-injection, as density calculation uncertainties are added to the uncertainty of produced fluids.

Incremental apparent viscosity during co-injection compared to the waterflood for all co-injections is shown in Figure 14.6. Generation of foam was observed during co-injection of NPA and SurfA, but the foam strength was considerably weaker than for foam achieved during co-injection of NPA and SurfB. The weak foam may be explained by the surface charge, as nonionic surfactants (SurfA) possibly do not adsorb on the negative silica nanoparticle surface. However, increased oil recovery and apparent viscosity can also be a result of different experimental conditions or the difference in surfactant concentration.

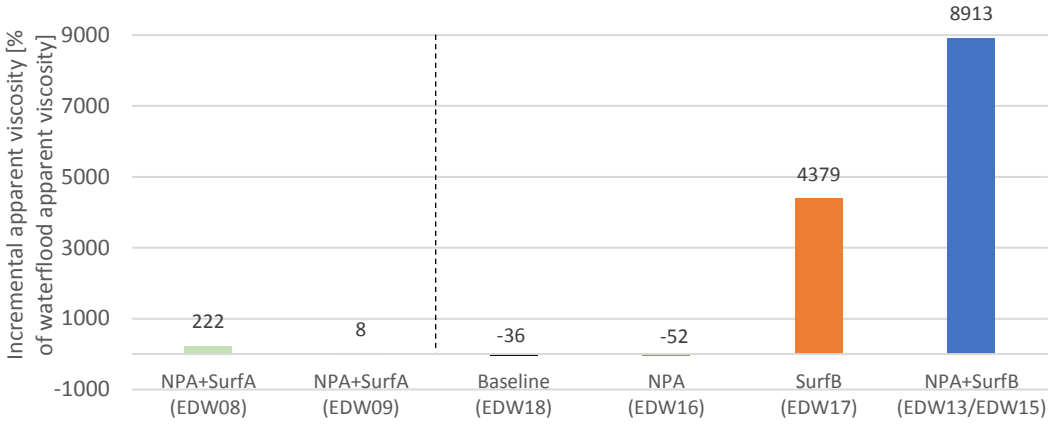

Figure 14.6 – Incremental apparent viscosity during co-injection compared to waterflood for different foaming agents. The blue column for NPA and SurfB as foaming agents is an average based on results from experiments conducted on EDW13 and EDW15. The dashed line separate co-injections performed under deviating conditions (left) and at and at 40°C and 175 bar (right).

Incremental Pressure Mechanisms

Foam generation adds a viscous component to the oil recovery process in addition to diffusion, resulting in high differential pressures and an increase of gas apparent viscosity. High apparent viscosity is therefore a measure of foam strength, indicating generation of strong foam for CO_2-foam stabilized by SurfB or SurfB combined with NPA. However, as discussed in Chapter 5.3, presence of emulsions also increase differential pressures and apparent viscosities. Often associated with high viscosity values, emulsions can restrict fluid flow through high-permeable layers and redirect fluids to low-permeable layers (Schramm, 1992). This high-permeable blocking effect resembles the effects of foam generation, and differential pressures will increase if the oil droplet size in emulsions exceeds the pore throat size.

Comparison of pressure gradients and oil recovery during co-injection in Figure 14.3 shows an increase in pressure gradient as oil recovery decreases. Foam generation does not occur if the oil saturation is higher than a specific maximum value (see Chapter 4.3), and it appeared as stronger foam was generated as oil saturation decreased. Increasing pressure gradients with decreasing oil saturation may therefore argue that foam generation was the primary mechanism for increased pressure gradients. On the other hand, the pressure gradient in Figure 14.2 displaying co-injection of CO_2, NPA and SurfA for EDW07 (in grey) indicates that pressure buildup could partially be a result of emulsions, as only emulsions were produced during this experiment, and emulsions were suspected to be present in the core from the initiation of the co-injection.

For reasons mentioned above, it is evident that further investigation is required for determining the primary mechanism of increased differential pressure, and to determine how foam is generated and affected by nanoparticles and surfactants in the presence of oil. Emulsions were visibly produced at the outlet, but emulsion generation could be a result of production through the BPR. Generation and behavior of foam and emulsions in porous media are complex processes that should be visually investigated via micromodels or imaging techniques. The significant differential pressures achieved during CO_2-foam EOR injections can cause injectivity issues in petroleum reservoirs, where limitations in injection well pressure and formation fracture pressures must be considered (Haugen et al., 2014). It is therefore crucial to determine the cause of increased pressure to be able to control reservoir pressures at field scale.

15. CO_2 Storage Potential in Sandstone and Limestone Cores

A quantitative investigation of carbon storage potential was conducted in sandstone and limestone cores to examine the possibility of carbon neutral/negative oil production during CO_2-foam EOR and pure CO_2 EOR (see Table 15.1). Supercritical CO_2 is beneficial for CO_2-storage because more carbon molecules can be stored per volume unit. The experimental conditions were therefore selected for optimum storage conditions (dense CO_2). Carbon storage potential was also calculated for all CO_2-foam EOR injections in limestone (see Chapter 14). This chapter shows that carbon negative oil production was achieved during co-injection of CO_2-foam in sandstone and during NPA-stabilized foam (with and without SurfA) in limestone, and that generation of foam and/or emulsions is beneficial for CO_2 storage. The storage potential was quantitatively determined by comparing the mass of carbon stored to the mass of carbon produced during combustion of hydrocarbon (mass element exchange). The section also emphasizes the effect of limestone dissolution on CO_2 storage capacity. Carbon calculations performed in this thesis do not consider the industrial effort and subsequent release of CO_2 associated with carbon capture, transport and storage.

Table 15.1 – Experimental parameters for CO_2-foam and CO_2 EOR injection

Core	Injection fluid	Superficial velocity [ft/day]	Experimental conditions	Brine
SS06	CO_2 + 0.5 wt.% SurfA	2	40°C / 140 bar	C
	CO_2			

15.1 Mass Element Exchange of Carbon

Physical and geochemical mechanisms of CO_2 trapping are discussed in Chapter 6.1. The rapid process of residual trapping was likely the primarily mechanism of CO_2 trapping during CO_2-foam EOR injections performed in this thesis, with CO_2 stored as a free phase. The volume of stored carbon dioxide (V_{CO_2}) as free phase was calculated based on material balance:

$$V_{CO_2} = PV - V_w - V_{HC} \tag{15.1}$$

where PV is the pore volume and V_w and V_{HC} are the volumes of water and hydrocarbons occupying the pore space, respectively. The physical properties of CO_2 (density and viscosity) are highly dependent on temperature and pressure (see Chapter 3.1), and these properties will consequently affect the amount of carbon stored in a reservoir. It is therefore beneficial to calculate the number of carbon atoms stored per unit reservoir volume, usually expressed as mol per unit volume (molar concentration).

Combustion of produced hydrocarbons releases CO_2 (see Eq. 6.1), and the produced amount of hydrocarbons must therefore be accounted for. The efficiency of carbon utilization and storage was quantitatively determined by mass element exchange (MEE), defined as the ratio of mass elements of carbon stored ($N_{C,stored}$) to the mass element of carbon produced during combustion ($N_{C,prod}$) of hydrocarbons recovered during CO_2-foam EOR injections (and pure CO_2 injection for SS06). CO_2-foam EOR injections are considered carbon neutral or carbon negative if the amount of stored carbon dioxide is equal to, or exceeds, the amount of carbon dioxide released during hydrocarbon combustion:

$$\frac{N_{C,stored}}{N_{C,prod}} > 1 \rightarrow Carbon\ negative\ oil\ production$$

$$\frac{N_{C,stored}}{N_{C,prod}} = 1 \rightarrow Carbon\ neutral\ oil\ production$$

$$\frac{N_{C,stored}}{N_{C,prod}} < 1 \rightarrow Carbon\ positive\ oil\ production$$

The total amount of carbon atoms stored is given as:

$$N_{C,stored} = V_{CO_2} \cdot c_{CO_2} \tag{15.2}$$

where c_{CO_2} is the molar concentration of CO_2. The amount of carbon released during hydrocarbon combustion was calculated as:

$$N_{C,prod} = V_{HC,prod} \cdot c_{HC} \cdot \gamma \tag{15.3}$$

where $V_{HC,prod}$ is the volume of produced hydrocarbons, c_{HC} is the molar concentration of the hydrocarbons and γ is the average number of carbon atoms in the hydrocarbon molecules. All hydrocarbons (except methane) consist of more than one carbon atom, and γ is therefore dependent on the oil composition. The oleic phase during all CO_2-foam EOR injections conducted in this thesis was n-Decane with γ = 10.

Oil recovery during tertiary co-injections and corresponding MEE is shown in Figure 15.1, with red lines representing a critical MEE (cMEE) specifying carbon neutral oil production. Carbon negative oil production is achieved when MEE exceeds the cMEE, which were profoundly affected by the experimental conditions as temperature and pressure determine the density of CO_2 and n-Decane.

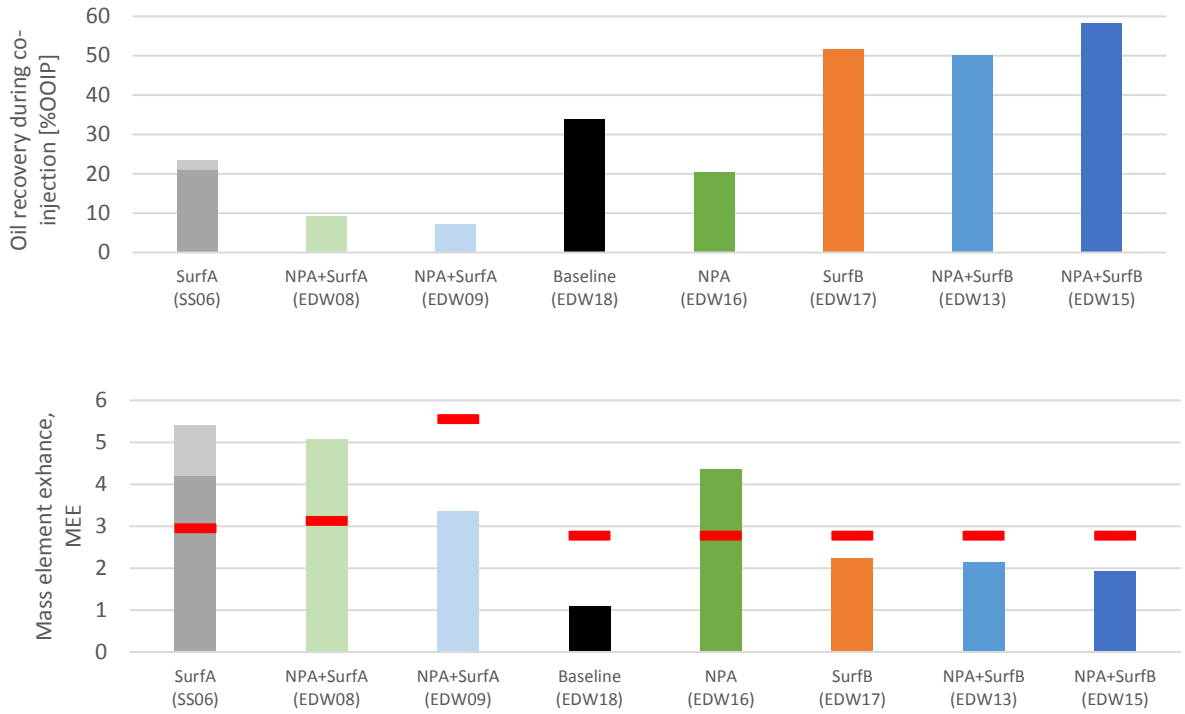

Figure 15.1 – Oil recovery (top) and corresponding mass element exchange (bottom) during co-injection of CO_2 and foaming agent (differentiated by colors). A pure CO_2 injection (light grey) was conducted in SS06 subsequent to the CO_2-foam injection (darker grey). Red markers indicate the critical MEE (cMEE), above which carbon negative oil production were achieved.

Carbon negative oil production was achieved during co-injection of CO_2 and SurfA in sandstone (SS06) and CO_2 and NPA with and without SurfA in limestone (EDW08 and EDW16). A trend of high MEE was observed for low oil recovery. Carbon negative oil production was, however, not achieved during co-injection of NPA and SurfA (EDW09) despite low oil recovery efficiency. This is explained by the difference in experimental conditions: higher experimental temperature (60°C compared to 40°C) reduces the CO_2 density, increasing the amount of stored CO_2 required to neutralize the amount of CO_2 produced during combustion of recovered hydrocarbons.

The aim of carbon negative oil production (store more CO_2 than produced during hydrocarbon combustion) is, to some extent, contradicting the aim of conventional oil recovery (produce as much hydrocarbons as possible), as high oil recovery reduces the MEE. However, higher MEE was achieved during co-injection of CO_2 and SurfB (with and without NPA) compared with the baseline, despite lower oil recovery during baseline. This suggests that generation of foam and/or emulsions is beneficial for CO_2 storage, with an increased water displacement relative to the baseline. The ratio between brine and oil production is lower during the baseline, resulting in low MEE.

15.2 Limestone Dissolution during Co-Injection of CO_2 and Foaming Agent

Six limestone core plugs were scanned with a computerized tomography (CT) at Haukeland University Hospital (HUS) prior and after CO_2-foam injections to qualitatively study the effect of limestone dissolution. Results from three cores (EDW09, EDW10, and EDW12) will be presented in this section to highlight the effect of dissolution on CO_2 storage potential.

Alteration of the limestone core was observed visually at the external surface after CO_2-foam injections (see Figure 15.2). The acidic flow of brine and supercritical CO_2 induce mineral dissolution of limestone, causing formation and growth of cavities, called vugs, and large-scale preferential channels for fluid flow (Espinoza et al., 2011). The dissolution was most eminent at the rock surface at the core inlet.

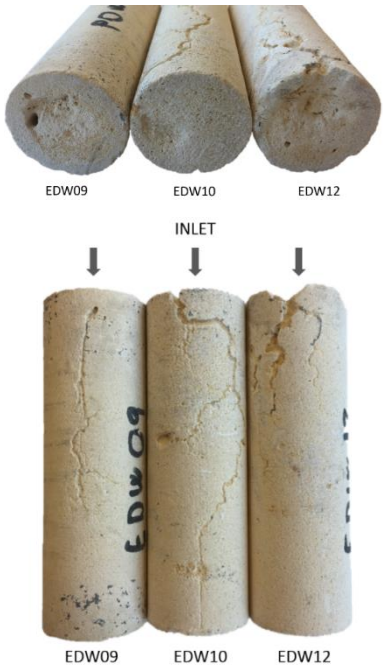

Figure 15.2 – Dissolution of limestone cores caused by acidic mixture of CO_2 and brine during CO_2-foam co-injections. Formation of large-scale preferential fluid flow channels (bottom) and severe dissolution at the core inlet (top) for limestone cores EDW09, EDW10 and EDW12.

Results from CT scans prior and after CO_2-foam injection revealed that the interior of the cores also was affected by rock dissolution (see Figure 15.3). Three distinct features are present in the CT images: white areas are high-density areas indicating high-density rock, grey areas indicate average density rock, and darker areas indicate low density. The low-density areas consist of cavities (vugs) in the core as visually observed at the core inlet (Figure 15.2). Vugs were observed in the cores both prior and after CO_2-foam injection. However, the acidic flow of brine and supercritical CO_2 caused formation of new vugs and growth of already present vugs prior to foam injection. The high-density rock (in white) was not profoundly affected by CO_2-foam injection

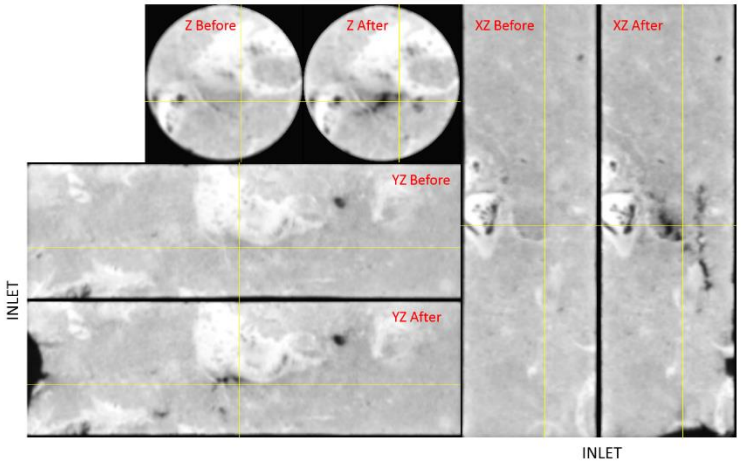

Figure 15.3 – Post- and pre-foam scan (quality scan and rate scan) CT images of EDW12 in the Z, XZ and YZ plane. The greyscale intensity indicates the density of the core: lighter areas indicate high-density rock matrix, whereas black areas are cavities (vugs).

Quantitative estimation of the vug volumes in EDW9, EDW10 and EDW12 both pre and post CO_2-foam injections was performed based on CT-image analysis by PhD candidate Tore L. Føyen. The low-density areas of the images, indicating cavities, were segmented out of the images using the Trainable Weka Segmentation tool (Arganda-Carreras et al., 2017) incorporated in the Fiji image processing package distribution of ImageJ (Schindelin et al., 2012). The CT-images consist of approximately 255 separate 2-dimensional image-slices stacked in the z-direction, constituting a 3-dimensional representation of the cores. The Weka Segmentation tool was used to segment out vugs from each image-slice, resulting in a 3-dimensional representation of the vug network, illustrated in 2D in Figure 15.4. A 3D Object Counter in ImageJ calculated the vug volumes based on the number of vug voxels. The CT-estimated vug volumes for the three core plugs pre and post CO_2-foam injection are included in Table 15.2.

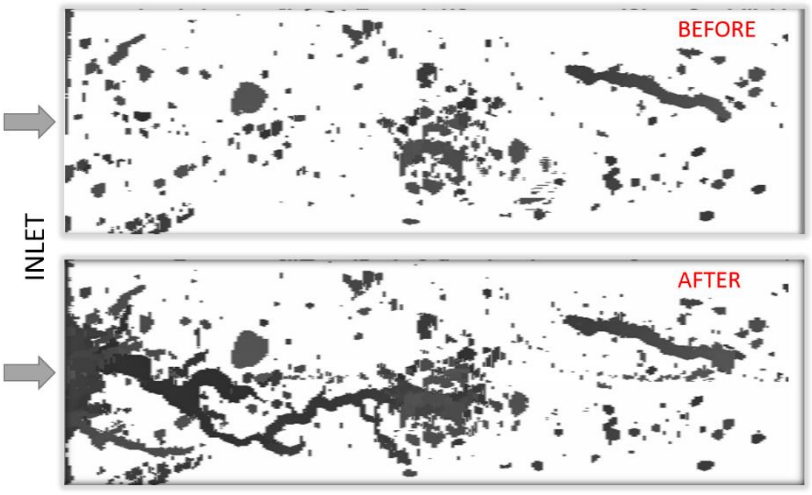

Figure 15.4 - Vugs (black areas) in core EDW12 pre and post foam injection segmented out from CT images using Trainable Weka Segmentation.

Pore volumes of the three limestone core plugs were measured after co-injections for comparison with the initial measured pore volume (see Table 15.2). The cores were vacuumed and saturated using the setup for porosity measurements in Appendix A. Increasing ΔPV due to a high degree of dissolution was observed with increasing duration of CO_2 exposure. Some uncertainties are associated with measurements of the new pore volume, due to loss of rock grains when handling the cores after co-injection experiments. The increase in pore volume at the exterior of the core plugs is not accounted for during the post foam pore volume measurements, as lack of capillary pressure prevents the water to stay in these cavities when temporarily removed from a water bath to measure the weight after saturation. However, this exterior increase in pore volume was accounted for during the CT-estimated pore volume increase, which can explain why the CT-estimated increase in PV is higher than the calculated increase in PV for EDW09 and EDW10, and that a negative ΔPV is measured for EDW10.

Table 15.2 – Limestone dissolution parameters

Core	CO_2 exposure [days]	PV prior to co-injection [ml]	PV after co-injection [ml]	ΔPV increase [ml]	ΔPV increase [%]	CT-estimated* increase in PV [%]
EDW09	9.5	70.2	71.9	1.7	2.3	3.6
EDW10	4	69.7	69.6	-0.1	-0.1	1.8
EDW12	10	64.9	68.2	3.3	5.2	4.9

*CT-estimated vug volumes were conducted by PhD candidate Tore L. Føyen.

Increased PV as a consequence of limestone dissolution did not influence calculated oil and brine volumes during CO_2-foam EOR injections, as these volumes were explicitly measured. The increase did, however, positively influence the storage potential as CO_2 could occupy additional pore space. An increase in PV without a change in produced water (V_w) or hydrocarbons (V_{HC}) increases the volume of stored CO_2 as free phase (Eq. 15.1). An increase in volume of stored CO_2 of 13% was achieved for EDW09 as a result of the ΔPV increase listed in Table 15.2 (measured, not CT-estimated values). This additional storage consequently increased the MEE by 15%. The other core plugs (EDW10 and EDW12) were not used for CO_2-foam EOR injections. However, if the ΔPVs obtained during co-injection in EDW09, EDW10 and EDW12 are representative for other cores used in CO_2-foam EOR injections, MEE is underestimated in Figure 15.1. Dissolution of limestone, increasing the pore volume, could therefore be considered as a mechanism of carbon dioxide storage.

Part IV – Conclusion and Future Work

16. Conclusions

This thesis reports experimental results on the synergy between nanoparticles and surfactant as foaming agents for CO_2-foam during EOR and CO_2 storage. Important parameters like foaming agent interactions, retention, foam stabilization and enhanced oil recovery were investigated to determine the feasibility of using nanoparticles and surfactants as a combined foaming agent for CO_2-foam. In particular, hydrophilic silica nanoparticles were combined with either a nonionic surfactant (0.5 wt.% SurfA) or a switchable cationic surfactant (1 wt.% SurfB) during co-injections in porous media. The following key observations and conclusions are drawn from this experimental study:

- Foam stabilization: Nanoparticles and surfactants (SurfA) remained stable during static test with reduced pH for more than 44 days. Nanoparticle injection in limestone resulted in aggregation and instability at elevated temperature (120°C) caused by dissolution of naturally occurring $CaCO_3$. Aggregation was mitigated with the presence of CO_2 during co-injections in limestone, believed to be related to reduced pH of the brine solution when contacted by CO_2. Oil has a detrimental effect on weak CO_2-foam during co-injections, whereas strong foams gain a stabilizing effect from the injected oil by oil-in-water emulsions.

- Nanoparticle retention: Retention of nanoparticle was in the lower range of reported foaming agent (surfactant) values during injection in sandstone and during co-injection with SurfA in limestone. The minor loss of nanoparticles to the rock formation is economically beneficial for CO_2-foam EOR operations.

- Oil recovery and foam performance: Combination of NPA and SurfB demonstrated better performance in terms of incremental oil recovery and foam strength compared with the combination of NPA and SurfA. In general, SurfB used separately or combined with NPA outperform the separate use of NPA and SurfA as foaming agents in limestone. Oil-in-water emulsions were observed during co-injection of CO_2 and foaming agent, and considerable amounts of emulsified oil were produced and must be accounted for to correctly measure final oil recovery.

- CO_2 storage potential: Carbon negative oil production was achieved during co-injection of CO_2-foam (SurfA) in sandstone and in limestone (NPA with and without SurfA). Generation of foam and/or emulsions is beneficial for CO_2 storage. The acidic effect of CO_2 and brine caused significant dissolution of limestone during co-injections, with a positive effect on carbon dioxide storage due to expansion of the pore volume.

The key observations and conclusions show that a combination of nanoparticles and surfactants are feasible for CO_2 mobility control in limestone, with high oil recovery and large pressure gradients. Experimental conditions between the two combinations (NPA+SurfA and NPA+SurfB) vary, and additional tests should be run to reach a firm conclusion if the nonionic or cationic is the preferred choice to combine with NPA. Suggestions for future work is presented in the following chapter.

17. Future Work

The experimental work presented in this thesis was a part of an ongoing CO_2-foam project run by the Reservoir Physics group at the Department of Physics and Technology, University of Bergen. Firm conclusions cannot be justified for all experiments conducted in this thesis, but important trends have been observed, which have improved the understanding of combining nanoparticles and surfactants for enhanced oil recovery by stabilizing CO_2-foam. Essential observations have been made, but results should be further verified through extensive lab work. Following is a list of suggestions for future work:

- Solution pH has proven to significantly affect the stability of nanoparticles and surfactants injected in limestone cores. A comprehensive study of the effect of pH should be conducted to optimize CO_2-foam EOR injections in limestone.

- Co-injections of CO_2, nanoparticles and surfactants should be conducted at elevated temperatures, where increased temperature might reduce the surfactant ability to stabilize foam.

- A screening study should be conducted to investigate foaming agent concentrations to optimize the synergy between nanoparticles and surfactants.

- Nanoparticle retention studies were performed with absence of CO_2 and oil. Retention studies could be performed with co-injection of foaming agent and CO_2 and with presence of oil to study the effect of CO_2 and oil on retention. Alternative methods should be considered for retention analyzes, as results from retention studies conducted in this experimental thesis are associated with significant uncertainties.

- Emulsions were produced during CO_2-foam EOR injections presented in this thesis. For an improved understanding of recovery methods during these co-injections, CT and/or PET scanning could be used to visualize the displacement process. CO_2-foam EOR injections should also be conducted in micromodels to obtain a better understanding of foam and/or emulsion behavior.

- Alternative methods should be considered for separation of dispersed foaming agent and oil to measure oil content of produced emulsions.

- Co-injections were performed at different experimental conditions during the experimental work of this thesis. Experiments should be conducted with comparable temperatures and pressures, and with constant surfactant concentrations to evaluate the effect of surfactant type. Experiments should also be replicated, as several of the conducted co-injections were only performed once.

- All CO_2-foam EOR injections were conducted with n-Decane as the displaced oleic phase. Experiments should be performed with crude oil to investigate the effect of oil type, and to study the interactions between CO_2, nanoparticles, surfactants and crude oil.

Part V – Nomenclature, Abbreviations, Appendix and References

Nomenclature

A	Cross sectional area
c_{CO2}	Molar concentration of CO_2
c_{HC}	Molar concentration of hydrocarbons
D	Diameter
f_g	Gas fraction
f_g^*	Critical foam quality
γ	Average number of carbon atoms in a hydrocarbon molecule
K	Absolute permeability
L	Length
m_{dry}	Mass of dry core
m_{sat}	Mass of saturated core
μ	Fluid viscosity
μ_{app}	Apparent foam viscosity
$N_{C,produced}$	Amount of CO_2 produced
$N_{C,stored}$	Amount of CO_2 stored
P	Pressure
ΔP	Differential pressure
∇P	Pressure gradient
φ	Porosity
Q	Flow rate
q_g	Gas flow rate
q_{liq}	Liquid flow rate
R_f	Total Recovery factor
$R_{f,w}$	Recovery factor from waterflood
$R_{f,co\text{-}inj}$	Recovery factor from co-injection
ρ	Density
S_o	Oil saturation
S_{oi}	Initial oil saturation
S_{or}	Residual oil saturation?
S_{iw}	Irreducible water saturation
S_w	Water saturation
V_b	Bulk volume
V_{CO2}	Volume of stored CO_2
V_{HC}	Volume of hydrocarbons occupying the pore space
V_{HC}	Volume of hydrocarbons produced
V_o	Volume oil produced
V_p	Pore volume
V_w	Volume of water occupying the pore space

Abbreviations

BPR	Back Pressure Regulator
CCS	Carbon Capture and Storage
CCUS	Carbon Capture, Utilization and Storage
cMEE	Critical Mass Element Exchange
CSC	Critical Salt Concentration
CT	Computerized Tomography
EDW	Edwards Limestone
EOR	Enhanced Oil Recovery
HUS	Haukeland University Hospital
IFT	Interfacial Tension
LPG	Liquefied Petroleum Gas
MEE	Mass Element Exchange
MMP	Minimum Miscibility Pressure
mPPM	Parts per million by mass
MRF	Mobility Reduction Factor
MRI	Magnetic Resonance Imaging
NCS	Norwegian Continental Shelf
NM	Not Measured
OOIP	Oil Originally in Place
POM	Polyformaldehyde
PV	Pore Volume
SAG	Surfactant Alternating Gas
SS	Bentheimer Sandstone
UoB	University of Bergen
wt.%	Weight percent

Appendix

A) Porosity and Permeability Measurements

Porosity Measurements

Porosity describes the presence of void space between grains in a porous media, and is highly determined by size, shape and distribution of the grains (Lien, 2004). The porosity of all core plugs were measured using the saturation method, where weight measurements and brine densities were used to determine the pore volume. Dried cores were weighted and placed in an evacuation apparatus (see Figure A1) to remove air occupying the pore space. The water container was filled with brine A, B or C depending on rock type, and the brine and core plug were separately vacuumed before pouring brine on to the vacuumed core plug. The submerged core was then stored in the evacuation apparatus overnight, before the final weight was measured. Porosity was calculated assuming 100% saturated cores.

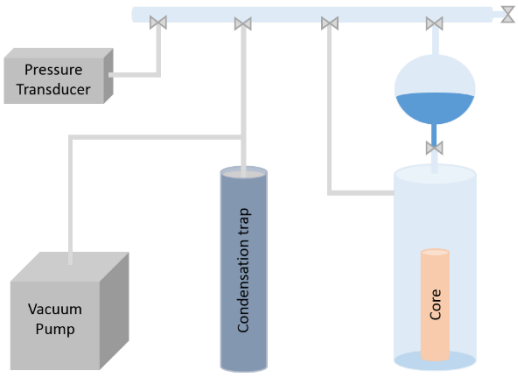

Figure A1 – Experimental setup for evacuation apparatus

As the brine density was known, and core weights were noted, Eq. A1 was used to calculate porosity:

$$\phi = \frac{V_p}{V_b} \cdot 100\% = \frac{m_{sat} - m_{dry}}{\rho_b \cdot \pi r^2 l} \cdot 100\% \quad \text{(A1)}$$

where V_p is the pore volume, V_b is the bulk volume found by measuring core dimensions r (radius) and l (length) , m_{dry} and m_{sat} is the mass of the core plug before and after saturation, and ρ_b is the brine density.

Absolute Permeability Measurements

Permeability is a porous medium's capability to transmit fluids through its network of interconnected pores, and absolute permeability can be regarded as a constant property for a specific medium if there only is a single fluid flowing through the medium (Zolotuchin & Ursin, 2000). As the cores were 100% saturated with brine, absolute permeability was measured prior to all core flooding experiments.

Figure A2 shows the setup for permeability measurements conducted on limestone cores EDW04-06 and sandstone core SS05. The 100% brine saturated core plug was placed in a Hassler core holder, and a confinement pressure of net 20 or 40 bar (for limestone and sandstone, respectively) above the pore pressure was applied to ensure that the injected fluids were transported through the core. Different confinement pressures were applied due to the mechanical strength of the core plugs. A Pharmasia pump was used to inject brine at three different rates, and the inlet pressure was measured using an ESI-pressure transducer. The outlet pressure was kept at ambient conditions, and the differential pressure was measured with periods of stable inlet pressure. Darcy's law was used to calculate the absolute permeability:

$$Q = \frac{KA\Delta P}{\mu L} \tag{A2}$$

where Q is the flow rate, K is the absolute permeability, ΔP is the differential pressure along the length of the core, L, and μ is the viscosity of the injected fluid.

The flow direction was reversed in order to evaluate the presence of directional permeability, but due to negligible variations, the remaining permeability measurements were only measured in one flow direction.

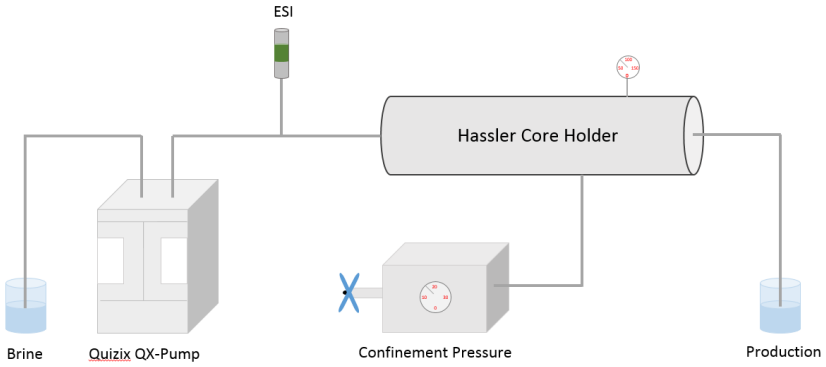

Figure A2 – Experimental setup for permeability measurements conducted on selected core plugs. A QX-pump was used to inject brine through the core at different rates, while the ESI-pressure transducer measured the differential pressure across the core plug. A confinement pressure of net 20 bar (limestone) or 40 bar (sandstone) above the pore pressure was applied to the core to ensure fluid flow through the core plug.

Permeability measurements for the remaining core plugs were performed using the experimental setup illustrated in Figure 7.5 (Chapter 7).

B) Foam Screening Results

Foam screening with different types of foaming agents (switching between injecting only nanoparticles (NPA), only surfactants (SurfA) or a combination of NPA and SurfA) was performed in limestone cores and a sandstone core partially saturated with CO_2 and oil. Foam screenings were performed directly after (and as an extension of) CO_2-foam EOR injections to investigate foam flow behavior using different foaming agents with and without the presence of oil. At the onset of foam screenings, oil saturation was equal to the final oil saturation after CO_2-EOR injections. Oil was therefore injected into the system simultaneously as CO_2 and foaming agent to evaluate the presence of oil during foam screening.

Results from foam screening in EDW08 (Figure B1), EDW09 (Figure B2) and SS06 (Figure B3) are shown below. The results were influenced by experimental difficulties when injecting CO_2 over extended periods and by pressure limitations of the experimental setup. All foam screening results are presented in this appendix for the entirety of the experimental work and for future evaluation.

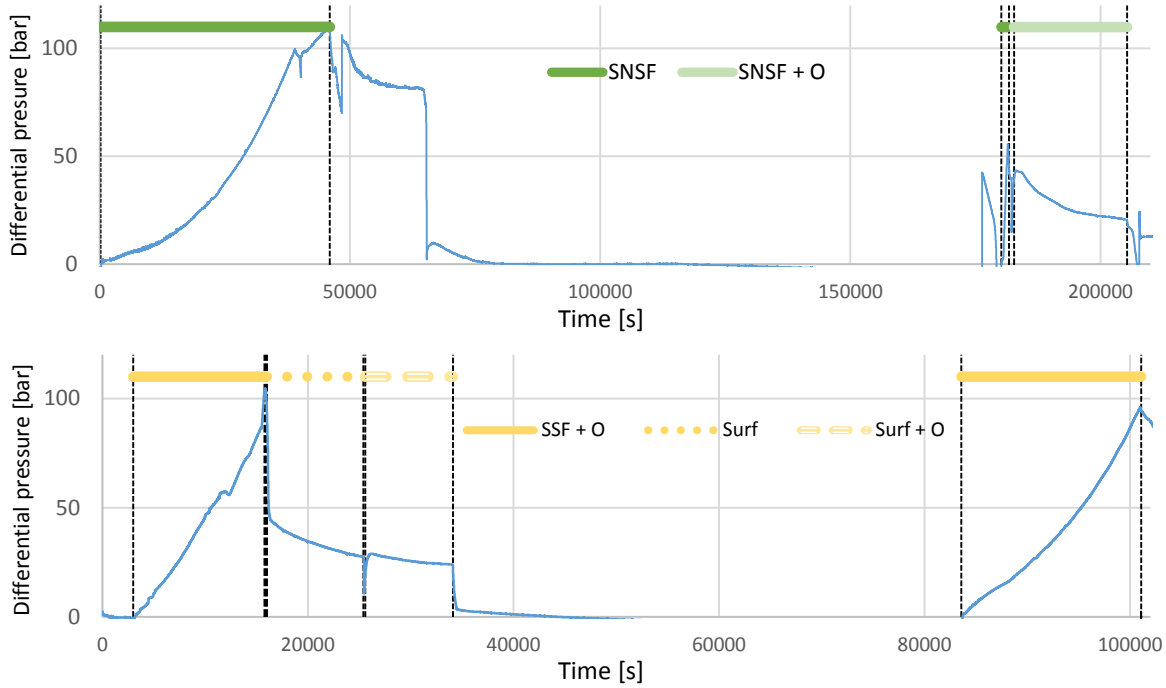

Figure B1 – Foam screening results for EDW08 with differential pressure as a function of time. A long shut-in period separates the co-injection of CO_2, SurfA and NPA without oil (surfactant-nanoparticle-stabilized foam, SNSF) and with oil (SNSF + O) (on top) and the co-injection of CO_2, SurfA and oil (SSF + O) or pure SurfA injection without (Surf) or with oil (Surf + O) (bottom). Co-injections were stopped or changed at 100 bar differential pressure due to pressure limitations of the experimental setup. Periods of no differential pressure are shut-in periods.

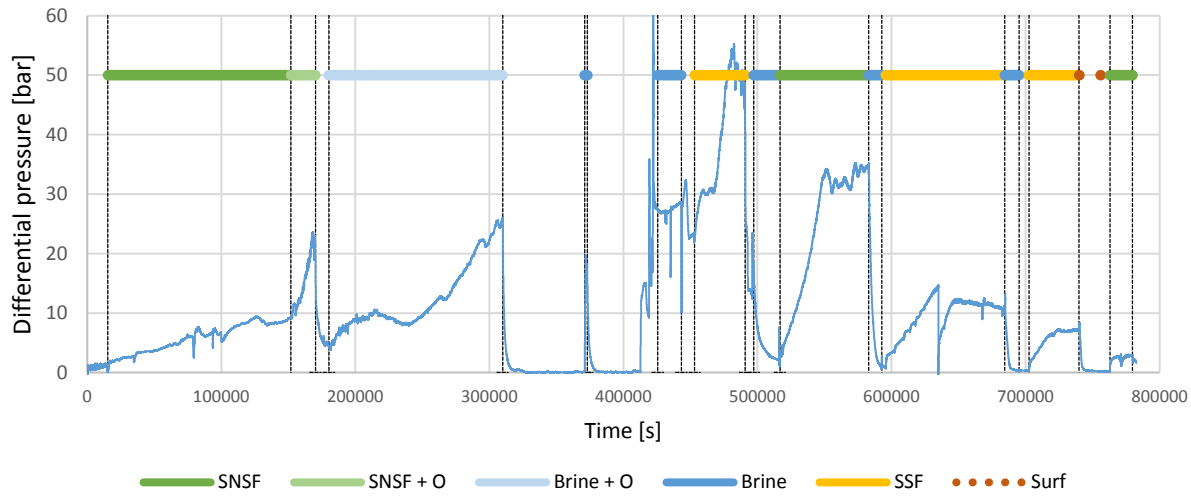

Figure B2 – Foam screening results for EDW09 with differential pressure as a function of time. Surfactant-nanoparticle-stabilized CO_2-foam with (SNSF + O) and without (SNSF) oil, surfactant-stabilized CO_2-foam (SSF), brine injection with and without oil and pure surfactant injection are differentiated by colors. Periods of no differential pressure are shut-in periods.

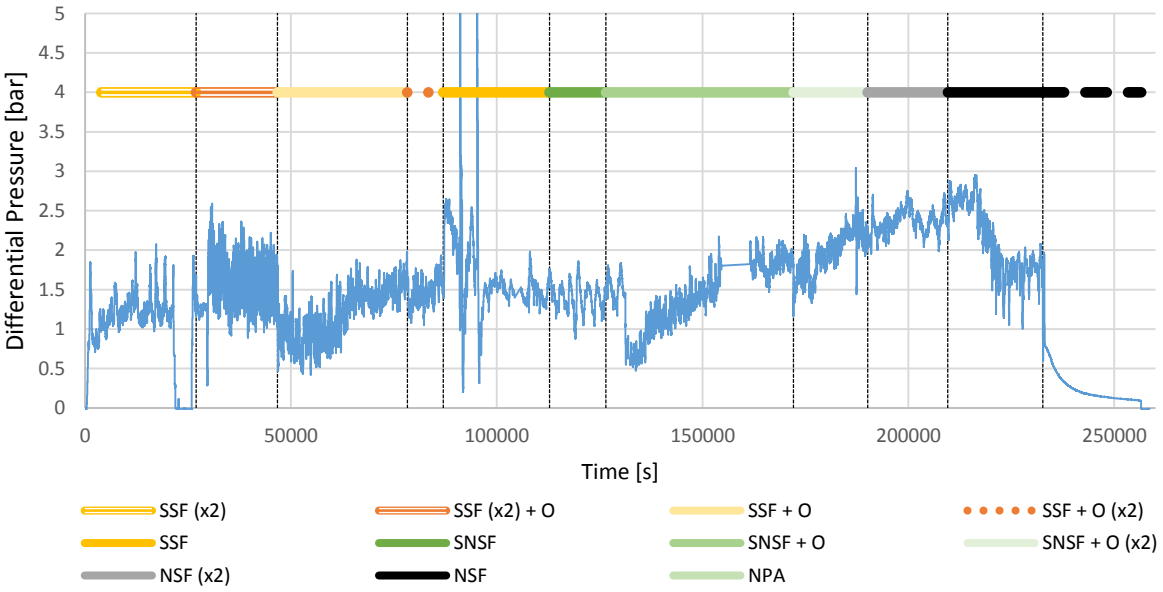

Figure B3 – Foam screening results for SS06 with differential pressure as a function of time. Surfactant-nanoparticle-stabilized CO_2-foam with (SNSF + O) and without (SNSF) oil, surfactant-stabilized CO_2-foam with (SSF + O) and without (SSF) oil, nanoparticle-stabilized CO_2-foam without oil (NSF) and pure nanoparticle injection (NPA) are differentiated by colors. The foaming agent or oil injection rate was doubled (x2) at different time steps. The period of no differential pressure is a shut-in period.

C) Uncertainty Calculations

Experimental measurements are dependent on uncertainties associated with the experimental method itself, and with the instruments used during experiments. Below is a list of equations used for uncertainty calculation during the work of this experimental thesis.

Addition and Subtraction

When addition or subtraction of independent variables $x, y, z, \ldots, i$, were used for calculation of an experimental value R, the uncertainty in R, S_R, was calculated based on the uncertainty in each of the independent variables $S_x, S_y, S_z, \ldots, S_i$:

$$S_R = \sqrt{\left(\frac{\delta R}{\delta x} S_x\right)^2 + \left(\frac{\delta R}{\delta y} S_y\right)^2 + \left(\frac{\delta R}{\delta z} S_z\right)^2 + \cdots + \left(\frac{\delta R}{\delta i} S_i\right)^2} \quad \text{(C1)}$$

Quotient and Product

If the value R was calculated as a product or quotient of a set of variables, $a^2x, b^2y, c^2z, \ldots, n^2i$, with inherent uncertainties $S_x, S_y, S_z, \ldots, S_i$, with $a^2, b^2, c^2, \ldots, n^2$ being constants, the uncertainty of R, S_R, was calculated by:

$$\frac{S_R}{R} = \sqrt{\left(a\frac{S_x}{x}\right)^2 + \left(b\frac{S_y}{y}\right)^2 + \left(c\frac{S_z}{z}\right)^2 + \cdots + \left(n\frac{S_i}{i}\right)^2} \quad \text{(C2)}$$

Standard Deviation

Standard deviation, used to quantify the amount of variation of individual variables of a data set, was used to calculate the uncertainty of mean values:

$$S = \sqrt{\frac{1}{N-1}\sum_{i=1}^{N}(x_i - \bar{x})^2} \quad \text{(C3)}$$

where N is the number of sample values, x, and $\bar{x}$ is the sample mean.

Table C.1 – Instrumental uncertainties for equipment used in the experimental work of this thesis

Instrument	Parameter	Uncertainty
Weight	Mass	± 0.01 g
Caliper	Length	± 0.002 cm
Ruler	Length	± 0.1 cm
ESI pressure transducer	Pressure	± 0.1 % of full scale
Differential pressure transmitter	Pressure	± < 0.032 bar
Graded cylinder (10 ml)	Volume	± 0.1 ml
Graded cylinder (5 ml)	Volume	± 0.05 ml

Volumetric Uncertainties during CO_2-Foam EOR Injections

Volumetric uncertainties during CO_2-foam EOR injections conducted at 40°C and 175 bar pore pressure are shown in Figure C1.

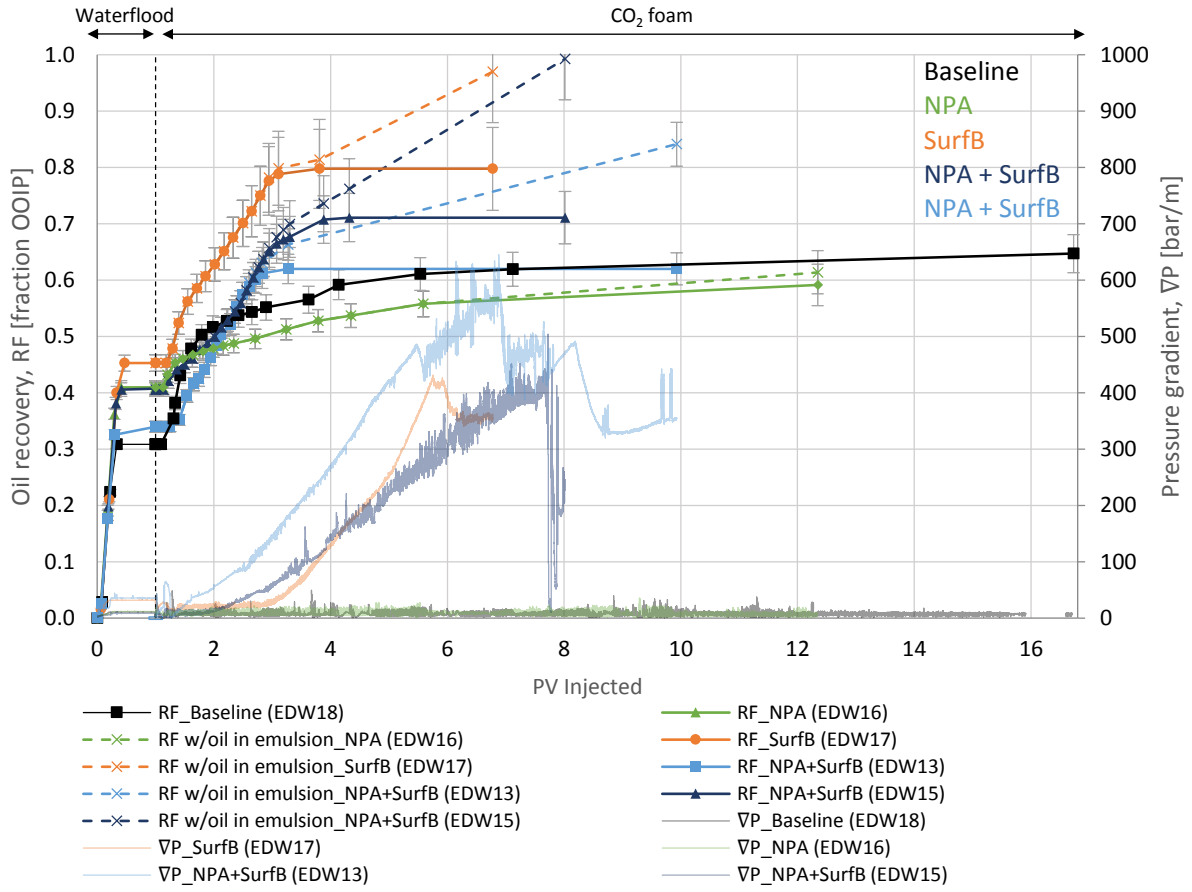

Figure C1 – Oil recovery and pressure gradient during waterflood and co-injection of CO_2 and foaming agent, where foaming agents are differentiated by colors: green for NPA (EDW16), orange for SurfB (EDW17), blue for NPA + SurfB (light for EDW13 and dark for EDW15) and black for the baseline. Solid lines are oil recovery without considering oil in emulsions, whereas additional oil content in emulsions is represented by dashed lines. The observed pressure gradient drop for co-injection in EDW13, EDW15 and EDW17 is a result of reduced injection rate.

D) Experimental Collaboration

The majority of core experiments conducted in this thesis have been performed in collaboration with PhD Øyvind Eide or PhD candidate Tore Lyngås Føyen. A detailed description of collaboration on each experiment is listed in Table D1 below.

Table D1 – Collaborating partners

Core	Experiment	Collaboration Partner
EDW03	Adsorption Test	Øyvind Eide
EDW04	Adsorption Study	Øyvind Eide
EDW05	Adsorption Study	Øyvind Eide
EDW06	Foam Quality Scan	Tore Lyngås Føyen
EDW07	EOR	Tore Lyngås Føyen
EDW08	EOR / Foam Screening	Tore Lyngås Føyen
EDW09	EOR / Foam Screening	Tore Lyngås Føyen
EDW10	Adsorption Test / Foam Quality Scan	Tore Lyngås Føyen
EDW11	Foam Quality Scan	Tore Lyngås Føyen
EDW12	Adsorption Study / Foam Scan	-
EDW13	EOR	Tore Lyngås Føyen
EDW14	Adsorption Test	-
EDW15	EOR	Tore Lyngås Føyen
EDW16	EOR	-
EDW17	EOR	-
EDW18	EOR	-
SS05	Adsorption Study	-
SS06	EOR / Foam Screening	Tore Lyngås Føyen

References

Abidoye, L. K., Khudaida, K. J., & Das, D. B. (2015). Geological Carbon Sequestration in the Context of Two-Phase Flow in Porous Media: A Review. *Critical Reviews in Environmental Science and Technology, 45*(11), 1105-1147. doi:10.1080/10643389.2014.924184

Ahr, W. M. (2008). *Geology of Carbonate Reservoirs: The Identification, Description, and Characterization of Hydrocarbon Reservoirs in Carbonate Rocks*. Hoboken, New Jersey: John Wiley & Sons, Inc.

Alagorni, A., Yaacob, Z., & Nour, A. (2015). An Overview of Oil Production Stages: Enhanced Oil Recovery Techniques and Nitrogen Injection. *International Journal of Environmental Sciences and Development, 6*(9), 693-701. doi:10.7763/IJESD.2015.V6.682

Alvarado, V., & Manrique, E. (2010). Enhanced Oil Recovery: An Update Review. *Energies, 3*, 1529-1575. doi:10.3390/en3091529

Aplisens. (2018). SMART DIFFERENTIAL PRESSURE TRANSMITTER PRE-28.SMART.

Arganda-Carreras, I., Kaynig, V., Rueden, C., Eliceiri, K. W., Schindelin, J., Cardona, A., & Sebastian Seung, H. (2017). Trainable Weka Segmentation: a machine learning tool for microscopy pixel classification. *Bioinformatics, 33*(15), 2424-2426. doi:10.1093/bioinformatics/btx180

Austad, T. (2013). Water-Based EOR in Carbonates and Sandstones: New Chemical Understanding of the EOR Potential Using "Smart Water". In J. J. Sheng (Ed.), *Enhanced Oil Recovery Field Case Studies* (pp. 301-335). Boston: Gulf Professional Publishing.

Azadgoleh, J. E., Kharrat, R., Barati, N., & Sobhani, A. (2014). Stability of Silica Nanoparticle Dispersion in Brine Solution: An Experimental Study. *Iranian Journal of Oil & Gas Science and Technology, 3*(4), 26-40. doi:10.22050/ijogst.2014.7485

Bennetzen, M. V., & Mogensen, K. (2014). *Novel Applications of Nanoparticles for Future Enhanced Oil Recovery*. Paper presented at the International Petroleum Technology Conference, Kuala Lumpur, Malaysia.

Benson, S., Cook, P., Anderson, J., Bachu, S., Nimir, H. B., Basu, B., . . . Zhou, D. (2005). Underground geological storage. In B. Metz, O. Davidson, H. d. Coninck, M. Loos, & L. Meyer (Eds.), *IPCC Special Report on Carbon Dioxide Capture and Storage*. New York: Cambridge University Press.

Binks, B. P., & Horozov, T. S. (2005). Aqueous Foams Stabilized Solely by Silica Nanoparticles. *Angewandte Chemie International Edition, 44*(24), 3722-3725. doi:10.1002/anie.200462470

Binks, B. P., Kirkland, M., & Rodrigues, J. A. (2008). Origin of stabilisation of aqueous foams in nanoparticle-surfactant mixtures. *Soft Matter, 4*(12), 2373-2382. doi:10.1039/B811291F

Binks, B. P., Rodrigues, J. A., & Frith, W. J. (2007). Synergistic Interaction in Emulsions Stabilized by a Mixture of Silica Nanoparticles and Cationic Surfactant. *Langmuir, 23*(7), 3626-3636. doi:10.1021/la0634600

Bjørlykke, K., & Jahren, J. (2010). Sandstones and Sandstone Reservoirs. In K. Bjorlykke (Ed.), *Petroleum Geoscience: From Sedimentary Environments to Rock Physics* (pp. 113-140). Berlin, Heidelberg: Springer Berlin Heidelberg.

Chambers, D. J. (1994). Foams for Well Stimulation. In *Foams: Fundamentals and Applications in the Petroleum Industry* (Vol. 242, pp. 355-404): American Chemical Society.

Chang, S.-H., & Grigg, R. B. (1999). Effects of Foam Quality and Flow Rate on CO2-Foam Behavior at Reservoir Temperature and Pressure. doi:10.2118/56856-PA

Dautriat, J., Gland, N. F., Youssef, S., Rosenberg, E., & Bekri, S. (2007). *Stress-Dependent Permeabilities of Sandstones and Carbonates: Compression Experiments and Pore Network Modelings*. Paper presented at the SPE Annual Technical Conference and Exhibition, Anaheim, California, U.S.A.

Derikvand, Z., & Riazi, M. (2016). Experimental investigation of a novel foam formulation to improve foam quality. *Journal of Molecular Liquids, 224*, 1311-1318. doi:10.1016/j.molliq.2016.10.119

Dicksen, T., Hirasaki, G. J., & Miller, C. A. (2002). *Conditions for Foam Generation in Homogeneous Porous Media*. Paper presented at the SPE/DOE Improved Oil Recovery Symposium, Tulsa, Oklahoma.

Dickson, J. L., Binks, B. P., & Johnston, K. P. (2004). Stabilization of Carbon Dioxide-in-Water Emulsions with Silica Nanoparticles. *Langmuir, 20*(19), 7976-7983. doi:10.1021/la0488102

El-Dessouky, H. T. (2002). Appendix A - Thermodynamic Properties. In H. M. Ettouney (Ed.), *Fundamentals of Salt Water Desalination* (pp. 525-563). Amsterdam: Elsevier Science B.V.

Enick, R. M., Olsen, D. K., Ammer, J., Boman, J., Kawecki, B., & Schuller, W. (2011). *Mobility and Conformance Control for Carbon Dioxide Enhanced Oil Recovery (CO_2-EOR) via Thickeners , Foams , and Gels – A Detailed Literature Review of 40 Years of Research*. Nationel Energy Technology Laboratory.

Enick, R. M., Olsen, D. K., Ammer, J. R., & Schuller, W. (2012). *Mobility and Conformance Control for CO2 EOR via Thickeners, Foams, and Gels -- A Literature Review of 40 Years of Research and Pilot Tests*. Paper presented at the SPE Improved Oil Recovery Symposium, Tulsa, Oklahoma, USA.

Espinoza, D. A., Caldelas, F. M., Johnston, K. P., Bryant, S. L., & Huh, C. (2010). *Nanoparticle-Stabilized Supercritical CO2 Foams for Potential Mobility Control Applications*. Paper presented at the SPE Improved Oil Recovery Symposium, Tulsa, Oklahoma, USA.

Espinoza, D. N., Kim, S. H., & Santamarina, J. C. (2011). CO_2 geological storage — Geotechnical implications. *KSCE Journal of Civil Engineering, 15*(4), 707-719. doi:10.1007/s12205-011-0011-9

Farajzadeh, R., Andrianov, A., Krastev, R., Hirasaki, G. J., & Rossen, W. R. (2012). Foam–oil interaction in porous media: Implications for foam assisted enhanced oil recovery. *Advances in Colloid and Interface Science, 183-184*, 1-13. doi:10.1016/j.cis.2012.07.002

Farajzadeh, R., Andrianov, A., & Zitha, P. L. J. (2010). Investigation of Immiscible and Miscible Foam for Enhancing Oil Recovery. *Industrial & Engineering Chemistry Research, 49*(4), 1910-1919. doi:10.1021/ie901109d

Fernø, M. A., Eide, Ø., Steinsbø, M., Langlo, S. A. W., Christophersen, A., Skibenes, A., . . . Graue, A. (2015a). Mobility control during CO2 EOR in fractured carbonates using foam: Laboratory

evaluation and numerical simulations. *Journal of Petroleum Science and Engineering, 135*, 442-451. doi:10.1016/j.petrol.2015.10.005

Fernø, M. A., Steinsbø, M., Eide, Ø., Ahmed, A., Ahmed, K., & Graue, A. (2015b). Parametric study of oil recovery during CO2 injections in fractured chalk: Influence of fracture permeability, diffusion length and water saturation. *Journal of Natural Gas Science and Engineering, 27*, 1063-1073. doi:10.1016/j.jngse.2015.09.052

Fernø, M. A., Torsvik, M., Haugland, S., & Graue, A. (2010). Dynamic Laboratory Wettability Alteration. *Energy & Fuels, 24*(7), 3950-3958. doi:10.1021/ef1001716

Freund, P. (2005). Properties of CO_2 and carbon-based fuels. In *Carbon Dioxide Capture and Storage*. New York: Cambridge University Press.

Friedmann, F., & Jensen, J. A. (1986). *Some Parameters Influencing the Formation and Propagation of Foams in Porous Media*. Paper presented at the SPE California Regional Meeting, Oakland, California.

Gao, C. (2007). Factors affecting particle retention in porous media. *Emirates Journal for Engineering Research, 12*(3), 1-7.

Green, D. W., & Willhite, G. P. (1998). *Enhanced Oil Recovery*. Richardson, TX: Henry L. Doherty Memorial Fund of AIME, Society of Petroleum Engineers.

Grigg, R. B., & Bai, B. (2005). *Sorption of Surfactant Used in CO2 Flooding onto Five Minerals and Three Porous Media*. Paper presented at the SPE International Symposium on Oilfield Chemistry, The Woodlands, Texas.

Grogan, A. T., Pinczewski, V. W., Ruskauff, G. J., & Orr, F. M., Jr. (1988). Diffusion of CO2 at Reservoir Conditions: Models and Measurements. doi:10.2118/14897-PA

Grogan, A. T., & Pinczewski, W. V. (1987). The Role of Molecular Diffusion Processes in Tertiary CO2 Flooding. doi:10.2118/12706-PA

Guo, F., & Aryana, S. (2016). An experimental investigation of nanoparticle-stabilized CO2 foam used in enhanced oil recovery. *Fuel, 186*, 430-442. doi:10.1016/j.fuel.2016.08.058

Hasan, M. M. F., First, E. L., Boukouvala, F., & Floudas, C. A. (2015). A multi-scale framework for CO2 capture, utilization, and sequestration: CCUS and CCU. *Computers & Chemical Engineering, 81*, 2-21. doi:10.1016/j.compchemeng.2015.04.034

Haugen, K. B., & Firoozabadi, A. (2006). On Measurement of Molecular and Thermal Diffusion Coefficients in Multicomponent Mixtures. *The Journal of Physical Chemistry B, 110*(35), 17678-17682. doi:10.1021/jp062382m

Haugen, Å., Mani, N., Svenningsen, S., Brattekås, B., Graue, A., Ersland, G., & Fernø, M. A. (2014). Miscible and Immiscible Foam Injection for Mobility Control and EOR in Fractured Oil-Wet Carbonate Rocks. *Transport in Porous Media, 104*(1), 109-131. doi:10.1007/s11242-014-0323-6

Heller, J. P. (1994). CO_2 Foams in Enhanced Oil Recovery. In *Foams: Fundamentals and Applications in the Petroleum Industry* (Vol. 242, pp. 201-234): American Chemical Society.

Hirasaki, G. J., & Lawson, J. B. (1985). Mechanisms of Foam Flow in Porous Media: Apparent Viscosity in Smooth Capillaries. doi:10.2118/12129-PA

Holm, L. W. (1986). Miscibility and Miscible Displacement. *Journal of Petroleum Technology, 38*(08). doi:10.2118/15794-PA

Hucknall, D. J. (1985). *Chemistry of hydrocarbon combustion*: Springer Netherlands.

Hudgins, D. A., & Chung, T. H. (1990). *Long-Distance Propagation of Foams*. Paper presented at the SPE/DOE Enhanced Oil Recovery Symposium, Tulsa, Oklahoma.

Keelan, D. K., & Pugh, V. J. (1975). Trapped-Gas Saturations in Carbonate Formations. doi:10.2118/4535-PA

Khatib, Z. I., Hirasaki, G. J., & Falls, A. H. (1988). Effects of Capillary Pressure on Coalescence and Phase Mobilities in Foams Flowing Through Porous Media. doi:10.2118/15442-PA

Kokal, S. L., Maini, B. B., & Woo, R. (1992). Flow of Emulsions in Porous Media. In L. L. Schramm (Ed.), *Emulsions: Fundamentals and Applications in the Petroleum Industry*. Washington: American Chemical Society.

Kovalchuk, N. M., & Starov, V. M. (2012). Aggregation in colloidal suspensions: Effect of colloidal forces and hydrodynamic interactions. *Advances in Colloid and Interface Science, 179-182*, 99-106. doi:10.1016/j.cis.2011.05.009

Lake, L. W., Johns, R., Rossen, B., & Pope, G. (2014). *Fundamentals of Enhanced Oil Recovery*. USA: Society of Petroleum Engineers.

Lee, S., & Kam, S. I. (2013). Chapter 2 - Enhanced Oil Recovery by Using CO2 Foams: Fundamentals and Field Applications In *Enhanced Oil Recovery Field Case Studies* (pp. 23-61). Boston: Gulf Professional Publishing.

Lemmon, E. W., McLinden, M. O., & Friend, D. G. (2018). Thermophysical Properties of Fluid Systems. In P. J. Linstrom & W. G. Mallard (Eds.), *NIST Chemistry WebBook, NIST Standard Reference Database Number 69*. Gaithersburg MD: National Institute of Standards and Technology.

Lien, J. R. (2004). *Grunnleggende reservoarfysikk*. Bergen: University of Bergen.

Mangalsingh, D., & Jagai, T. (1996). *A Laboratory Investigation of the Carbon Dioxide Immiscible Process*. Paper presented at the SPE Latin America/Caribbean Petroleum Engineering Conference, Port-of-Spain, Trinidad.

McAuliffe, C. D. (1973). Oil-in-Water Emulsions and Their Flow Properties in Porous Media. *Journal of Petroleum Technology, 25*(06). doi:10.2118/4369-PA

Mei, L., Chou, T.-H., Cheng, Y.-S., Huang, M.-J., Yeh, L.-H., & Qian, S. (2016). Electrophoresis of pH-regulated nanoparticles: impact of the Stern layer. *Physical Chemistry Chemical Physics, 18*(15), 9927-9934. doi:10.1039/C5CP05728K

Metin, C. (2012). *Characterization of Nanoparticle Transport in Flow Through Permeable Media* (PhD dissertation), The University of Texas at Austin, Texas.

Metin, C. O., Lake, L. W., Miranda, C. R., & Nguyen, Q. P. (2011). Stability of aqueous silica nanoparticle dispersions. *Journal of Nanoparticle Research, 13*(2), 839-850. doi:10.1007/s11051-010-0085-1

Morel, D., Bourbiaux, B., Latil, M., & Thiebot, B. (1993). Diffusion Effects in Gasflooded Light-Oil Fractured Reservoirs. doi:10.2118/20516-PA

Muller, T., & Lake, L. W. (1991). Theoretical Study of Water Blocking in Miscible Flooding. doi:10.2118/20206-PA

Nordbotten, J. M., & Celia, M. A. (2012). *Geological Storage of CO2: Modeling Approaches for Large-Scale Simulation*. John Wiley & Sons, Inc: Hoboken, New Jersey.

Ogolo, N. A., Olafuyi, O. A., & Onyekonwu, M. O. (2012). *Enhanced Oil Recovery Using Nanoparticles*. Paper presented at the SPE Saudi Arabia Section Technical Symposium and Exhibition, Al-Khobar, Saudi Arabia.

Osei-Bonsu, K., Grassia, P., & Shokri, N. (2017). Relationship between bulk foam stability, surfactant formulation and oil displacement efficiency in porous media. *Fuel, 203*, 403-410. doi:10.1016/j.fuel.2017.04.114

Perkins, T. K., & Johnston, O. C. (1963). A Review of Diffusion and Dispersion in Porous Media. doi:10.2118/480-PA

Pratsinis, S. E. (1998). Flame aerosol synthesis of ceramic powders. *Progress in Energy and Combustion Science, 24*(3), 197-219. doi:10.1016/S0360-1285(97)00028-2

Prigiobbe, V., Worthen, A. J., Johnston, K. P., Huh, C., & Bryant, S. L. (2016). Transport of Nanoparticle-Stabilized CO_2-Foam in Porous Media. *Transport in Porous Media, 111*(1), 265-285. doi:10.1007/s11242-015-0593-7

Prud'homme, R. K., & Khan, S. A. (1996). *Foams: Theory, measurements, and applications*. New York: Marcel Dekker.

Ransohoff, T. C., & Radke, C. J. (1988). Mechanisms of Foam Generation in Glass-Bead Packs. *Society of Petroleum Engineers*. doi:10.2118/15441-PA

Rognmo, A., Al-Khayyat, N., Heldal, S., Vikingstad, I., Eide, O., Fredriksen, S., . . . Fernø, M. (2018a). *Performance of Silica Nanoparticles in CO2-Foam for EOR and CCUS at Tough Reservoir Conditions*. Paper presented at the SPE Norway One Day Seminar, Bergen.

Rognmo, A. U., Heldal, S., & Fernø, M. A. (2018b). Silica nanoparticles to stabilize CO2-foam for improved CO2 utilization: Enhanced CO2 storage and oil recovery from mature oil reservoirs. *Fuel, 216*, 621-626. doi:10.1016/j.fuel.2017.11.144

Rognmo, A. U., Horjen, H., & Fernø, M. A. (2017). Nanotechnology for improved CO2 utilization in CCS: Laboratory study of CO2-foam flow and silica nanoparticle retention in porous media. *International Journal of Greenhouse Gas Control, 64*, 113-118. doi:10.1016/j.ijggc.2017.07.010

Romero-Zerón, L. (2012). Advances in Enhanced Oil Recovery Processes. In L. Romero-Zerón (Ed.), *Introduction to Enhanced Oil Recovery (EOR) Processes and Bioremediation of Oil-Contaminated Sites*. InTech.

Ross, S., & McBain, J. W. (1944). Inhibition of Foaming in Solvents Containing Known Foamers. *Industrial & Engineering Chemistry, 36*(6), 570-573. doi:10.1021/ie50414a019

Schindelin, J., Arganda-Carreras, I., Frise, E., Kaynig, V., Longair, M., Pietzsch, T., . . . Schmid, B. (2012). Fiji: an open-source platform for biological-image analysis. *Nature methods, 9*(7), 676.

Schlumberger. (2007). Carbonate Rerservoirs.

Schramm, L. (2014). *Emulsions, Foams, Suspensions, and Aerosols: Microscience and Applications, 2nd Edition*: John Wiley & Sons, Inc.

Schramm, L. L. (1992). Petroleum Emulsions: Basic Principles. In L. L. Schramm (Ed.), *Emulsions: Fundamentals and Applications in the Petroleum Industry*. Washington: American Chemical Society.

Schramm, L. L. (1994). Foam Sensitivity to Crude Oil in Porous Media. In *Foams: Fundamentals and Applications in the Petroleum Industry* (Vol. 242, pp. 165-197): American Chemical Society.

Schramm, L. L., & Wassmuth, F. (1994). Foams: Basic Principles. In L. L. Schramm (Ed.), *Foams: Fundamentals and Applications in the Petroleum Industry* (Vol. 242, pp. 3-45): American Chemical Society.

Sheng, J. (2010). *Modern Chemical Enhanced Oil Recovery: Theory and Practice*. Boston: Gulf Professional Publishing.

Sheng, J. (2013). Chapter 11 - Foams and Their Applications in Enhancing Oil Recovery. In *Enhanced Oil Recovery Field Case Studies* (pp. 251-280). Boston: Gulf Professional Publishing.

Skarestad, M., & Skauge, A. (2012). *PTEK213 Reservoarteknikk II*. Bergen, Norway: University of Bergen.

Skauge, T., Spildo, K., & Skauge, A. (2010). *Nano-sized Particles For EOR*. Paper presented at the SPE Improved Oil Recovery Symposium, Tulsa, Oklahoma, USA.

Skjæveland, S., & Kleppe, J. (1992). *SPOR Monograph—Recent Advances in Improved Oil Recovery Methods for North Sea Sandstone Reservoirs*. Stavanger, Norway: Norwegian Petroleum Directorate.

Smallwood, I. M. (1996). n-Decane. In *Handbook of Organic Solvent Properties* (pp. 23-25). Oxford: Butterworth-Heinemann.

Sofla, S. J. D., James, L. A., & Zhang, Y. (2018). Insight into the stability of hydrophilic silica nanoparticles in seawater for Enhanced oil recovery implications. *Fuel, 216*, 559-571. doi:10.1016/j.fuel.2017.11.091

Song, Y.-C., Zhu, N.-J., Liu, Y., Zhao, J.-F., Liu, W.-G., Zhang, Y., . . . Jiang, L.-L. (2011). Magnetic Resonance Imaging Study on the Miscibility of a CO_2/n-Decane System. *Chinese Physics Letters, 28*(9).

Svorstol, I., Vassenden, F., & Mannhardt, K. (1996). *Laboratory Studies for Design of a Foam Pilot in the Snorre Field*. Paper presented at the SPE/DOE Improved Oil Recovery Symposium, Tulsa, Oklahoma.

Talebian, S. H., Masoudi, R., Tan, I., & Zitha, P. (2014). Foam assisted CO2-EOR: A review of concept, challenges, and future prospects. *Journal of Petroleum Science and Engineering, 120*. doi:10.1016/j.petrol.2014.05.013

Talebian, S. H., Masoudi, R., Tan, I. M., & Zitha, P. L. J. (2013). *Foam assisted CO2-EOR; Concepts, Challenges and Applications*. Paper presented at the SPE Enhanced Oil Recovery Conference, Kuala Lumpur, Malaysia.

Weaire, D. (1999). *The physics of foams*. Oxford: Clarendon Press.

Wergeland, C. (2017). *Field Pilot Preparations - Determining CO_2 Foam Quality for Optimal EOR Mobility Control*. (Master thesis), University of Bergen, Bergen.

Worthen, A. J., Bagaria, H. G., Chen, Y., Bryant, S. L., Huh, C., & Johnston, K. P. (2013). Nanoparticle-stabilized carbon dioxide-in-water foams with fine texture. *Journal of Colloid and Interface Science, 391*, 142-151. doi:10.1016/j.jcis.2012.09.043

Yellig, W. F., & Metcalfe, R. S. (1980). Determination and Prediction of CO2 Minimum Miscibility Pressures. doi:10.2118/7477-PA

Zhang, T., Davidson, D., Bryant, S. L., & Huh, C. (2010). *Nanoparticle-Stabilized Emulsions for Applications in Enhanced Oil Recovery*. Paper presented at the SPE Improved Oil Recovery Symposium, Tulsa, Oklahoma, USA.

Zhang, Z., L. Freedman, V., & Zhong, L. (2009). *Foam Transport in Porous Media - A Review*. Richland, Washington: United States Department of Energy.

Ziegler, V. M., & Handy, L. L. (1981). Effect of Temperature on Surfactant Adsorption in Porous Media. doi:10.2118/8264-PA

Zolotuchin, A. B., & Ursin, J.-R. (2000). *Introduction to petroleum reservoir engineering*. Kristiansand: Høyskoleforl.